QATAR UNIVERSITY

COLLEGE OF ENGINEERING

NEW APPROACH OF PIPELINES JOINING USING FIBER REINFORCED PLASTICS COMPOSITES

BY

MOHAMED HOSSAMELDIN FARAG

A Thesis Submitted to

the Faculty of the College of

Engineering

in Partial Fulfillment

of the Requirements

for the Degree of

Masters of Science in Mechanical Engineering

January 2018

COMMITTEE PAGE

The members of the Committee approve the Thesis of Mohamed Farag

defended on 13/12/2017.

_____

Prof. Elsadig Mahdi Saad
Thesis/Dissertation Supervisor

_____

Prof. Tahir Khan
Committee Member

_____

Prof. Faris Tarlochan
Committee Member

_____

Prof. Lazhar Ben-Brahim
Committee Member

Approved:

_____

Khalifa Al-Khalifa, Dean, College of Engineering

ABSTRACT

FARAG,MOHAMED,HOSSAMELDIN, Masters : January : [2018:],

Masters of Science in Mechanical Engineering

Title: NEW APPROACH OF JOINING PIPELINES USING FIBER REINFORCED PLASTICS COMPOSITES

Supervisor of Thesis: Elsadig, Mahdi, Saad.

It is well known that maintenance of pipelines failures due to leakage or rupture caused by either corrosion or lack of strength is a significant challenge for pipelines engineers. Pipelines joining is considered as a significant challenge since many of pipelines failure cases have been observed to be related to joining. The classic methods of joining pipelines including welding have many limitations that result in properties weakening, accelerate corrosion, and hence lead to failure and unexpected shutdowns in oil and gas field. This study aims to introduce a different solution for pipes joining using fiber-reinforced plastics (FRP) composites. An investigation of the effect of different types of FRP on the mechanical behavior of joints regarding bending behavior and internal pressure capacity compared to welding has been carried out through six phases. In phase 1, a fabrication processes in which aluminum pipes have been prepared to be used later for wrapping with different FRP and welding. The FRP used are Kevlar fiber/epoxy (KFRP), carbon fiber/epoxy (CFRP), and glass fibers/epoxy (GFRP). These fiberes have been cut into strips and utilized in the joining systems using fabric winding method. On the other hand, two types of welding have been used to study their effect on pipe's mechanical behavior. These are V-welding technique and normal faced butt-welding technique. Optimization of fiber orientation of joining system under three-point bending test, where CFRP has been used with $0^0/90^0$ and $\pm 45^0$ orientations has been discussed and

presented in phase 2. The results showed that $0^0/90^0$ orientation has the highest flexural load. In phase 3, evaluation of fiber type effect on bending behavior of joined pipes has been carried out for different FRP composites types with four layers and compared to welding. Accordingly, the non-joined aluminum pipe has been investigated under three-point bending test as a control for the study. In addition, the V-welded pipes, as well as normal faced butt-welded pipes, have been investigated under three-point bending test. The results for V-welded pipes showed higher mechanical performance than normal faced butt-welded pipes. To this extent, KFRP showed the highest flexural load, and CFRP showed higher value of flexural load than welding techniques, while the GFRP showed similar flexural load to welding techniques. In addition, phase 4 involved assessment of FRP hybridization on bending behavior of joined pipes, where GFRP/CFRP and KFRP/CFRP of four layers and eight layers have been assessed. The results showed that four layers the of FRP hybridization are insignificant compared to four layers of single FRP type, while eight layers resulted in improvement in flexural loads compared to four layers of single FRP type. Based on the bending results, phase 5 has been dedicated to evaluate the internal pressure capacity of the optimized pipes, in which two types of pipes have considered. These are pipes joined with four layers of KFRP and eight layers of KFRP/CFRP. The results showed improvement in the pipe's internal pressure capacity compared to welding. Finally, corrosion test has been carried out in Phase 6. The results showed that FRP joining systems have higher corrosion resistance compared to welded and non-joined pipes. These results revealed that using FRP composites in pipes joining showing a promising future for pipes joining.

DEDICATION

I dedicate this work to my parents and my beloved wife and son as well as my friends for their appreciative support and trust on me through my master's journey

ACKNOWLEDGMENTS

Great thanking to almighty God for giving me the patience and ambitious and blessing me to complete this work.

I would like to give my sincere thanks also to my supervisor, professor Dr. Elsadig Mahdi Saad for his supporting, encouraging and advising throughout the thesis preparation, and for his assisting and providing of all necessaries to carry out this work.

Finally, yet importantly, I would like to express my thanks and appreciate to the workshop team at Qatar University, Mr. Sunith & Mr. Judith for their help in preparing the pipe samples, and to Eng. Mohamed Karim & Eng. Mohamed Gebril for their exceptional efforts and help in carrying out the experiments.

TABLE OF CONTENTS

LIST OF TABLES

LIST OF FIGURES

CHAPTER 1

INTRODUCTION

This chapter contains a brief about the problem statement and objectives for carrying this work as well as the general outline of this thesis.

1.1 Background

Oil and Gas industry goes through extreme growth over the entire world. It is well known that the energy demand increases because of increasing the world population and due to the higher level of lifestyles today which require more energy. All these factors led to substantial growth in oil & gas industry and other energy industries improvements concerning of production quantities and its technologies.

Pipelines are the most preferred option for transporting oil & gas due to its low cost and its capability to carry and transport large quantities of oil & gas. It is also used for drinking water networks to supply the society with water demands. Thousands of miles of pipelines enter the service annually. The pipelines are joined together in different ways. One of the most common methods for joining metal pipes is welding techniques.

Although those pipelines contribute as an active factor in oil and gas industry, transportation via pipelines still suffers from different problems and obstacles. Failure due to various causes, like the strength capacity of the pipes and due to corrosion and fatigue are widely known. The cost of corrosion in pipelines annually is about $ 589

million out of total cost of corrosion related to oil and gas industry, which is $ 1.372 billion. (Popoola L. T., Grema, Latinwo, Gutti, & Balogun, 2013).

It is well known today among all researchers that joining processes, which carried out classically through welding, contribute as a significant factor in failure process. However, the heat-affected zone (HAZ) is the weakest zone associated with welded parts, which leads to different failure types like severe corrosion. These problems are added to some other issues, like the permanent nature of welding, which does not offer an alternative solution but only cutting in case of any modification or repair. These issues also appear in other types of joining like threaded joints and flanges, due to high-stress concentration points that lead to failure.

This study aims to outline a different solution for joining pipes using fiber-reinforced plastics composites (FRP) and investigate the effect of different FRP composites on the mechanical behavior of joints.

1.2 Significance of the problem

The outcome of the proposed study to existing knowledge is significant, including preventing the cost of lost capital due to corrosion damage related to classical joining methods and improving pipeline joining by optimizing material type, fiber orientation angle, stacking sequence that produces high damage tolerance and handles high internal pressure, and bending load. It is also expected to reduce the number of the shutdown of process and risks to life and the environment. Furthermore, achieving life extension of pipelines and related facilities and in so doing to enhance the productivity of oil and gas

producers. Moreover, using composite in joining in gas and oil industry will help in reducing safety risks, decrease pipeline shutdown, prevent gas and oil leakage, which result in reducing the negative impact on the environment.

1.3 Objectives

The objectives of this thesis are classified below:

1. To investigate the effect of joining types on the mechanical behavior of joints.
2. To evaluate the effect of fibers joining types on the mechanical behavior of joints.
3. To examine the effect of fiber orientation on the mechanical behavior of joints.
4. To determine the effect of hybridization of fibers joining on the mechanical behavior of joints.

1.4 Outline of thesis

This study contains five chapters, and it is divided as follows:

Chapter 1: Contains the introduction about the problem.

Chapter 2: Contains the literature review about the problem.

Chapter 3: Contains the methodology used to carry out the experiments.

Chapter 4: Contains the results and discussion of the observed data from the experiments.

Chapter 5: Contains the conclusion and recommendations.

CHAPTER 2

LITERATURE REVIEW

This chapter addresses the literature about transportation pipelines, pipelines challenges, mainly, joining methods and its limitations regarding failure due to corrosion or lack of properties. This chapter covers as well the mechanics of fiber composites and its fabrication processes.

2.1 Transportation Pipeline

Pipelines have been used for a long time to supply towns and cities with drinking water. (Kennedy, 1993). While, for oil and gas industry, first using of pipelines was in mid of the 1800s in the United States. (Mahmoodian & Li, 2016). The main objective of pipelines is to carry the oil and gas from its sources like crude oil or gaseous to the processing facilities and distribution units. High demands on energy around the world require a fast and effective way of transporting huge amounts of oil or gas. Accordingly, the most effective and practical way of oil and gas transportation has been used for a long time is pipelines. Depends on needs, pipelines can vary from few kilometers to reaches thousands of kilometers to deliver oil or gas to different destinations across the country or even to other countries. Accordingly, Pluvinage & Elwany stated that the total length of gas transportation pipelines around the world is estimated to be around 1 million km; 450,000 km is in the USA, while 235,000 km in Russia. (Pluvinage & Elwany, 2008).

Meanwhile, Mahmoodian & Li stated that the United States has 800,000 km of pipeline for transporting products like natural gas, crude oil, and petroleum products. (Mahmoodian & Li, 2016). Pipelines can be classified based on the materials as conventional pipelines (i.e., mostly metallic) and composites pipelines. More details about these two types are given in below sections.

2.1.1 Conventional pipeline

Conventional pipelines in oil and gas transportation mostly are made from different steel types. (Sharma & Maheshwari, 2017). It is well known that carbon steel pipes, as well as high strength low alloy steel pipes, has been widely used for oil and gas transportation due to their high strength properties. (Mathias, Sarzosa, & Ruggieri, 2013) & (Zhu, Xu, Chang, Hub, & Lu, 2014). High-pressure capacity and high strength properties of pipelines are essential factors for oil and gas transportation in different environmental conditions like offshore or onshore, buried or above the ground (Sharma & Maheshwari, 2017) & (Eliyan, Mahdi, & Alfantazi, 2012). It is also worth to mention that the practice of designing pipelines is based on well-known standards and codes such as ASME and API.

2.1.2 Composite pipeline

Fiber reinforced polymer composite (FRP) pipelines become an alternative for metallic pipelines because FRP has a good performance and cost-effective. Among these composite materials, glass fiber composites (GFRP) has been widely used in low-pressure pipelines. FRP pipelines usually contain an inner non-penetrable barrier with a protection layer for oil or gas transportation, while the outer face of the pipelines has another barrier with a protection layer. (Krikanov & Soni, 1995). FRP pipelines have many advantages over the conventional pipelines. FRP composites pipelines have lower specific weight than conventional pipeline and higher corrosion resistance to many high corrosive chemicals including H_2S. (Fukunaga & Chou, 1988). In addition, in failure mechanism, the global international reporting (GRI) has discussed new high strength steels and FRP composites, which, leak before rupturing and showed that FRP pipelines have higher properties for large diameters pipes and massive operations. (Toutanji & Dempsey, 2001). Today, FRP pipelines have been used for many applications in onshore and processing facilities where low and moderate pressure and temperatures experienced. The offshore applications are still not supported much with FRP composites pipelines, where high temperatures and pressure are expected. (Vasiliev, Krikanov, & Razin, 2003).

2.2 Challenges in pipelines Design

Piping techniques have many challenges to meet the requirements for design and operation, which is usually specified in codes and standards primarily in oil and gas industry. It is well known that maintenance of pipelines failures due to leakage or rupture that caused by either corrosion or lack of strength is a significant challenge for pipelines engineers. Maintenance of pipelines is costly activity, which can be increased in case of offshore pipelines or the buried pipelines. On the other hand, extended networks of pipelines need joining techniques to connect thousands of kilometers of pipelines. Pipelines joining is considered as a significant challenging in pipeline design. It is also evident that the type and location of joints controlled the failure of the pipeline. (Kumar, Singh, & Kumar, 2007). This is because designers consider joints as critical locations (i.e., stress risers). Moreover, in the case of elbow and T-joints, the stress concentration is attributed to the abrupt change in geometry of pipeline, which leads to catastrophic failures in pipelines. (Lee & Chang, 2013) & (Lotsberg, 2008). In addition to the joining challenge, the effect of corrosion on the pressure capacity of the pipeline is very significant, and deteriorate the pipeline integrity and shortening its lifetime. Furthermore, the combination of these factors, if not adequately considered in the design, will lead to an unplanned shutdown. (Vanaei, Eslami, & Egbewande, 2017) & (Xu, Wang, Li, Wang, & Su, 2016). As mentioned earlier, there are two significant challenges arise in pipelines, which is corrosion and joining, these two significant challenges are discussed in below sections.

2.2.1 Corrosion in conventional pipelines

Corrosion is one of the most critical issues in pipelines. Popoola, L.T et al. Studied corrosion problems during oil and gas production and its mitigation. Their study showed that cost of corrosion is about 3% to 5% of the gross national product of industrial countries. The same study showed that total cost of corrosion in oil and gas production industries is $1.372 billion annually. Out of this $589 million is the annual cost related to surface pipelines and facilities, while $463 million is the annual cost for tubing expenses. The other $320 million is the annual cost for corrosion capital expenditures. (Popoola L. T., Grema, Latinwo, Gutti, & Balogun, 2013). The corrosion in pipelines can be either external or internal. The external corrosion in pipelines results from coating degradation or coating defects. While the surrounding environment is a significant contributing factor for external corrosion, the reaction with wet soil and moisture in buried pipelines is a common cause of external corrosion. Also, submerged pipes external corrosion is determined by water chemistry. (Vanaei, Eslami, & Egbewande, 2017). On the other hand, internal corrosion is anticipated in oil and gas transportation, which involves a very high corrosive media like hydrogen sulfide (H_2S) and carbon dioxide (CO_2). CO_2 and H_2S when reacting with free water cause internal corrosion within the internal pipelines surfaces. Continuing internal corrosion process will lead to material degradation and accordingly reduction of pipelines thickness. This result in a reduction of mechanical properties and strength and hence affects the lifetime of the pipeline. (Popoola L. T., Grema, Latinwo, & Gutti, 2013).

There are different types of corrosion observed in pipelines. The uniform/general

corrosion/metal loss is a very famous type of corrosion that results in a reduction of pipeline thickness and causes metal loss and hence failure due to rupture or leakage. (Figure 2.1-a). In addition, The pitting corrosion which is one of the most commonly observed corrosion forms in pipelines and it is considered a severe corrosion that causes cavities and pits to appear on the pipeline surface, and hence leads to failure when it due to penetration through the pipeline's wall (Figure 2.1-b). This form of corrosion can occur either internally or externally. The cavitation corrosion is another type of corrosion in pipelines, which result from the pressure drop of the fluid below the vapor pressure causing bubbles and pockets to form in the internal pipeline surface (Figure 2.1-c). The erosion-corrosion is another type of corrosion, which is observed in pipelines, and it is usually related to the particulates found in the fluids that strike the pipeline internally. The stray current corrosion attacks the external pipeline surface when there is a stray current stream inside the pipelines. It causes pinholes and pits to appear on the surface (Figure 2.1-d). Also, microbiologically influenced corrosion (MIC), which caused by the metabolic activity of microorganisms. This type is divided into two types: anaerobic and aerobic. The Sulfate SO_4^{-2} reducing bacteria is considered the most reason for a severe form of an anaerobic type of this corrosion form (Figure 2.1-e). (Vanaei, Eslami, & Egbewande, 2017). Finally, the galvanic corrosion, which results from electrical current due to the electrical coupling of different electrodes in an electrolyte. (Hack, 2010). Moreover, it is defined as ''accelerated corrosion of metal because of an electrical contact with a more noble metal or nonmetallic conductor in a corrosive environment'' (ASTM, 2006). In this type of corrosion, the charge of metal atoms changes from zero in the metal to a positive value for metal ions in the solution. Accordingly, this reaction is

called an anodic reaction. This reaction generates free electrons that involve other reactions where the charge is reduced and corrosion proceeds. (Hack, 2010).

In pipelines, one or more forms of corrosion can be observed in the same pipe. The combination of two or more forms of corrosion can lead to another form of corrosion and accelerate the failure process as well. (Vanaei, Eslami, & Egbewande, 2017).

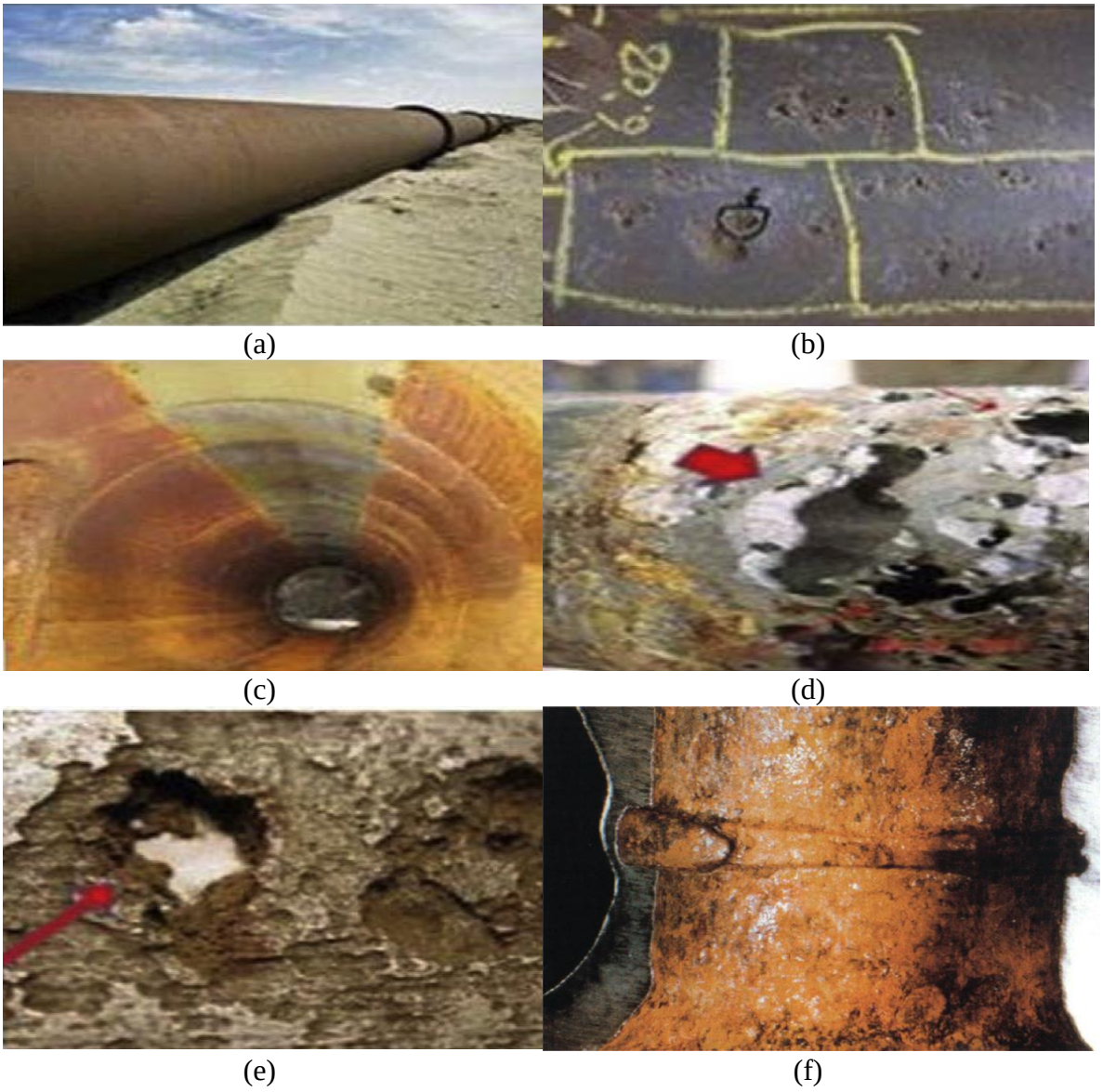

Figure 2.1: Different corrosion forms on transmission oil and gas pipelines. (a): Uniform corrosion, (b): Pitting corrosion, (c): Cavitation and erosion-corrosion, (d): Stray current corrosion, (e): Microbiologically-influenced corrosion, (f): Corrosion of a carbon steel weld in piping carrying partially deaerated seawater. *(Francis, 2001).* & *(Vanaei, Eslami, & Egbewande, 2017).*

2.2.2 Joining of pipelines

Pipelines consist of many pipes joined together. There are many types of joining used to joining pipelines parts. The most common type, which is used in conventional pipelines, is joining two pipes with the welding process. Flanges also is another type for joining pipelines especially in locations where there is a need to change direction or limiting the space and in connection to facilities or pumps. There are some other types of joining pipes also like adhesive bonding and tying components together. Each type of these joining methods has its advantages and its weaknesses. (Kumar, Singh, & Kumar, 2007).

Welding is one of the most widely used techniques to join steel pipes. This technique involves a high temperature, which is necessary for melting and fusion to connect the two pipes. High temperature during welding process cause distortion and cracks within the weldment in the area known as heat affected zone (HAZ) near the welding center. Accordingly, joints by welding become the weakest part of the pipeline where most of the failures in pipelines as result of corrosion or fatigue occurs at HAZ. (Kumar, Singh, & Kumar, 2007). There are different types of welding used for pipes including, metal inert gas (MIG), tungsten inert gas (TIG), arc welding and Oxy Acetylene Welding. (Welding and Pipe Fabrication: Different Processes for Different Grades of Piping, 2015).

Flanges joining has limitations too. Flanges are considered expensive since it contains a sealing casket and many bolts, and it needs to be welded also. Accordingly, it combines limitations of welding in addition to some other limitations. (Barsoum & Khalaf, 2015). The bolts in flanges are considered high-stress points, which can be a failure point. In addition, it needs more effort of inspection to prevent the leakage and hence increase its

operating cost. (Kumar, Singh, & Kumar, 2007).

The other types of joining in pipelines are not used intensively, and it has some disadvantages too. The adhesive bonding usually is deficient in tension, while tying components lead to failure in the tow and appearance of the knots in many cases. (Kumar, Singh, & Kumar, 2007).

- **Effect of welding on corrosion behavior of welded pipelines**

The relation between corrosion behavior and welding is highly considered in corrosion studies. Usually, the stress concentration, residual stresses, and high temperature are the critical factors that affect the lifetime of welded metals, but when these structures like pipelines are subjected to a highly corrosive environment, the failure in welded zones due to corrosion become one of the leading issues. (Xu, Wang, Li, Wang, & Su, 2016) & (Chaves & Melchers, 2011).

Shanhua Xu et al. studied the effect of corrosion on surface characterization and mechanical properties of butt-welded joints. Their study considered the three zones (base metal, weld metal, and HAZ) to investigate their pitting corrosion behavior. Their results showed that pitting corrosion occurred in all three zones, while it was severe in HAZ than other zones (Figure 2.2). (Xu, Wang, Li, Wang, & Su, 2016).

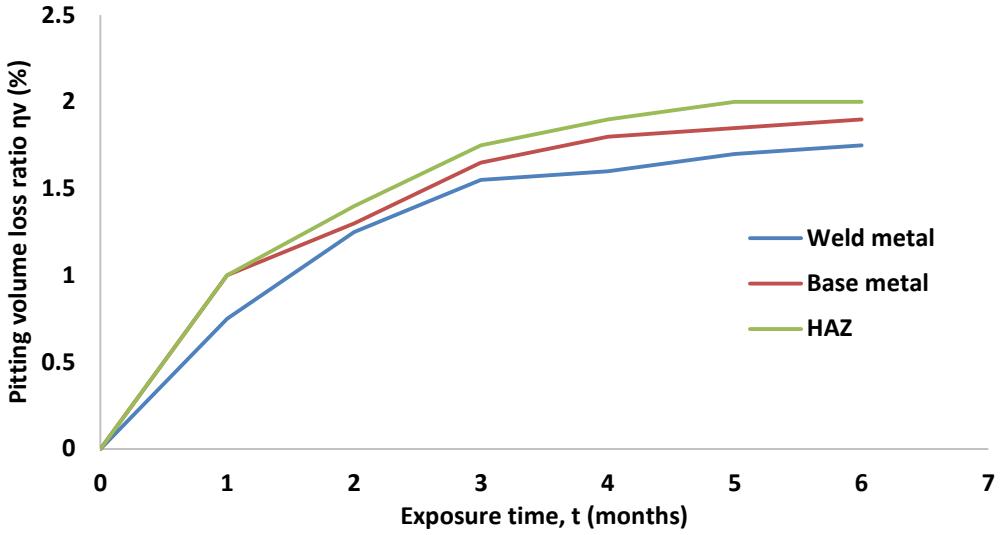

Figure 2.2: Time-dependent trends of pitting volume loss ratio ηv. (reproduced from (Xu, Wang, Li, Wang, & Su, 2016)).

Similar results obtained by Igor A. Chaves et al. They studied the pitting corrosion in pipeline steel weld zones. They found that pitting corrosion was 25% higher in HAZ than other zones in 0-55 weeks, while it reached 50-100% higher in HAZ than other zones after that (Figure 2.3 & Figure 2.4). (Chaves & Melchers, 2011).

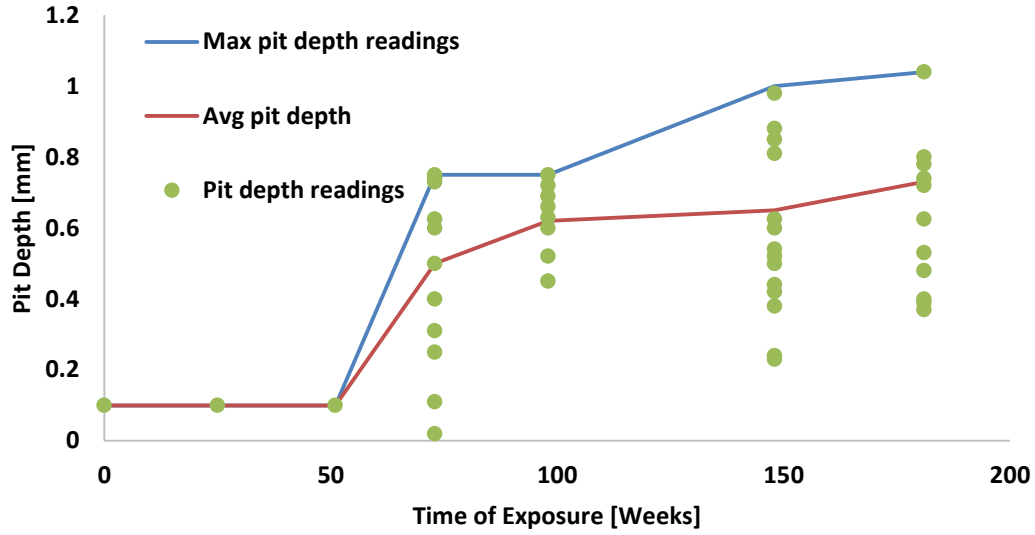

Figure 2.3: Pit depth data for observed deepest pits, mean and maximum trends for parent metal. (reproduced from (Chaves & Melchers, 2011)).

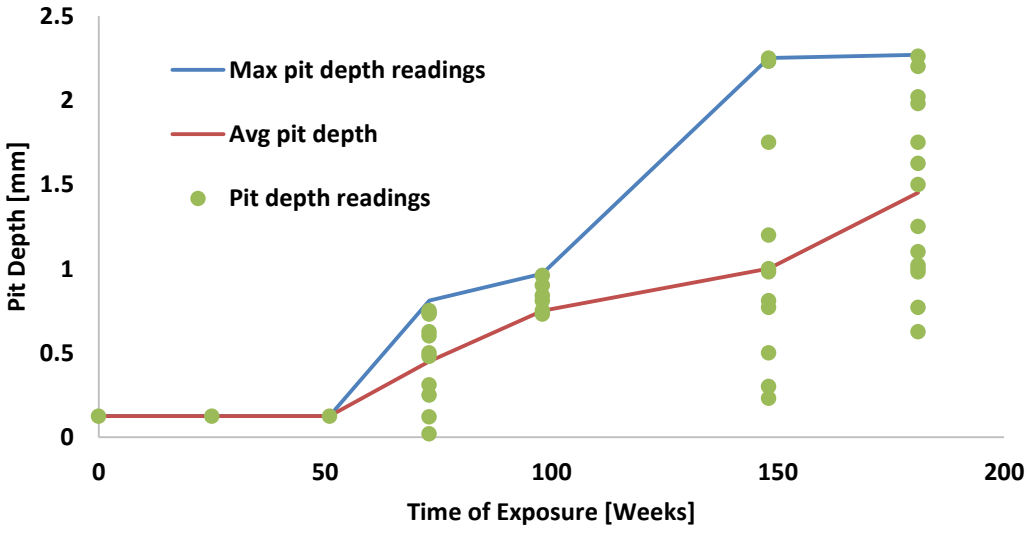

Figure 2.4: Pit depth data for observed deepest pits, mean and maximum trends for HAZ. (reproduced from (Chaves & Melchers, 2011)).

- **Effect of welding on pipes mechanical properties**

Welding process involves high temperatures that affect the microstructures of welded metal and hence result in a reduction of its mechanical properties. Inhomogeneous microstructure and defects in HAZ lead to inhomogeneous hardness distribution, where most of the failures occur usually. Zhu et al. studied microstructures and mechanical properties of welded joints of novel 3Cr pipeline steel using an in-house and two commercial welding wires. They conducted a tensile test and found that fracture occurred at the lowest hardness region in the joints. The failure occurred at HAZ for A-3Cr and in the center of the welded zone in B-3Cr (Figure 2.5). (Zhu, Xu, Chang, Hub, & Lu, 2014).

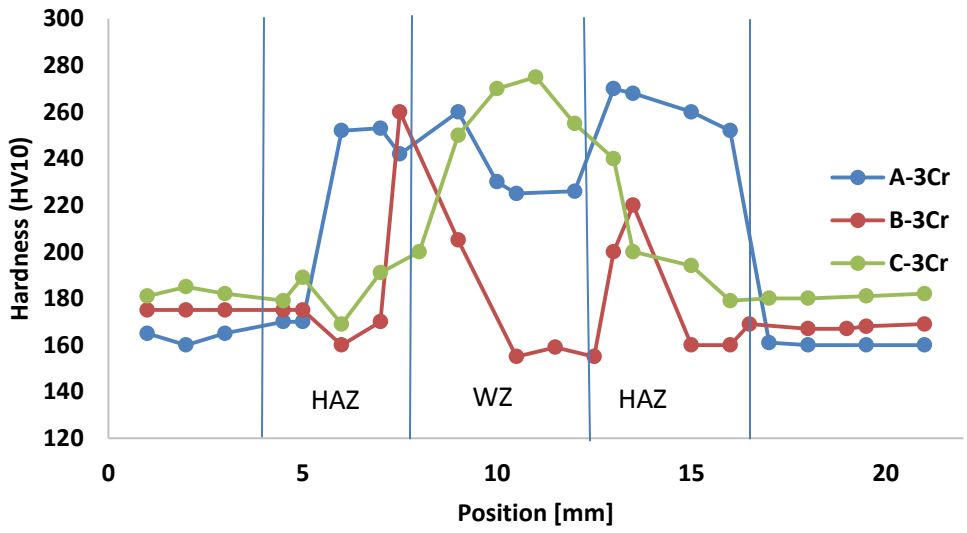

Figure 2.5: Vickers hardness distribution of the joints. (reproduced from (Zhu, Xu, Chang, Hub, & Lu, 2014)).

Many studies conducted to investigate the mechanical properties reduction due to welding processes. Yonghe Yang et al. studied the Fracture toughness of the materials in welded joint of X80 pipelines. They have conducted the tensile test and fracture toughness test. Their result showed that the critical fracture toughness parameters for base metal were higher than HAZ. The whole weld zone suffered regarding fracture toughness, while it was worse in HAZ. (Yang, et al., 2015).

Another study conducted by Xu Chen et al., to investigate fracture toughness at different locations of longitudinal submerged arc welded and spiral submerged arc welded joints of API X80 pipeline steels. They concluded that fracture toughness of base metal was the highest compared to HAZ. (Chen, Lu, Chen, & Wang, 2015).

- **Effect of welding on pipes pressure behavior**

Stress concentrations appear due to circumferential butt welds, welds at buckling arrestors and welds at flanges connectors in pipelines. Those stress concentrations affect the lifetime of pipelines due to cyclic internal pressure due to starting and shutdown of operations or in gas transportation where the pressure changes inside the pipelines. (Lotsberg, 2008).

In addition, residual stresses induced by welding process have a significant effect on the plastic behavior of pressurized pipes with girth-welds subjected to cyclic bending because of enhancing the hoop strain rate comparing to pressurized pipes with no girt-welds. It has been found that hoop strain increase as bending load or the internal pressure

increase. (Bae, Chang, & Lee, 2016).

Lee and Chang have studied the residual stresses in girth-welded steel pipes and their evolution under internal pressure. Their obtained results showed that the internal pressure that applied to girth-welded pipes with open-ends showed compressive hoop stress in the girth-weld due to circumferential shrinkage result from the welding process. This lead to secondary axial bending moment, where tensile axial stresses are presented at the outside surface of the pipe and compressive stresses on the inside surface of the pipe in and around the weld. While for the internal pressure that applied to girth-welded pipes with closed-ends, an extra bending moment at girth-weld attributed to the reduced diameter during the welding process is produced in addition to the secondary bending moment. (Lee & Chang, 2013).

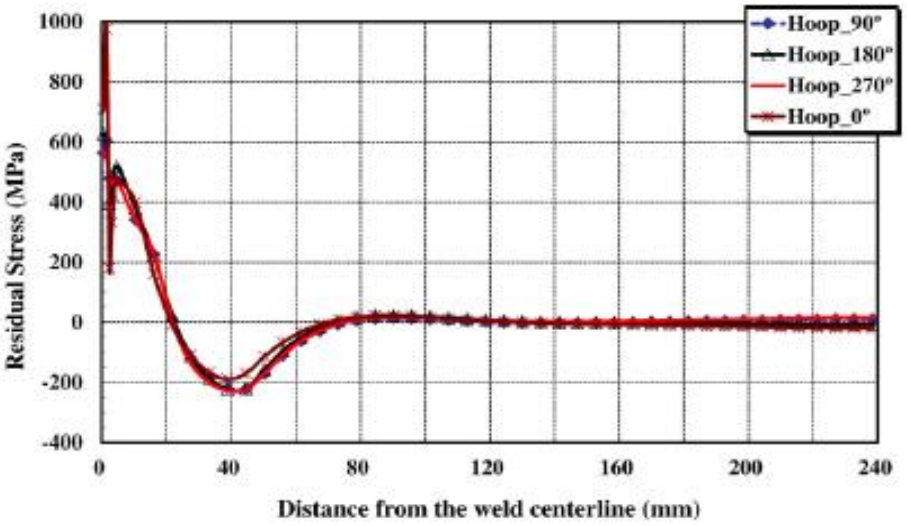

(a)

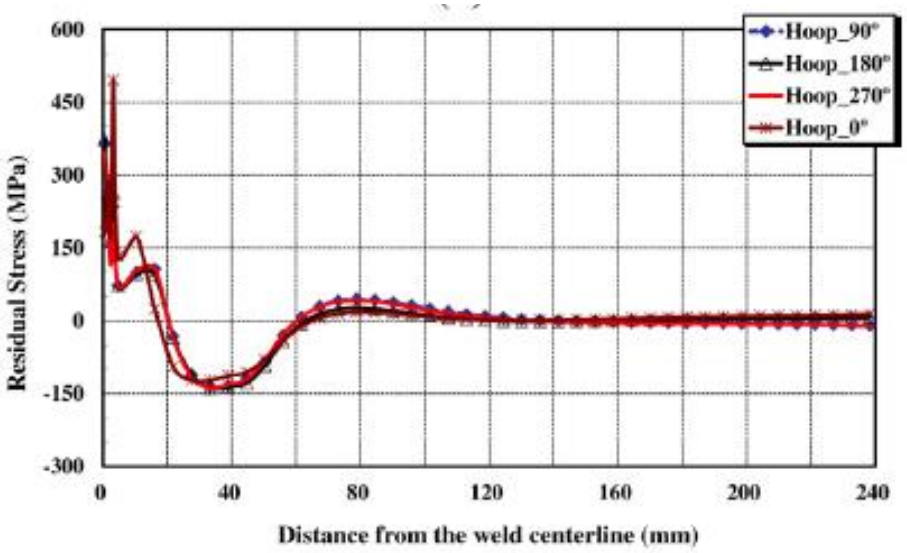

(b)

Figure 2.6: Hoop residual stresses at the four locations: (a) inside surface, and (b) outside surface (Lee & Chang, 2013).

2.3 Mechanics of fiber reinforced polymer composites (FRP)

In mechanics of materials, the deformation of materials, stresses & strain resulted from mechanical and thermal loads are considered an area of extensive research. For metals materials such as steels and aluminum, which considered homogenous and isotropic materials, the properties are not depending on location or orientation. Unlikely, fiber reinforced composites (FRP) are orthotropic and inhomogeneous materials. Orthotropic materials have three orthogonal planes where the material properties are different in all directions. Orthogonal planes contain three axes (1, 2 & 3) called principal material directions (Figure 2.7). The different mechanical behaviors for isotropic, orthotropic and anisotropic materials are presented in (Figure 2.8). (Mallick, 2007).

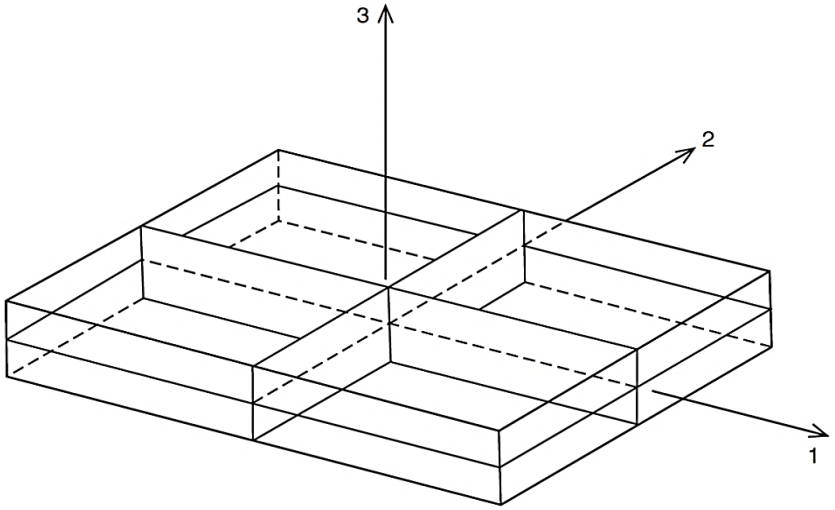

Figure 2.7: Orthotropic material with three planes of symmetry. (Mallick, 2007).

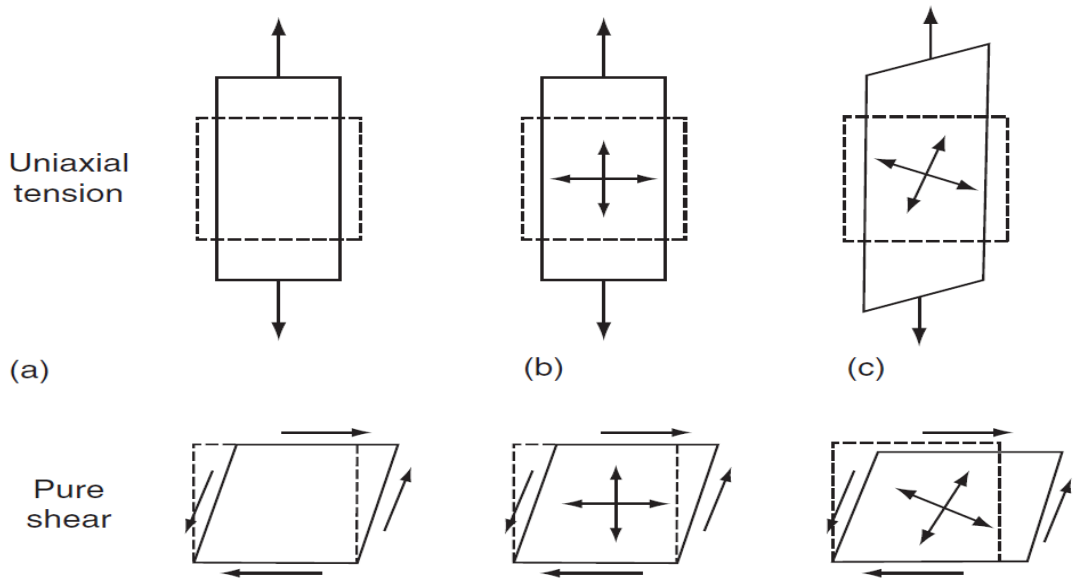

Figure 2.8: Isotropic, orthotropic and anisotropic materials deformations with uniaxial tension and pure shear stresses. (a) Isotropic (b) Special orthotropic, (c) General orthotropic and anisotropic. (Mallick, 2007).

For isotropic materials, when normal tensile stresses are applied in any direction, they cause an elongation in the same direction and contraction in the other two transverse directions. The same behavior can happen in orthotropic materials when normal stresses are applied in only one principal material direction, while an extensional and shear deformations will be observed if the stresses are applied in any the other direction. For anisotropic material, it is observed that there is a combined extensional and shear deformation that results from normal stresses when they are applied in any direction. This cause combination of extensional and shear deformation and known as "extension-shear coupling." It is well known that for isotropic materials, stress-strain characteristics are given using three elastic constants: E, ν, and G, which is Young's modulus, Poisson's ratio, and shear modulus respectively, where two of them are considered independent

according to the following equation:

$$G = \frac{E}{2(1+\nu)} \tag{2.1}$$

The numbers of independent elastic constants needed for orthotropic materials characterization are 9. They are $E_{11}, E_{22}, E_{33}, G_{12}, G_{13}, G_{23}, \nu_{12,}\nu_{13}, \nu_{23}$. Fibers elastic properties in 12 plane are equal in the 2-3 direction. Therefore, $E_{22} = E_{33}$, $\nu_{12,} = \nu_{13}$, and $G_{12} = G_{13}$. Accordingly, the new equation for expressing G_{23} is generated as following:

$$G_{23} = \frac{E_{22}}{2(1+\nu_{23})} \tag{2.2}$$

The number of independent elastic constants for unidirectional orientation fiber is reduced to five constants: E_{11}, E_{22}, ν_{12}, G_{12} and ν_{23}. These are called transversely isotropic. In this case, ν_{12}, and $\nu_{31} \neq \nu_{13}$, while, $\nu_{31} = \nu_{21}$. Though, ν_{21} is related to ν_{12} through the following equation, knowing that it is non-independent elastic constant.

$$\nu_{21} = (\frac{E_{22}}{E_{11}})\nu_{12} \tag{2.3}$$

In a unidirectional fiber reinforced composites the relation between ν_{23} with fibers in the first direction can be linked to ν_{12} and ν_{21} in the following equation:

$$\nu_{23} = \nu_{32} = \nu_{12}\frac{(1-\nu_{21})}{(1-\nu_{12})} \tag{2.4}$$

Therefore, the numbers of constants are reduced from five to four. The fiber reinforced polymer composites (FRP) mechanics are divided into two levels: macro mechanics and micromechanics. In macro mechanics, the material behavior related to mechanical and thermal loads is studied as a macro scale where the material is assumed homogeneous

and orthotropic elasticity equation can be used for stress-strain calculations. Nevertheless, in microscale, the interaction of the constituent materials is studied, and elastic and thermal characters of the lamina are described by micromechanics equations. Understanding the interaction within constituents in the matrix is necessary to understand the failure modes of FRP. (Mallick, 2007).

2.4 Mechanics in fiber-matrix interaction in a unidirectional lamina

Describing mechanics of fiber and matrix interaction in a unidirectional lamina due to tensile and compressive loadings require the following assumptions:

1. Uniform distribution of fiber throughout the matrix.
2. Fibers and matrix have excellent bonding.
3. No voids provided in the matrix.
4. Forces applied to the matrix are parallel or normal to the fiber direction.
5. Stress-free state condition of the lamina, where both matrix and fiber has no residual stresses.
6. Matrix and fiber have linear elastic materials behavior.

(Mallick, 2007).

2.4.1 Longitudinal tensile loading

In longitudinal tensile loading, applied forces are parallel to the lamina's fibers. In addition, these forces are in unidirectional continues, discontinues, and micro-failure modes in longitudinal tension. For unidirectional continuous fibers with the assumption of excellent bonding between the fibers and matrix, the following equation is valid:

$$\varepsilon_f = \varepsilon_m = \varepsilon_c \tag{2.5}$$

This represents the longitudinal strain in fibers (ε_f), matrix (ε_m) and composite (ε_c). The respective longitudinal stresses can also be given, with the assumption of elastic behavior:

$$\sigma_f = E_f\varepsilon_f = E_f\varepsilon_c \tag{2.6}$$

$$\sigma_m = E_m\varepsilon_m = E_m\varepsilon_c \tag{2.7}$$

From above equations, it is noted that $E_f > E_m$, accordingly, it is concluded that $\sigma_f > \sigma_m$. Additionally, sharing between fibers and matrix for the forces in the composite lamina, where tension forces applied is given by:

$$P_c = P_f + P_m \tag{2.8}$$

Knowing that $F = \sigma * A$, so:

$$\sigma_c A_c = \sigma_f A_f + \sigma_m A_m \tag{2.9}$$

$$\sigma_c = \sigma_f \frac{A_f}{A_c} + \sigma_m \frac{A_m}{A_c} \tag{2.10}$$

Where,

σ_c: Average stress for tensile in the composite.

A_f: Fibers net cross-sectional area.

A_m: Matrix net cross-sectional area, where $A_c = A_m + A_f$.

As, $V_f = \frac{A_f}{A_c}$ and $V_m = \frac{A_m}{A_c} = (1 - V_f)$

Therefore,

$$\sigma_c = \sigma_f V_f + \sigma_m V_m = \sigma_f V0_f + \sigma_m (1 - V_f) \qquad (2.11)$$

Additionally, and by dividing both sides of equations by ε_c, result in the following equation for longitudinal modulus:

$$E_L = E_f V_f + E_m V_m = E_f V_f + E_m (1 - V_f) = E_m + V_f (E_f - E_m) \qquad (2.12)$$

This equation is named the rule of mixtures, and it illustrates that for the unidirectional continuous fiber composites, the longitudinal modulus has an intermediate value compared to both fiber modulus and matrix modulus, where linearity increases as fiber volume fraction increases.

The fraction of load that fiber under longitudinal tensile stress can carry is:

$$\frac{P_f}{P_c} = \frac{\sigma_f V_f}{\sigma_f V_f + \sigma_m (1 - V_f)} = \frac{E_f V_f}{E_f V_f + E_m (1 - V_f)} \qquad (2.13)$$

For polymer matrix composites, the fiber modulus is considerably higher than matrix modulus, and hence fibers carry about (70%) of the load in composites. Accordingly, the fiber load fraction and composite load increases as fiber volume fraction increases. The matrix failure strain is higher than fiber failure strain. Under the assumption that entirely fibers have equivalent tensile strength and the failure in fibers occur at the same time of composites failure, the longitudinal tensile strength can be predicted by:

$$\sigma_{Ltu} = \sigma_{fu} V_f + \sigma"_m (1 - V_f) \qquad (2.14)$$

Where,

σ_{fu}: Fiber tensile strength.

σ''_m: Matrix stress at the fiber failure strain ($\varepsilon_m = \varepsilon_{fu}$).

In the case of longitudinal tensile loading, the fiber strength follows a statistical distribution, and hence some fibers that have low stress will break first, while the other fibers may carry higher stresses. Accordingly, broken fiber will cause stress concentrations at voids as well as shear stress concentrations near ends of fibers within the matrix. These stress concentrations can lead to different micro failure modes, like the deponding of fibers from its surrounding matrix. Initiation of cracks within the fibers can occur because of stress concentrations (Figure 2.9). (Mallick, 2007).

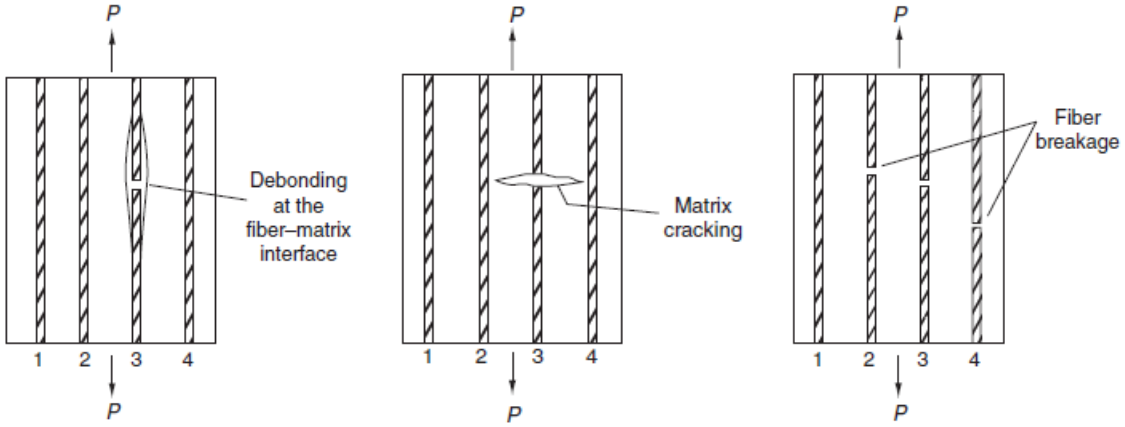

Figure 2.9: Possible micro failure modes following fiber breakage. (Mallick, 2007).

2.4.2 Transverse tensile loading

In the case of transverse tensile loading, the fibers are considered hard inclusions within the matrix and hence, not carrying the load as principal members. In addition, the matrix modulus is increased due to existence fibers, while the local stresses and strains in the matrix are higher compared to the applied stresses. Radial tensile stress near the fiber – matrix interface is about 50% more than applied stress. Accordingly, the cracks which are normal to the loading direction can be in the fiber – matrix interface or the matrix at (θ=90º). The equation for transverse modulus is derived from the following assumptions:

1. The total deformation in the transverse direction is equal to the sum of deformation for both the fiber and the matrix. ($\Delta W_c = \Delta W_f - \Delta W_m$).
2. Tensile stress in the composite equal to the tensile stress of both matrix and fiber. ($\sigma_f = \sigma_m = \sigma_c$).

Since the $\varepsilon_f = \frac{\Delta W_f}{\Delta w}$ and hence, for composite as well as a matrix, the deformation equation can be written as:

$$\varepsilon_c W_c = \varepsilon_f W_f + \varepsilon_m W_m \qquad (2.15)$$

Noting that, $V_f = \frac{W_f}{W_c}$ and $V_m = \frac{W_m}{W_c}$, the equation becomes:

$$\varepsilon_c = \varepsilon_f V_f + \varepsilon_m V_m \qquad (2.16)$$

Since, $\varepsilon_c = \frac{\sigma_c}{E_t}$, $\varepsilon_f = \frac{\sigma_f}{E_f}$ and $\varepsilon_m = \frac{\sigma_m}{E_m}$

The equation becomes:

$$\frac{1}{E_t} = \frac{V_f}{E_f} + \frac{V_m}{E_m} \tag{2.17}$$

By rearranging:

$$E_t = \frac{E_f E_m}{E_f V_m + E_m V_f} = \frac{E_f E_m}{E_f - V_f(E_f - E_m)} \tag{2.18}$$

This equation illustrates that, as fiber volume fraction increases, the transverse modulus is increasing nonlinearly. Unlike the longitudinal tensile modulus, the transverse modulus is affected further by the matrix modulus rather than fiber modulus.

Tensile strength prediction equation is:

$$\sigma_{Tut} = \frac{\sigma_{mu}}{K_\sigma} \tag{2.19}$$

Where,

$$K_\sigma = \frac{1 - V_f[1 - (E_m/E_f)]}{1 - (4V_f/\pi)\text{^}0.5[1 - (E_m/E_f)]} \tag{2.20}$$

The tensile strength equation considers that the transverse tensile strength of the composite is affected by the matrix ultimate tensile strength. In addition, K_σ is representing the maximum stress concentration in the matrix. This equation also shows that transverse tensile strength decreases as fiber modulus and fiber volume fraction increases. (Mallick, 2007).

2.4.3 Longitudinal compressive loading

Longitudinal compressive loading is critical since matrix should support laterally loading and be stable under these conditions. Polymer matrix composites have a lower modulus than fibers itself, and hence, failure in the case of longitudinal compressive loading is usually initiated by localized buckling of fibers. This failure can be described as elastic microbuckling and fiber kinking, depending on the elastic mode or plastic deformation. Microbuckling is categorized into the extensional mode and shear mode (Figure 2.10). (Mallick, 2007).

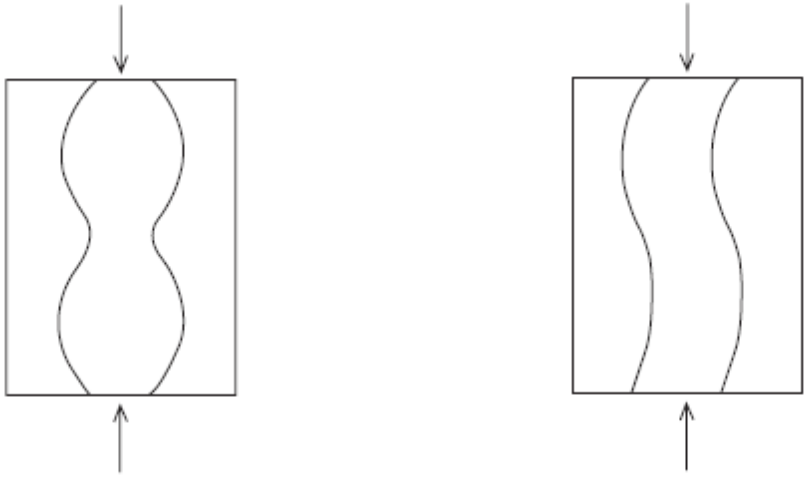

(a) (b)

Figure 2.10: Microbuckling modes due to longitudinal compressive loading for unidirectional continuous fiber composite: (a): extensional mode, (b): shear mode. (Mallick, 2007).

Extensional mode of microbuckling failure is found in low fiber volume fractions, where ($V_f < 0.2$), and it causes extensional strain in the matrix due to out-of-phase buckling. The shear mode of microbuckling is found in high fiber volume fractions, and it causes shear strain in the matrix due to in-phase buckling. (Mallick, 2007).

The prediction of compressive strength in extensional has been found by Rosen as:

$$\sigma_{Lcu} = 2V_f(\frac{V_f E_m E_f}{3(1 - V_f)})\text{^}0.5 \quad (2.21)$$

While for Shear mode it is:

$$\sigma_{Lcu} = \frac{G_m}{(1 - V_f)} \quad (2.22)$$

Where,

G_m: The matrix shear modulus.

V_f: The fiber volume fraction.

The other failure mode in longitudinal compressive mode, which is kinking failure mode, is found in high-localized areas, where the fibers are slightly misaligned from the compressive loading direction. This allows fibers to tilt or rotate at an additional angle and hence form kink bands (Figure 2.11). (Mallick, 2007).

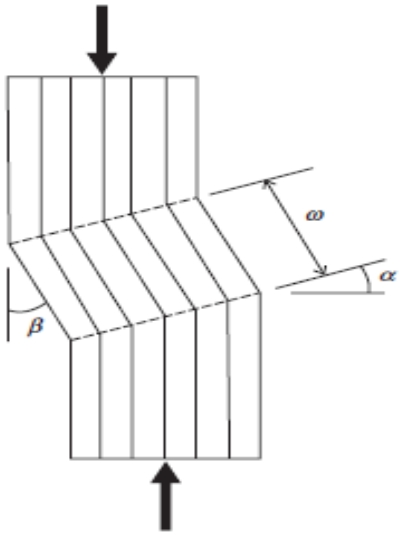

Figure 2.11: Kink band geometry, where, α is Kink band angle, β is Fiber tilt angle, and ω is the kink bandwidth. (Mallick, 2007).

The prediction of stress at kinking initiation has been made by Budiansky and Fleck as following:

$$\sigma_{ck} = \frac{\tau_m}{(\varphi + \gamma_m)} \qquad (2.23)$$

Where,

τ_m: Matrix shear yield strength.

γ_m: Matrix shear yield strain.

φ: Fiber misalignment initial angle.

(Budiansky & Fleck, 1993)

There are some other failure modes observed in longitudinal compressive loading for unidirectional continuous FRP, such as shear failure, yielding of the reinforcement, compressive failure, longitudinal splitting in the matrix as result of poisons ratio effect,

matrix yielding, interfacial debonding, and fiber splitting or fibrillation. (Mallick, 2007).

To improve the longitudinal compressive loading for unidirectional composites, it is necessary to increase the matrix shear modulus, fiber tensile modulus, fiber diameter, matrix ultimate strain and fiber-matrix interfacial strength. It is important also, to notice that misalignment or bowing cause reduction in the longitudinal compressive strength. (Mallick, 2007).

2.4.4 Transverse compressive loading

In case of transverse compressive loading, the applied load is normal to the fiber direction, where the shear failure along the planes parallel to fiber direction and inclined to the loading direction is the most common failure mode can be observed. Debonding in fiber matrix is the cause that initiates this failure mode. It is found that the transverse compressive modulus and strength are lower than longitudinal compressive loading. In addition, the transverse compressive modulus is higher than matrix modulus and is found to be close to that of the transverse tensile modulus. It is also found to be independent of fiber volume fraction. (Mallick, 2007).

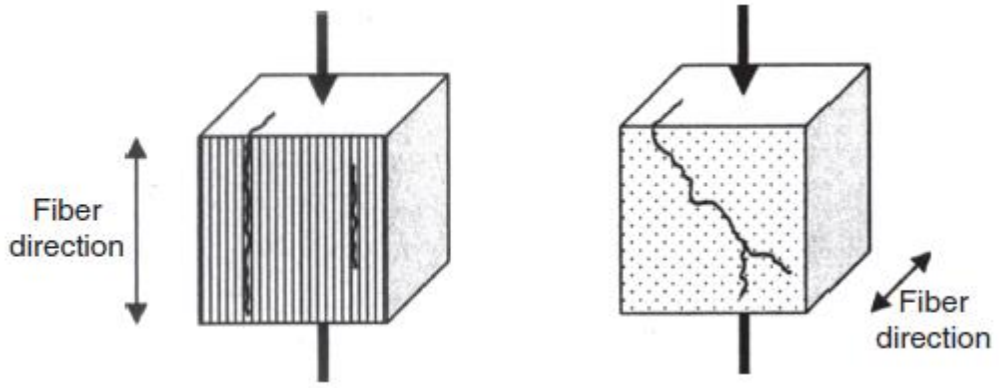

(a) (b)

Figure 2.12: failure in (a): longitudinal compression, (b): transverse compression. (Mallick, 2007).

2.5 Mechanics in fiber-matrix interaction in a woven fabric fiber lamina

Fibers come in Woven fabric laminates with (0^0 & 90^0) has balanced properties compared to unidirectional laminates. Balanced properties can also be obtained using multilayered unidirectional laminates, but the layup process of woven fabric is faster than multilayered unidirectional laminates. It has been noticed that tensile strength of the woven fabric is lower than multilayered laminates. This is due to the presence of fiber yarns in the wrapping direction that behaves like an interlocked structure. In addition, woven fabric fibers usually experience additional mechanical handling during weaving process and hence reduce its tensile strength. (Mallick, 2007). Zheng Ming Huang has developed a micromechanics model called bridging model for woven and braided fibers. (Huang, 2000). The general form of a bridging matrix is:

$$[A_{y^{\cdot\cdot}}] = \begin{bmatrix} a_{11} & a_{12} & a_{13} & a_{14} & a_{15} & a_{16} \\ 0 & a_{22} & a_{23} & a_{24} & a_{25} & a_{26} \\ 0 & 0 & a_{33} & a_{34} & a_{35} & a_{36} \\ 0 & 0 & 0 & a_{44} & a_{45} & a_{46} \\ 0 & 0 & 0 & 0 & a_{55} & a_{56} \\ 0 & 0 & 0 & 0 & 0 & a_{15} \end{bmatrix} \quad (2.24)$$

(Huang, 2000)

For elastic response, the fiber and matrix are subjected to elastic deformation, all elements in the bridging equation are zero, except a_{12} and a_{13}, and accordingly:

$$a_{13} = a_{12} = \frac{(S_{f12} - S_{m12})(a_{11-}a_{22})}{(S_{f11} - S_{m11})} \quad (2.25)$$

Where, S_{ij} are independent elements.

Accordingly:

$$E_{11} = V_f E_{f11} + V_m E_m \quad (2.26)$$

And

$$v_{12} = V_f v_{f12} + V_m E_m \quad (2.27)$$

And

$$E_{22} = \frac{(V_f + V_m a_{11})(V_f + V_m a_{22})}{(V_f + V_m a_{11})(V_f S_{f22} + a_{22} V_m S_{m22}) + V_f V_m (S_{m21} - S_{f21}) a_{12}} \quad (2.28)$$

For transverse tensile load, the ultimate strength (σ_{22}) is obtained by the following equation:

$$\sigma_{22} = \min\{\frac{\sigma_{uf} - (\alpha_{fe2} - \alpha_{fp2})\sigma_{022}}{\alpha_{fp2}}, \frac{\sigma_{um} - (\alpha_{me2} - \alpha_{mp2})\sigma_{022}}{\alpha_{mp2}}\} \quad (2.29)$$

Where,

$$\sigma_{022} = \min\{\frac{\sigma_{mY}}{\alpha_{me2}}, \frac{\sigma_{fu}}{\alpha_{fe2}}\} \quad (2.30)$$

$$\alpha_{fe2} = \frac{E_{f22}}{V_f E_{f22} + 0.5(1 - V_f)(E_m - E_{f22})} \quad (2.31)$$

$$\alpha_{me2} = \frac{0.5(E_{f22} + E_m)}{V_f E_{f22} + 0.5(1 - V_f)(E_m - E_{f22})} \quad (2.32)$$

$$\alpha_{fp2} = \frac{E_{f22}}{V_f E_{f22} + 0.5(1 - V_f)(E_{mT} - E_{f22})} \quad (2.33)$$

$$\alpha_{mp2} = \frac{0.5(E_{f22} + E_{mT})}{V_f E_{f22} + 0.5(1 - V_f)(E_{mT} - E_{f22})} \quad (2.34)$$

For in-plane shear load, the ultimate strength (σ_{12}) is obtained by the following equation:

$$\sigma_{u12} = \min\{\frac{\sigma_{uf} - (\alpha_{fe3} - \alpha_{fp3})\sigma_{012}}{\alpha_{fp3}}, \frac{\sigma_{um} - (\alpha_{me3} - \alpha_{mp3})\sigma_{012}}{\alpha_{mp3}}\} \quad (2.35)$$

$$\sigma_{012} = \min\{\frac{\sigma_{mY}}{\sqrt{3}\alpha_{me2}}, \frac{\sigma_{fu}}{\alpha_{fe2}}\} \quad (2.36)$$

$$\alpha_{fe3} = \frac{G_{f12}}{V_f G_{f12} + 0.5(1 - V_f)(G_m - G_{f12})} \quad (2.37)$$

$$\alpha_{me3} = \frac{0.5(G_{f12} + G_m)}{V_f G_{f12} + 0.5(1 - V_f)(G_m - G_{f12})} \quad (2.38)$$

$$\alpha_{fp3} = \frac{3G_{f12}}{3V_f G_{f12} + 0.5(1 - V_f)(E_{mT} - 3G_{f12})} \quad (2.39)$$

$$\alpha_{mp3} = \frac{0.5(3G_{f12} + E_{mT})}{3V_f G_{f12} + 0.5(1 - V_f)(E_{mT} - 3G_{f12})} \quad (2.40)$$

(Huang, 2000).

2.6 Failure Criteria of polymeric composites

Traditional design approaches for isotropic materials like steels or aluminum cannot be used to describe failure criteria of polymeric composites such as FRP. Polymeric composites such as FRP is considered orthogonal materials. Therefore, new approaches for design methods and failure predictions for FRP materials has been established. Four types of failure theories named as: maximum stress theory, maximum strain theory, Azzi-Tsai-Hill theory and Tsai-Wu failure theory are discussed in following. (Mallick, 2007).

i. Maximum stress theory

In this theory, it has been suggested that the failure is expected when stress in any principal material direction equal or exceed the corresponding ultimate stress for the unidirectional lamina.

ii. Maximum strain theory

In this theory, it has been suggested that the failure is expected when strain in any principal material direction equal or exceed the corresponding ultimate strain for the unidirectional lamina.

iii. Azzi-Tsai-Hill theory

In this theory, Azzi and Tsai suggested that the failure occurs in an orthotropic lamina when the following equation is fulfilled:

$$\frac{\sigma_{11}^2}{S_{Lt}^2} - \frac{\sigma_{11}\sigma_{22}}{S_{Lt}^2} + \frac{\sigma_{22}^2}{S_{Lt}^2} + \frac{\tau_{12}^2}{S_{Lt}^2} = 1 \qquad (2.41)$$

Both tensile stresses are positive, and for compressive stresses, the corresponding compressive strengths are used in the same equation. (Mallick, 2007).

iv. Tsai-Wu Failure Theory

Tsai and Wu have proposed that under the plane stress conditions, the failure is predicted if the following equation is satisfied:

$$F_1\sigma_{11} + F_2\sigma_{22} + F_6\tau_{12} + F_{11}\sigma_{11}^2 + F_{22}\sigma_{22}^2 + F_{66}\tau_{12}^2 + 2F_{12}\sigma_{11}\sigma_{22} = 1 \qquad (2.42)$$

Where F_i, are strength coefficients.

A comparison between the failure theories has been made using experimental data for carbon fiber-epoxy lamina (Figure 2.13). It is noted that failure envelope described by Tsai-Wu theory is a continuous ellipse. (Mallick, 2007).

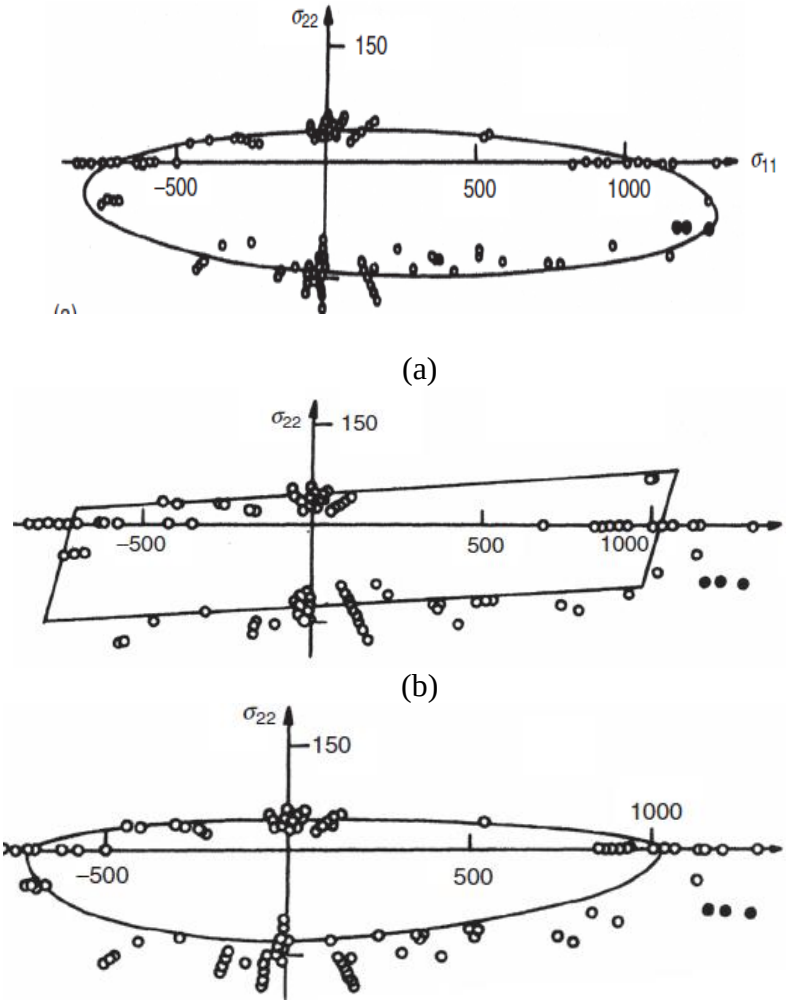

Figure 2.13: Comparison of failure theories, (a): Tsai-Wu, (b): maximum strain, (c): Azzi-Tsai-Hill failure theories with biaxial strength data of a carbon fiber-reinforced epoxy composite (Mallick, 2007).

2.7 Manufacturing process of composites

Cost effective and reliability of production method are the most critical factors that affect the production, which, define an efficient production for a material or component. The early method used for FRP structural parts manufacturing is hand layup technique. Layup technique is considered a reliable process but is very slow and involve an expensive labor cost. The revolution of the automotive industry has been involved in FRP manufacturing to support the high production rates. Compression molding, pultrusion, and filament winding are three manufacturing processes existed for a long time. Resin transfer molding (RTM) is another manufacturing process that becomes a significant process due to its ability to support the production of complex shapes, high production rates, and fast curing resins, especially in aerospace and automotive industries. (Mallick, 2007). In the following section, the winding process is highlighted in details.

i. Winding process:

Winding processes involves wrapping fibers around rotating mandrel, where fibers are continuously immersed in resin before wrapping with different angles (Figure 2.14). Usually, this process which uses filament fibers and called filament-winding process. This process is widely used in different industries applications, including automotive industries for drive shafts, aircrafts industries as well as pipelines and storage tanks for oil and gas industry. Winding process can also be used, with fiber strips instead of filament fibers, as the case in this study. In this case, only one strip of fiber each time can

be used for feeding in resin bowl to the rotating mandrel. For in-site fabrication, winding using a hand can be done as well, although this involves lower tension applied to the pipelines. Another way is to use a developed device for such purpose, which can rotate itself around the pipeline applying wrapping with wet fibers under certain tension.

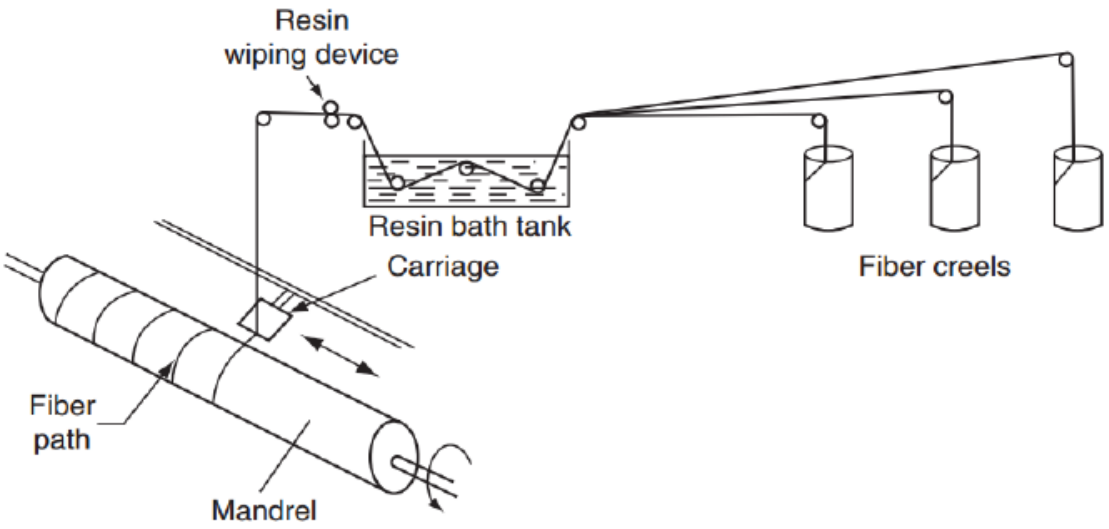

Figure 2.14: Schematic of a filament-winding process. (Mallick, 2007).

ii. Curing process

Fiber-reinforced thermoset polymers are considered a composite after it is cured through the curing process. Curing process involves elevated temperatures and pressure for the preset length of time. This process is necessary for transferring partially cured or uncured

material to fully cured solid. Curing process also involves high pressure, which used to allow the high viscous resin in the fiber-resin mixture to be distributed. The magnitude and duration of these two parameters are important. Hence, it affects the quality and performance of the product. (Mallick, 2007).

iii. Viscosity

The viscosity of a fluid is known as a resistance of flow under shear stresses. Fluids with low molecular weight fluids, such as water or motor oil, have low viscosities and flow readily. Other fluids that have high molecular weight such as polymer melts have high viscosities and high stresses are necessary to flow. Temperature and shear stress are the most critical factors that determine the viscosity of the fluid. Although shear stress does not affect the low molecular weight fluids, it affects high molecular weight fluids where the viscosity is either increase (shear thickening) or decrease (shear thinning). High-molecular-weight fluids Polymer melts are considered a shear thinning fluids as their viscosities decrease with increasing the shear stress. The starting material for thermoset resin is considered a low viscous fluid. Nevertheless, its viscosity increases through the curing process, and it reaches high values until it is completely converted to a solid. (Mallick, 2007).

2.8 Stress analysis for pipes

Pipes Design involves essential factors, such as pipes thickness, diameter, and material. Designing composites pipes is an intensive field of research among engineers working in oil and gas industry. (Sebaey & Mahdi, 2014) & (ASTM-G46, 2013). The composites optimization involves its fiber orientation, stacking sequence as well as the type of fiber. Pipes, in reality, are subjected to different types of loading, such as static and pseudo-static loading. (Mahdi E. , 2015). Bending due to pipe weight, internal pressure inside the pipe, thermal stress due to a temperature gradient, creep due to thermal loading, moisture strain, and soil – pipe interaction is considered examples for static and pseudo-static loading. While, vibration from the hydrodynamic forces, fluid impact and waves of sea and winds are examples of dynamic load. Accordingly, pipe design should consider combined loading in the optimization process.

The lamination theory shall be considered to correlate different loading condition with deformation by stiffness.

$$\begin{bmatrix} N \\ M \end{bmatrix} = \begin{bmatrix} A & B \\ B & D \end{bmatrix} \begin{bmatrix} \varepsilon \\ \kappa \end{bmatrix} \qquad (2.43)$$

Where, [A] is the membrane stiffness, [B] is coupling stiffness and [D] is bending stiffness.

The stiffness matrix components are calculated using the following equations:

$$
\begin{aligned}
A_{ij} &= \sum_{k=1}^{n} \overline{Q}_{ijk}(z_k - z_{k-1}) \\
B_{ij} &= \frac{1}{2}\sum_{k=1}^{n} \overline{Q}_{ijk}({z^2}_k - {z^2}_{k-1}) \\
D_{ij} &= \frac{1}{3}\sum_{k=1}^{n} \overline{Q}_{ijk}({z^3}_k - {z^3}_{k-1})
\end{aligned}
\tag{2.44}
$$

Where Q is the stiffness matrix of layer k, n is the number of layers and z is the distance between the layer k and the laminate axis of symmetry.

Critical bending moment due to the own pipe weight, the weight of fluid or working environment is an important parameter which shall be considered in designing, can be calculated as following (Sebaey & Mahdi, 2014):

$$
M_{cr} = \frac{2\,\overline{E} I_{yy} a_{11} \lambda_{cr}}{D} \tag{2.45}
$$

Where, λ_{cr} is the minimum eigenvalue. Additionally, a_{11} can be obtained from compliance matrix $[a] = [A]^{-1}$.

$$
EI_{yy} = \frac{\pi D}{2}\left(\frac{D}{2a_{11}} + \frac{1}{d_{11}}\right) \tag{2.46}
$$

Buckling due to pipe external pressure is another parameter that needs to be considered during the design. It can be calculated:

$$
\begin{aligned}
&P \\
&= 3\left[\frac{A_{Ani}D_{Ani} - B_{Ani}^2}{A_{Ani}(D/2)^3 + 2B_{Ani}(D/2)^2 + D_{Ani}(D/2)}\right]
\end{aligned}
\tag{2.47}
$$

Where,

$$
\begin{bmatrix} A_{Ani} & B_{Ani} \\ B_{Ani} & D_{Ani} \end{bmatrix} = \begin{bmatrix} A_{22} & B_{22} \\ B_{22} & D_{22} \end{bmatrix} - [L_1]^T [L_2]^{-1} [L_1] \tag{2.48}
$$

$$[L_1] = \begin{bmatrix} A_{12} & B_{12} \\ A_{26} & B_{26} \\ B_{12} & D_{12} \\ B_{26} & D_{26} \end{bmatrix} \quad (2.49)$$

$$[L_2] = \begin{bmatrix} A_{11} & A_{16} & B_{11} & B_{16} \\ A_{16} & A_{66} & B_{16} & B_{66} \\ B_{11} & B_{16} & D_{11} & D_{16} \\ B_{16} & B_{66} & D_{16} & D_{66} \end{bmatrix} \quad (2.50)$$

Where, [A], [B] and [D] are the stiffness matrix determined previously (Mahdi, Rauf, Ghani, El-Noamany, & Pakari, 2013).

For internal pressure, the general equation for the pipe as described in Shegly's mechanical engineering design:

$$\sigma_t = \frac{P_i r_i \hat{}2 - P_o r_o \hat{}2 - r_i \hat{}2 r_o \hat{}2 (P_o - P_i)/r \hat{}2}{(r_o \hat{}2 - r_i \hat{}2)} \quad (2.51)$$

$$\sigma_r = \frac{P_i r_i \hat{}2 - P_o r_o \hat{}2 - r_i \hat{}2 r_o \hat{}2 (P_o - P_i)/r \hat{}2}{(r_o \hat{}2 - r_i \hat{}2)} \quad (2.52)$$

Where,

σ_t: Tangential stress

σ_r: Radial stress

P_i: Internal pressure

P_o: External pressure

r_i: Internal diameter

r_o: Outer diameter

(Budyans & Nisbett, 2011)

These equations are considered as guidance for unified or combined loading. Considering

the weight of the pipe is essential for pipe handling, transportation and installing. Furthermore, the maximum strain criterion is the most common theory for stacking sequence optimization. Where, the Tsai-Wu theory is the most common for industry (Eliyan, Mahdi, & Alfantazi, 2012). These two failure criteria are simple in implementation. Moreover, these two failure criteria do not consider the shear effect, nonlinearity, lamina position and thickness in the failure index. LaRC failure criteria is an example of these criteria. (Sebaey T. , Mahdi, Shamseldin, & Eltai, 2014).

Ghiasi et al. reviewed different optimization techniques that are considered for stacking sequence design of the laminated composites. Accordingly, they found that for the optimizing the stacking sequence of composite laminates, the gradient direct optimization methods has limitations. This is related to the discrete nature of the problem variables and to the vast number of local optima where the gradient methods can converge without reaching the global optimal. (Mahdi, Hamouda, Sahari, & Khalid, 2003) & (Mahdi, Hamouda, Sahari, & Khalid, 2003). In fact, the enumeration technique can be used for laminates with small numbers of layers and combinations of possible fiber orientations. While, when considering a large number of layers and possible orientations, the enumeration technique does not work (Mahdi, Mokhtar, Asari, Elfaki, & Abdullah, 2006). Accordingly, the metaheuristic search algorithms are considered the most suitable for solving problems, which their objective function can be discontinuous, non-differentiable, stochastic, or highly nonlinear (Lyu Jin. A, 2014). The ACO algorithm falls in this category of optimization algorithms and is a simulation of the behavior of the real ants when traveling between the nest and the food source. (Senkine & Shin, 1999) & (Gohari, Golshan, Mostakhdemin, Mozafari, & Momenzadeh, 2012). Mixing all these

theories and techniques can help in the well understanding of the behavior of hybrid composite/metal pipeline under different loading and environmental conditions.

Summary:

In this chapter, literature review covering related topics has been addressed to provide the necessary understanding of the background of this study. This chapter covered a brief about pipelines in oil and gas industry and addressed two of the most common problems in that field, which is corrosion and joining. The relation between these two problems has been discussed and clarified. The chapter also covered, the mechanics of fiber reinforced polymer composites (FRP) including its equations and its failure modes. In the proceeding chapter, a detailed experimental program methodology is presented.

CHAPTER 3

METHODOLOGY

In this chapter, a detailed methodology that has been used to carry out this research study including procedures and preparation for different types of experiment are described. The methodology has been divided into six phases as described below:

3.1 Methodology phases

Phase 1: Fabrication process

In this phase, aluminum pipes and three types of fibers reinforcement plastics (FRP) have been used for pipe joining, (KFRP, CFRP, and GFRP). These types have been prepared for joining the pipes by cutting them as long strips and making grooves in the aluminum pipes for joining. The fabrication has been done by wrapping the joined pipes with fibers strips from groove to groove manually by wrapping technique. Additionally, for welding, the delegated pipes specimens have been prepared and welded (V-welding and Normal faced butt-welding) with aluminum alloy filler (4043).

Phase 2: Optimization of fiber orientation under bending test

An optimization of fiber orientation has been carried out on CFRP for two orientation ($0^0/90^0$ and $\pm45^0$) under three-point bending test. The outcomes of this phase have been considered in the following phase.

Phase 3: Evaluation of fiber type effect on bending behavior of joined pipes

Various FRP types (KFRP, CFRP, and GFRP) have been used as joining material for the aluminum pipes with the optimized orientation (phase 2). These FRP joining systems have been investigated under three-point bending test and compared to welding systems.

Phase 4: Assessment of FRP hybridization on bending behavior of joined pipes

The hybridization has been made for KFRP/CFRP & GFRP/CFRP, where both KFRP & GFRP have been chosen as starting material in contact with aluminum pipes due to their corrosion resistance comparing to CFRP. These FRP joining systems have been investigated under three-point bending test and compared with single FRP joining systems.

Phase 5: Performance of optimized joining types under internal pressure test

Optimization process has been established for different FRP joining systems considering the previous phases. The optimized joining systems have been investigated under internal pressure test. This test included combined radial and axial test as well as pure radial test.

Phase 6: Corrosion investigation of FRP and joining types

The FRP joining systems as well as non – joined and welded pipes are investigated for corrosion and compared with each other.

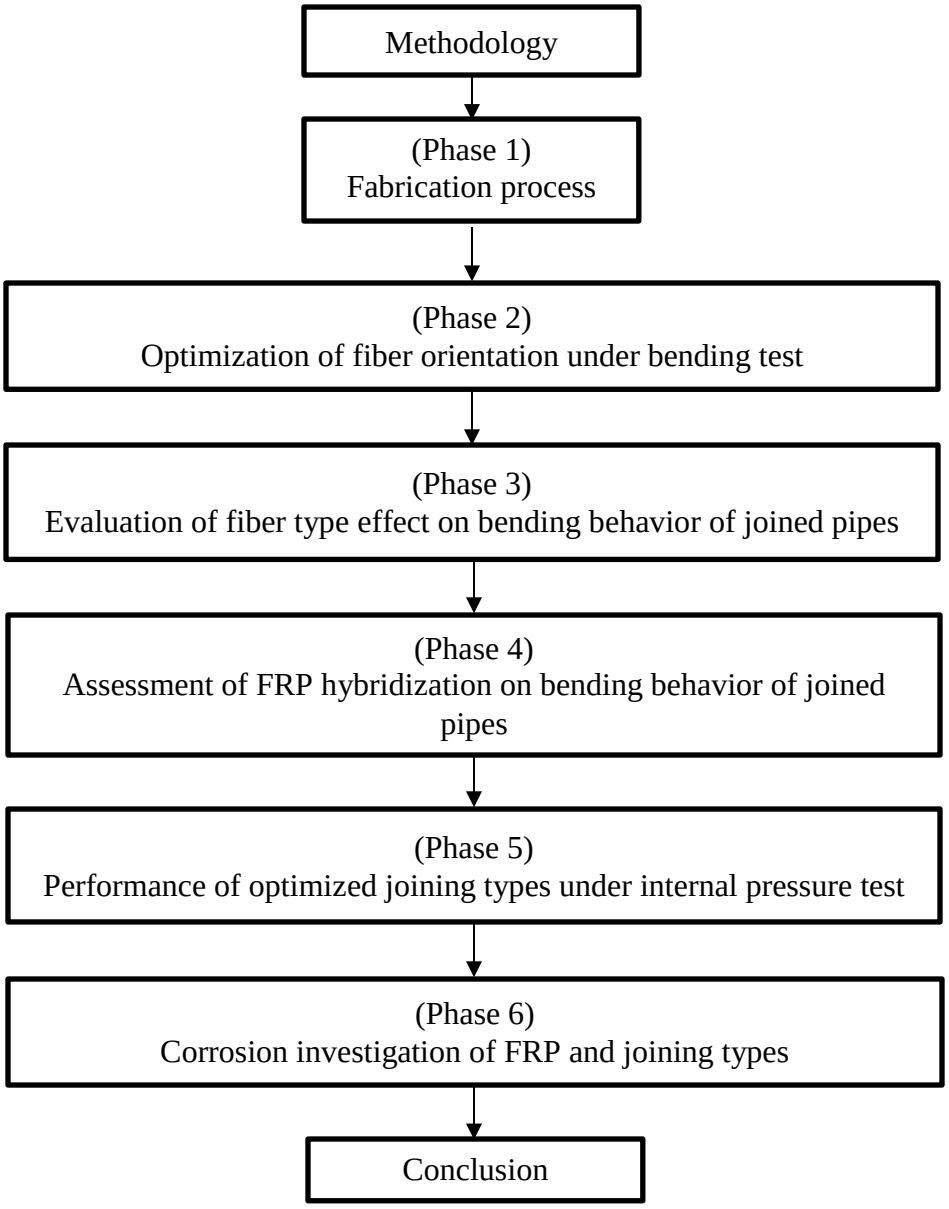

Figure 3.1: Methodology outline.

3.2 Materials

Used materials included aluminum pipes of 50 mm outer diameter, 3 mm thickness (Figure 3.2). These pipes have been prepared for welding, and FRP joining. FRP materials included KFRP, CFRP, and GFRP. The fibers were woven fabric rolls (Figure 3.3). The aluminum has been chosen instead of steel due to the limitations of internal pressure machine capacity. The internal pressure test has been designed to reach the bursting limit, and accordingly it is difficult to be reached with steel pipes. Moreover, the material type of pipes is not under investigation in this study, which focus on the joint behavior. All these reasons support using of metallic aluminum pipe for investigating the behavior of joints in terms of internal pressure as well as flexural loads.

Figure 3.2: Aluminum pipe with (50 mm) outer diameter and (3 mm) thickness.

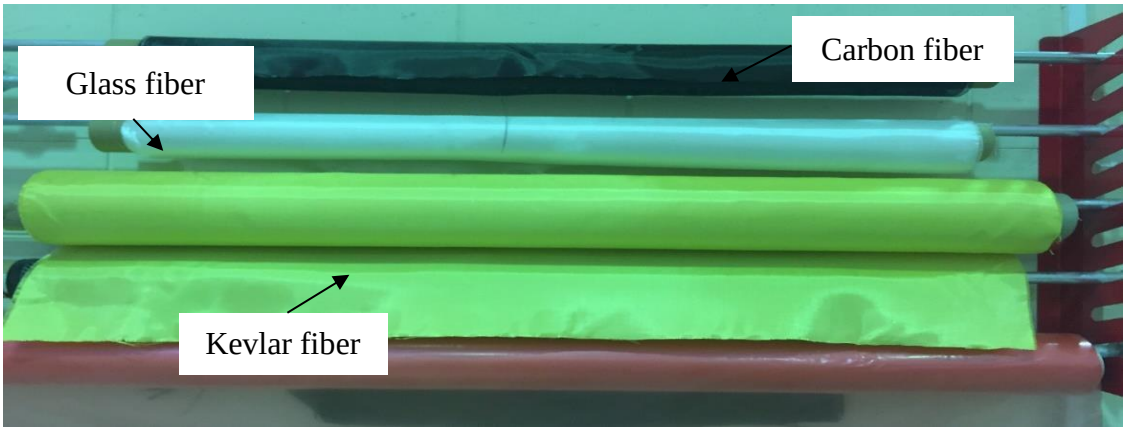

Figure 3.3: Woven fabric fibers.

3.3 Specimens preparation

3.3.1 Welding of pipes

Aluminum pipes of 1m total length have been cut in the middle and subjected to MIG welding using filler wire of aluminum alloy (4043), which has the following chemical composition:

Table 3.1: Chemical composition of welding filler aluminum alloy (4043)

Material	**Si**	**Mn**	**Cu**	**Zn**	**Fe**	**Ti**
Wire/Strip (%)	5	<0.05	<0.10	<0.10	<0.60	<0.15

Table 3.2: Mechanical properties of welding filler aluminum alloy (4043)

Yield strength (MPa)	Tensile strength (MPa)
55	165

The welding process involved two different methods: (V-welding & normal faced butt-welding). For V-welding, the pipes have been prepared by removing material from pipes edge in a slope to form V-shape when connected. This method has been done to allow the filler material to be intensively distributed through the joint and to provide higher welding quality. For faced butt-welding method, the pipes have been faced together after cutting, and welding has been applied directly to join the two pipes.

3.3.2 Preparation for FRP composites joining

Aluminum pipes of 1m total length have been cut in the middle, and the groove of 1.5 mm depth and 5 cm width has been applied as shown in Figure 3.4 to allow for wrapping process and to prevent the joint from slipping under different loading conditions. The total length of the joint is 25 cm from groove to groove.

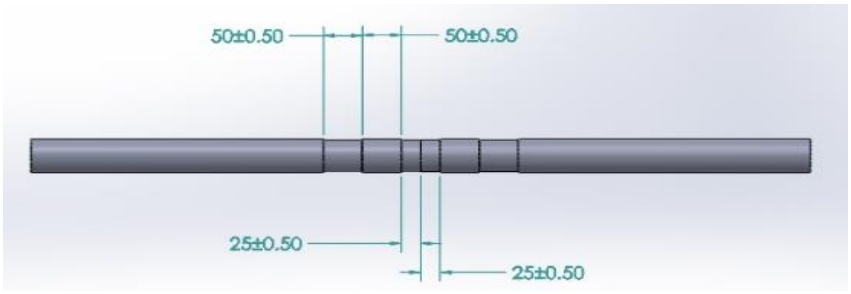

(a)

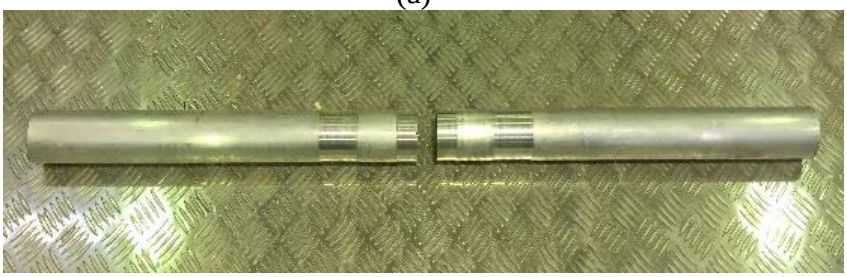

(b)

Figure 3.4: Aluminum pipe prepared for the fabrication process, (a): dimensions produced by Solidworks, (b): Sample after preparation.

3.3.3 Fibers reinforcement preparation

All used fibers (Kevlar, Carbon fiber & Glass fiber) are in woven rolls form. Woven rolls have been cut to very long strips of 5 cm width (Figure 3.5). These strips have been used in the wrapping of $0^0/90^0$ as well as $\pm 45^0$ by adjusting the angle of wrapping manually. Other orientations were challenging to be wrapped since it needs manual adjusting for the orientation.

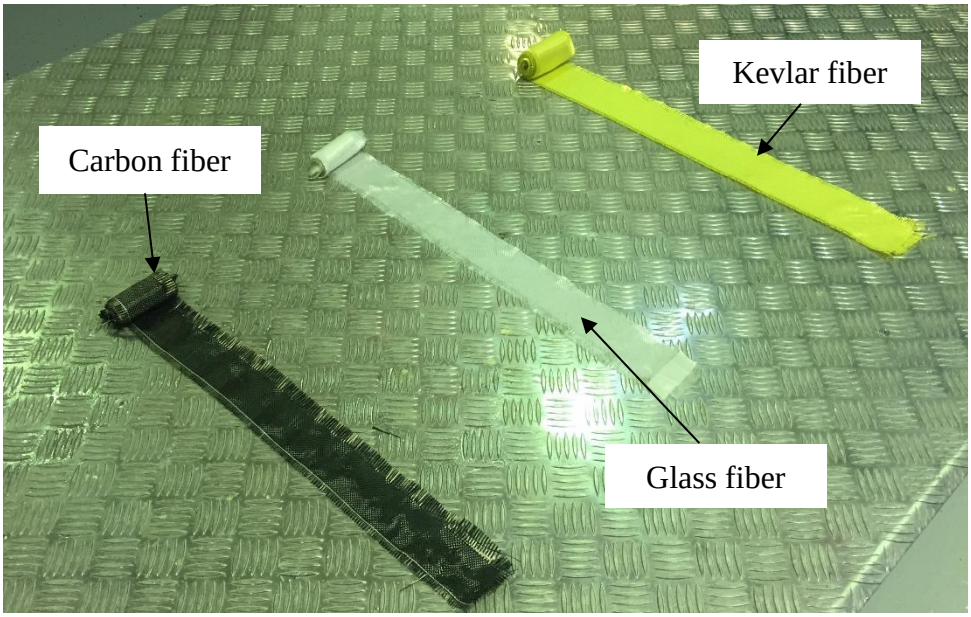

Figure 3.5: Woven rolls strips fibers**.**

3.4 Fabrication process

Pipes has been coupled by placing a solid cylindrical piece of aluminum inside the two parts of pipes to prepare them for fabrication. This piece of aluminum has been covered with a layer of nylon to ease its removal after the resin is cured. The pipes have been placed in a winding machine to allow it for rotating while wrapping. The fabrication has been done by wrapping the joined pipes with fibers strips from groove to groove (Figure 3.7). This method is considered as wet wrapping or winding method. The fiber strips are subjected to resin while wrapping using a brush to apply the resin. The resin was a fast curing resin by using (EL2 epoxy laminating resin) mixed with (AT30 Fast epoxy hardener), which has a curing time of 4-6 hours (Figure 3.6). The epoxy to hardener

mixing ratio was 100-30 parts per weight. Although there are many other methods for fiber composite preparation, this is suitable for pipeline joining, since this process, in reality, need to be done after installing pipes in their destinations, and accordingly, other methods will be difficult for pipelines joining, unless separate tools for wrapping are invented for such application in the future.

(a) (b)

Figure 3.6: (a): Epoxy hardener, (b): Laminating resin.

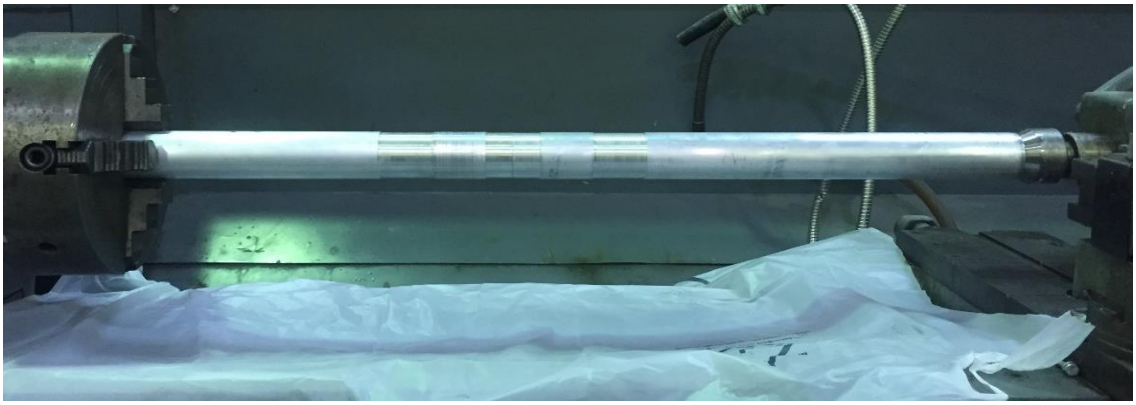

(a)

(b)

(c)

Figure 3.7: Fabrication process, (a): coupled pipe. (b): wrapping process using KFRP. (c): fabricated sample with CFRP.

3.5 Three-point bending test procedure

Three-point bending test has been carried out using the Instron machine (Figure 3.8 - a). Bending has been performed on the pipes using steel Mandrel T-shape (load pin), (Figure 3.8 - c), which applies bending load on the joint. This tool represents one of the three points. The pipes rest on a two supporting point (Figure 3.8 - b), which represents the

other two points with a total length of 33 cm point to point. The test has been run under the general compression test built-in program with speed of 15 mm/min and performed until failure occurred.

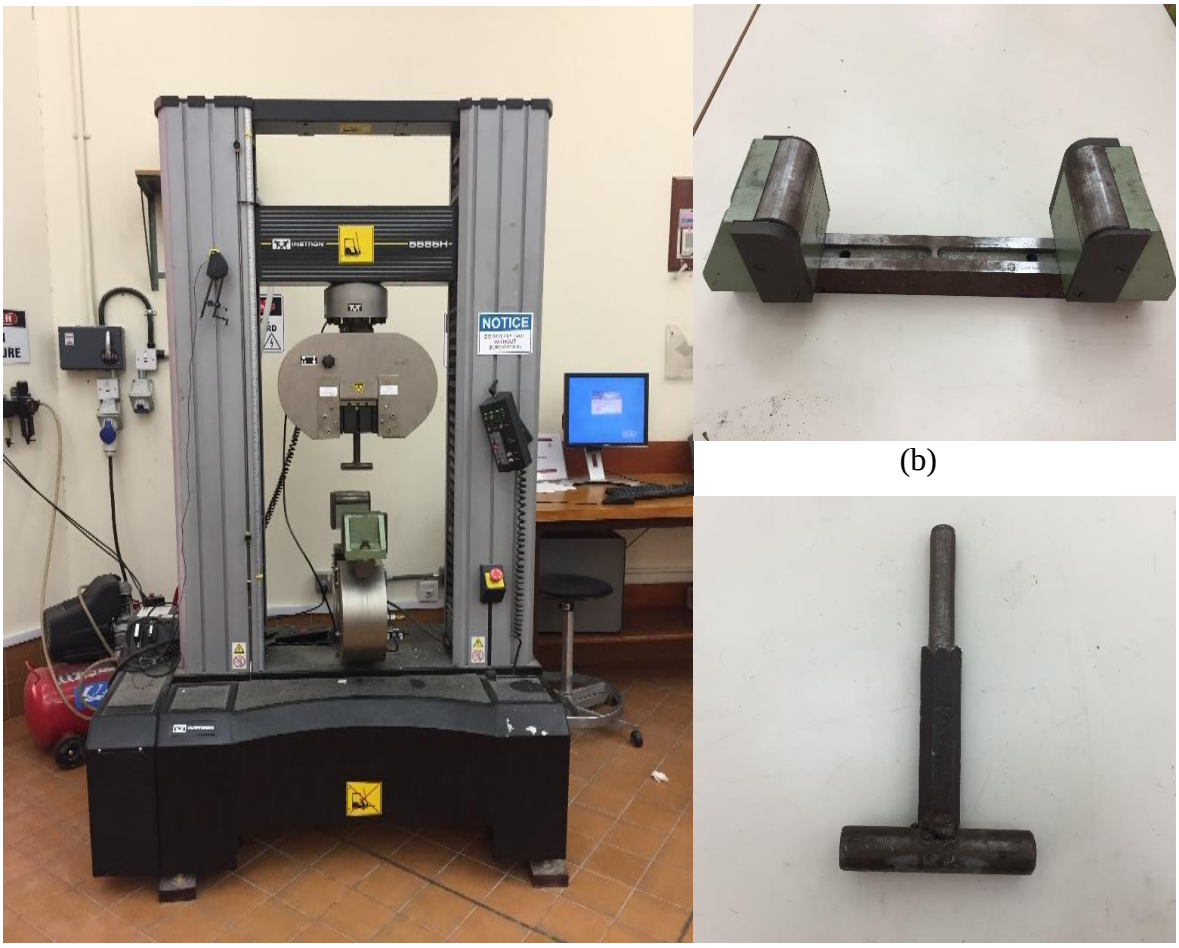

(a) (b) (c)

Figure 3.8: (a): Instron machine with 250 Ton capacity, (b): Two points support, (c): T-tool.

3.6 Internal pressure test procedure

The internal pressure test has been carried out using Resato high-pressure machine model SPU-CC-2000 (Figure 3.9). The machine applies pressure using corrode oil fluid pressurized by a high-pressure air pump, with a maximum capacity of 2000 bar. The test is a cyclic pressure test. It starts with filling the pipe, then, perform low pressure to ensure there is no leak before cyclically conducting the pressure test until failure occurs.

Figure 3.9: Resato high-pressure testing machine.

After fabrication, the pipes delegated for internal pressure test has been threaded from each side to fit in prepared fixtures for this purpose (Figure 3.10 - a). These two fixtures have been fabricated to allow the inlet and outlet hoses of the machine to be fixed to the pipes (Figure 3.11).

For radial internal pressure test, a new fixation has been used as a case to hold both sides of the pipe (Figure 3.12). This fixation has been designed as two plates connected to each other using four long threaded rods with nuts for tiding. These two plates have a cup groove where the original two fixtures of the pipe can be placed.

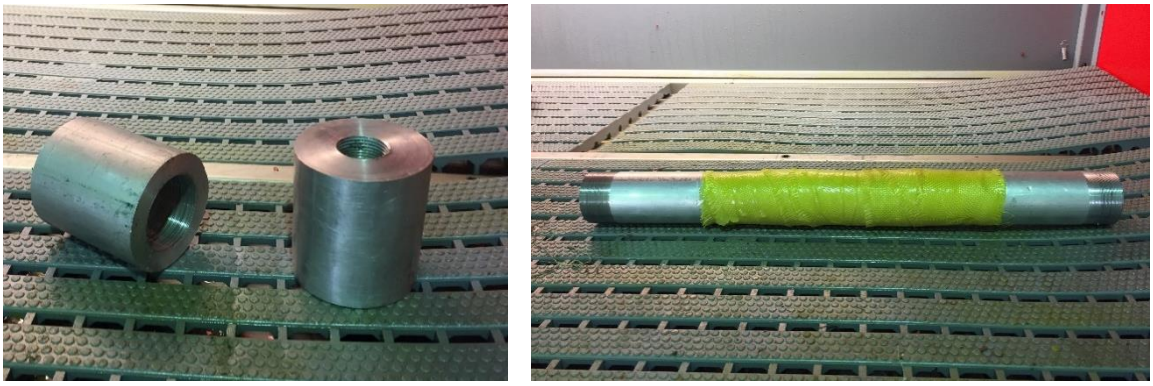

(a) (b)

Figure 3.10: (a): Fixtures, (b): Pipe with threads.

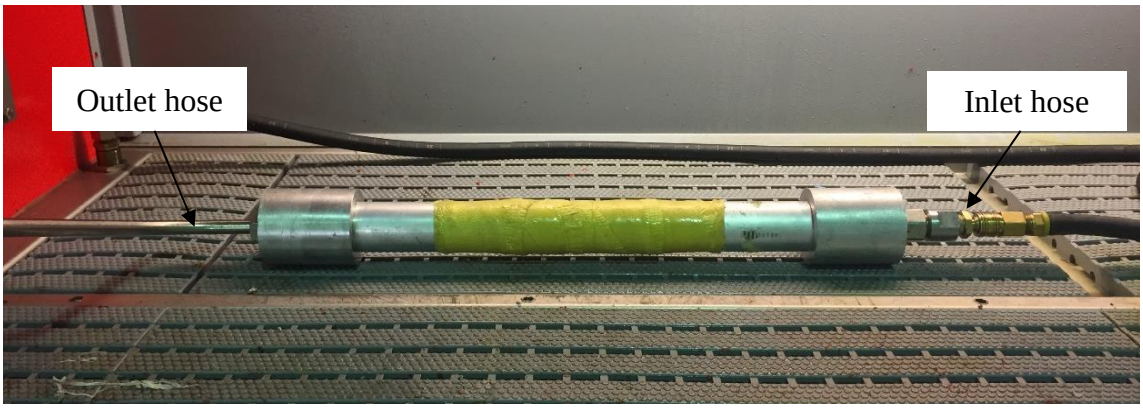

Figure 3.11: Pipe after fixation with inlet and outlet hoses for combined axial and radial internal pressure test.

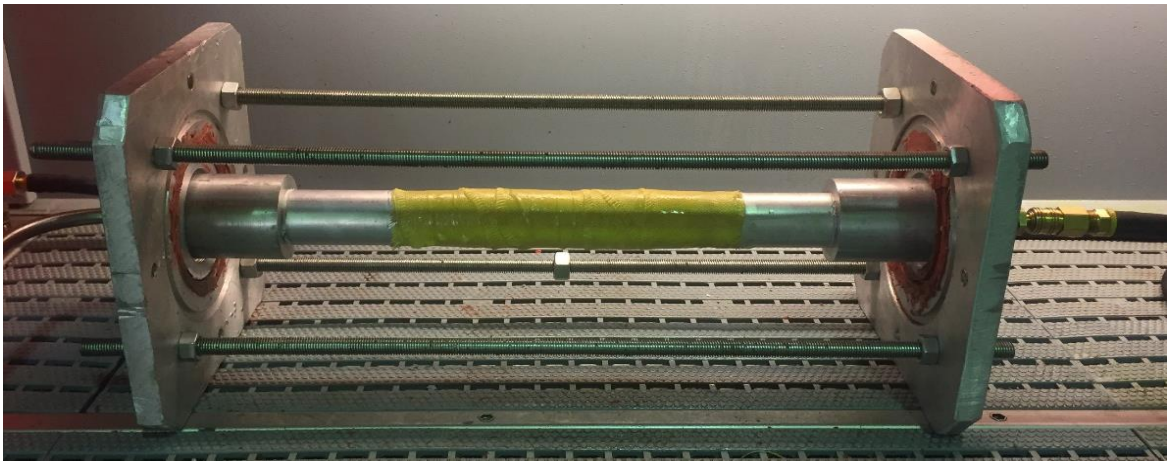

Figure 3.12: Fixation for radial internal pressure test.

3.7 Corrosion investigation procedure

Corrosion investigation has been carried on the three types of FRP composites joining (CFRP, KFRP, and GFRP) as well as for the welded pipe and non – joined pipe. The pipes specimens have been sealed from one side using chemical resistant sealing to prevent the solution from entering the pipe (Figure 3.14). The investigation has been done using 1.5 M of HCl solution as corrosive media. The specimens have been immersed in the beakers containing the solution and monitored for corrosion formation for few days. To corrosion acceleration, a heater contains water at a temperature of 50^{o} degree has been used as a surrounding media to the solution, where the beakers with HCl are immersed. (Figure 3.13).

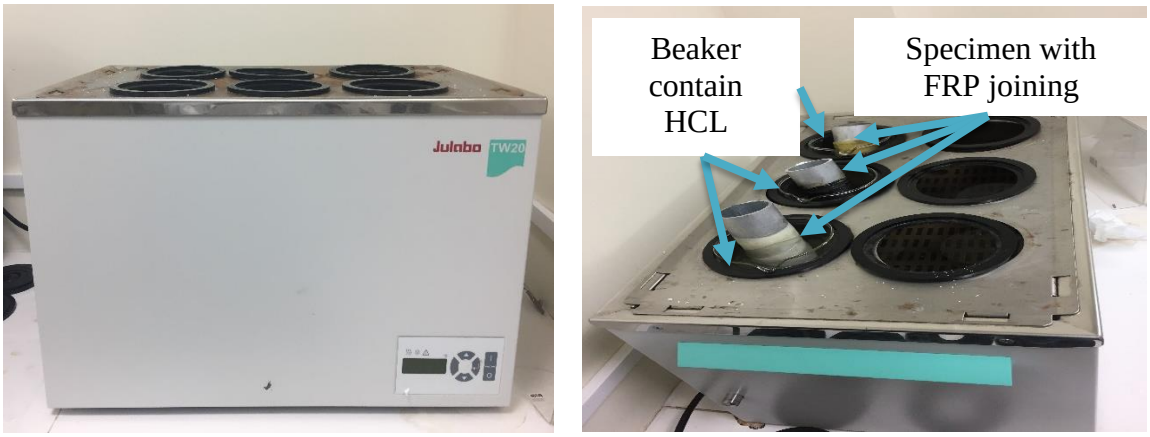

(a) (b)

Figure 3.13: (a): Water heater, (b): Beakers contain solution and specimens immersed in the heater.

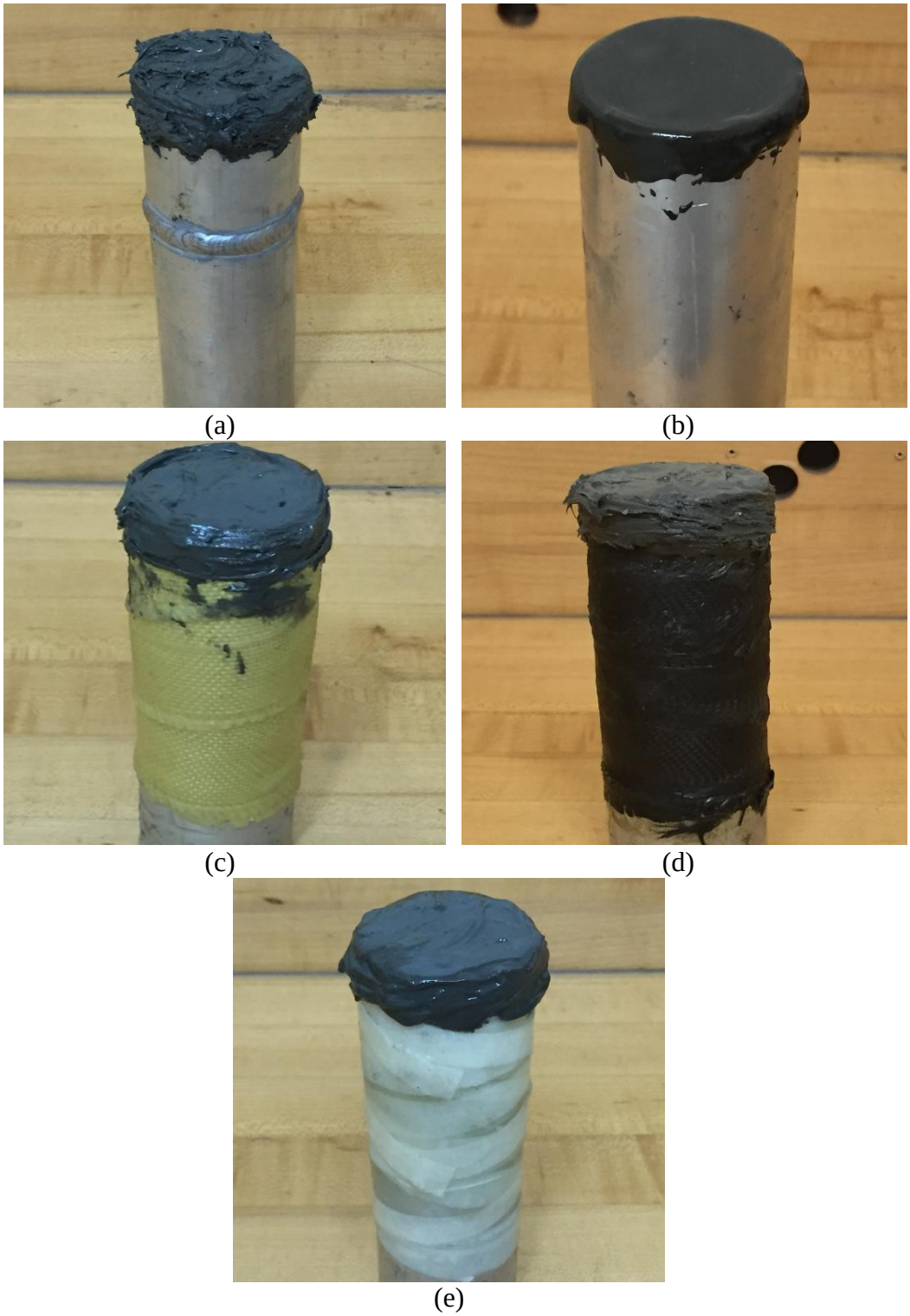

Figure 3.14: Specimens before corrosion experiment, (a): Welded aluminum pipe, (b): Non-welded aluminum pipe, (c): KFRP, (d): CFRP and (e): GFRP.

CHAPTER 4

RESULTS & DISCUSSION

In this chapter, full optimization process has been carried out to evaluate different types of joining following the methodology procedures (Chapter. 3). Three-point bending test, internal pressure test, and corrosion test have been used throughout this study. The results for joined metallic pipes (aluminum) under bending are presented and discussed in details. The joined pipes included FRP joining and welding joining. The V-welding and normal faced butt-welding methods have been considered under the classical joining types. For FRP joining, three types of fiber have been used to join pipes, including KFRP, CFRP, and GFRP. In addition, hybrid composite joining system has been established and discussed in details. The optimized types of joining have been studied for internal pressure capacity, and the results are discussed. Finally, corrosion investigation outcomes for different joining types are presented and discussed.

4.1 Bending behavior of joined metallic pipes

Bending behavior of different types of FRP joining systems and welding joining systems are evaluated, presented and discussed in detail in this section. To this end, bending behavior of non – joined aluminum pipes have been examined under three-point bending test. The results of this test are used as a control for evaluating the performance of the FRP composite and welding joining systems.

4.1.1 Non-joined aluminum pipe

This test is designed to be a baseline for the study. Therefore, the aluminum pipe has been tested under three-point bending. Figure 4.1 shows the bending behavior of the aluminum pipe. As seen for the tested non-joined aluminum pipe, it can be classified into four stages. In the first stage, elastic deflection was found to be 1.1 mm. As the pipe - deflected beyond this point, the pipe's response entered the second stage, where, the flexural load no longer proportional to deflection and plastic deformation was observed to occur (Figure 4.1). The change in pipe behavior from elastic to plastic has been noticed to be a gradual process, which results in the onset of plastic deformation. The attained plastic deformation is explained as it is corresponding to the breaking of atomic bonding between elastically deformed atom neighbors and then rearranging bonds with new neighbors as large numbers of atoms or molecules move relative to one another. Because Aluminum is crystalline solids, the plastic deformation is achieved by means of a slipping process, which involves motion (i.e., dislocations) of many atoms. At this stage, and since the pipe experiences gradual elastic–plastic change, the yielding point has been determined as the point, after which the curve departures from linearity of the flexural load-deflection curve. After attaining plastic deformation, the yielding stage has been found to continue without a significant increase in the pipe load carrying capacity. The deflection measured to be about 14.7 mm. Then after, the bending behavior of the tested pipe entered the third stage, where, the load necessary to continue plastic deformation in pipe increases and the pipe demonstrated its ultimate load carrying capacity to 10.37 kN. After that, the failure stage occurred (i.e., the fourth stage), and the load decreased.

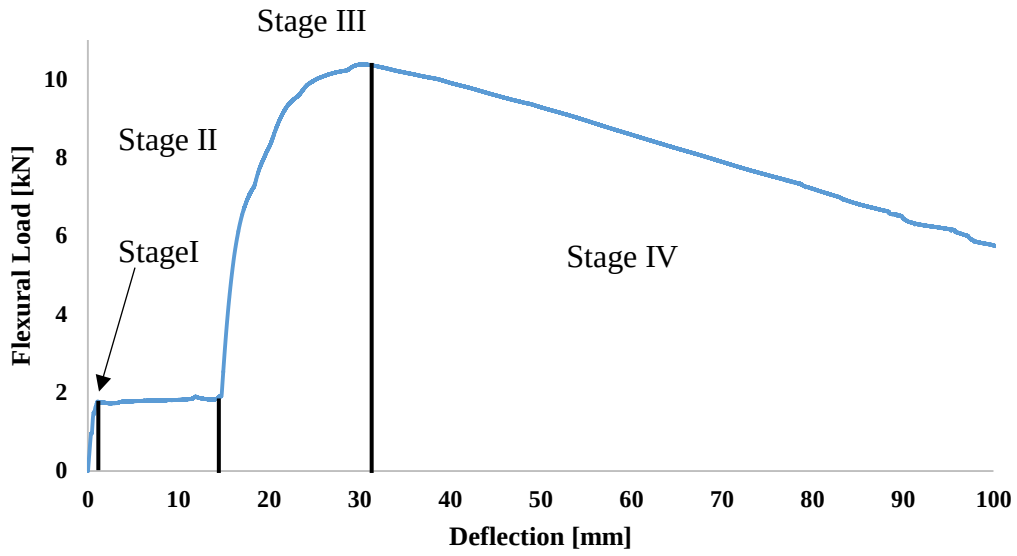

Figure 4.1: Flexural load vs. deflection curves for the non-joined aluminum pipe.

4.1.2 Welded aluminum pipes

Two different types of welding have been considered in this section as described earlier in methodology (Chapter 3). These types are V-welding & normal faced butt-welding.

- **V-welded aluminum pipe**

Figure 4.2 shows the bending behavior of V-welded aluminum pipes. Similar to the bending behavior of aluminum pipes, the flexural load-deflection curves observed to be classified into four stages. In the first stage, elastic deflection was found to be 0.5 mm, and linearity controls the relationship between the flexural load and deflection. Following this stage, the second stage, in which the pipe starts to yield at the heat-affected zone. As

the pipe deflected beyond this point, the flexural load no longer proportional to deflection and plastic deformation was observed to occur. At this stage, and since the pipe experiences gradual elastic–plastic change, the yielding point has been determined as the point, after which the curve departures from linearity of the flexural load-deflection curve. After attaining plastic deformation, the yielding stage has been found to continue without a significant increase in the pipe load carrying capacity. The deflection measured to be about 13 mm. Then after, the bending behavior of the tested pipe entered the third stage, where, the load necessary to continue plastic deformation in pipe increases and the pipe demonstrated its ultimate load carrying capacity to 6.6 kN, while the deflection reached 33.5 mm. After that, the failure stage occurred (i.e., the fourth stage), and the load decreased.

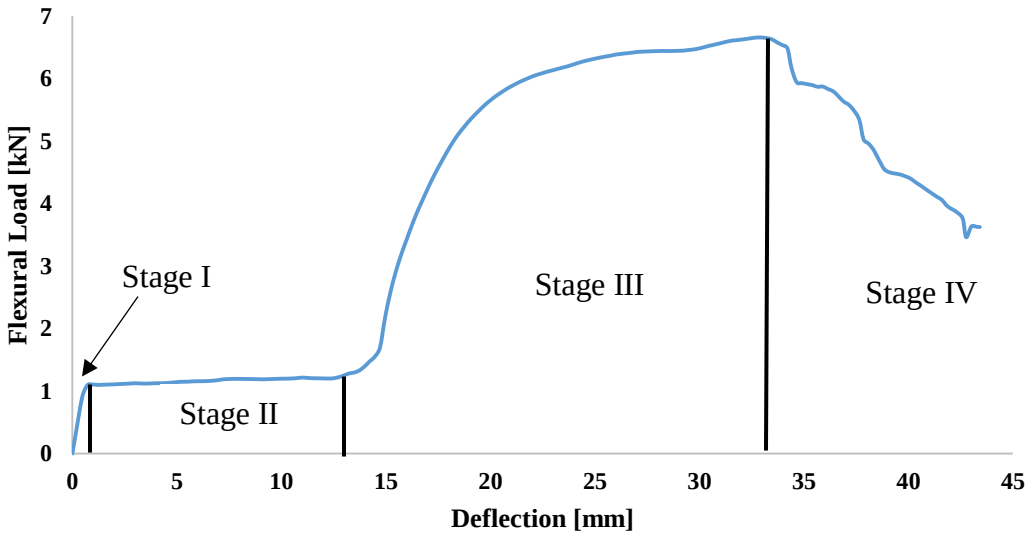

Figure 4.2: Flexural load vs. deflection curve for the V-welded aluminum pipe.

- **Normal faced butt-welded aluminum pipe**

Figure 4.3 shows the bending behavior of normal faced butt-welded aluminum pipe. Dissimilar to V-welding, this behavior can be classified into five stages. In the first stage, elastic deflection was found to be 0.75 mm and linearity control the relation between the flexural load and deflection. As the pipe deflected beyond this point, the second stage starts, where the flexural load no longer proportional to deflection and plastic deformation was observed to occur. At this stage, and since the pipe experiences gradual elastic–plastic change, the yielding point has been determined as the point, after which the curve departures from linearity of the flexural load-deflection curve. After attaining plastic deformation, the yielding stage has been found to continue without a significant increase in the pipe load carrying capacity. The deflection measured to be about 13 mm. Then after, in the third stage, the load necessary to continue plastic deformation in pipe increases and the pipe demonstrated its ultimate load carrying capacity to 6.1 kN while the deflection reached 22.2 mm. After that, the fourth stage occurred where failure started, and the load decreased until the deflection reached 25 mm, and the deflection continued without a significant increase in the load until 28 mm. Finally, the fifth stage started where the complete failure occurred.

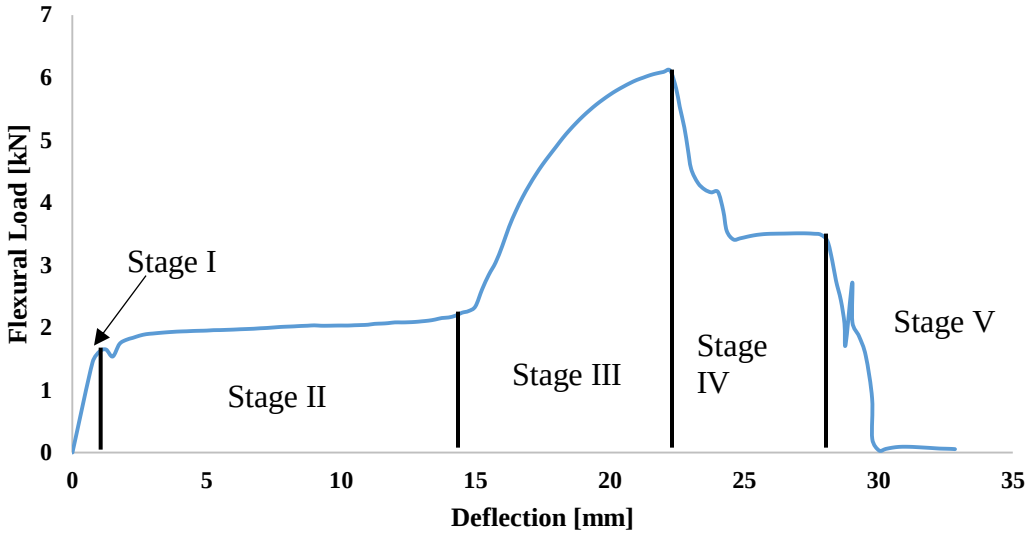

Figure 4.3: Flexural load vs. deflection curve for the normal faced butt-welded aluminum pipe.

- **Welded pipes versus non-joined pipe**

Figure 4.4 shows both types of welding bending behavior versus non-joined aluminum pipe. Normal faced butt-welding showed elastic deflection at 0.75 mm, higher than V-welding that was 0.5 mm. Both welding types showed lower elastic deflection than the aluminum pipe elastic deflection, which was 1.2 mm. The aluminum pipe showed yielding (initial failure) of 1.7 kN, higher than normal faced butt-welding, which was 1.4 kN and V-welding, which was 1.1 kN. The deflection in yielding stage of both types of welding was 13 mm, which found to be lower than the aluminum pipe, which was 14.7 mm. The ultimate flexural load found to be 6.1 kN for normal face welding, which is lower than V-welding, which was 6.6 kN. The deflection at the failure of both types of

welding was different. The V-welding value showed 33.5 mm deflection, which is much higher than normal faced butt-welding 22.2 mm. Both types of welding resulted in significant reduction of ultimate flexural load compared to the non-joined aluminum pipe. It has been observed that V-welded pipe showed higher deflection at failure than non – joined pipe.

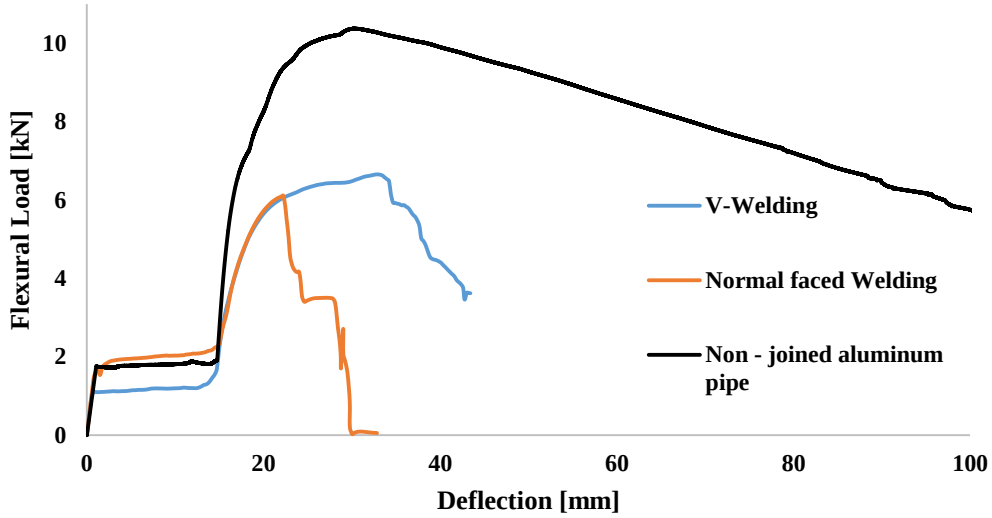

(a)

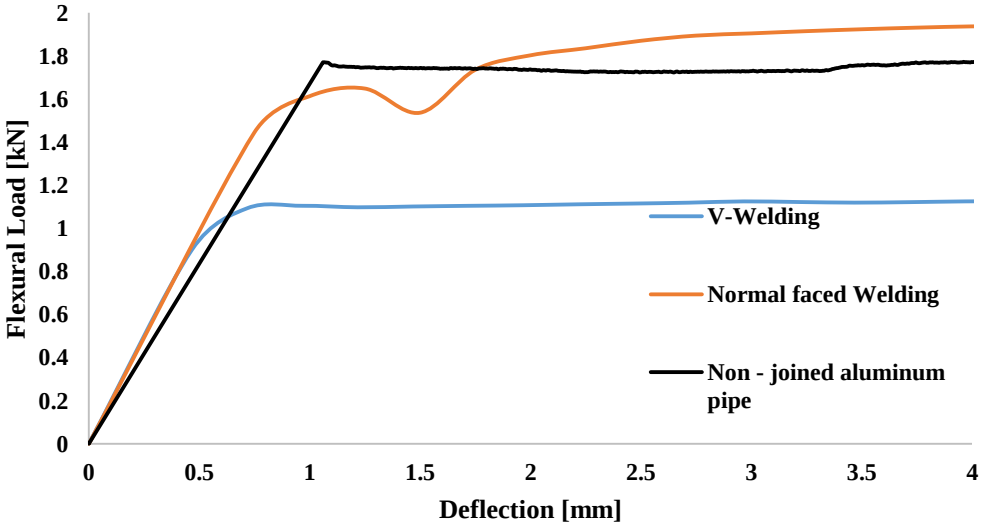

(b)

Figure 4.4: Flexural load vs. deflection curves for V-welded pipes & normal faced butt-welded pipes, (a): full curve, (b): zoomed curve for initial failure.

Table 4.1: Observations summary for bending behavior of welded aluminum pipes and non welded aluminum pipe

Type of joining	Yielding		Ultimate failure	
	Load [kN]	Deflection [mm]	Load [kN]	Deflection [mm]
V-welding	1.1	0.5	6.6	33.5
Normal faced welding	1.4	0.75	6.1	22.2
Non-joined Al pipe	1.7	1.1	10.37	30.25

For failure investigation in the non-joined aluminum pipe, it has been observed that there is no fracture at the macro level. The pipe deformed until blockage due to bending (Figure 4.6 – a & b). On other hands, the SEM results showed that there is a micro crack in lower side (tension) and sides (Figure 4.7 – b, c & d), while the upper side experienced micro crushing due to applied bending load by Mandrel T-shape tool (Figure 4.7 – a). In addition, for V-welded pipes, the fracture occurred at the bottom side, which is under tension. The fracture occurred at the weakest point, which known as heat affected zone (HAZ) (Figure 4.6 – b & c). HAZ is a result of residual stresses that form due to the welding process, which cause lack of properties due to these stresses and it is always at a certain distance from the welded zone. The shape of pipe cross section became oval due to applied bending load. For the normal faced welded pipes, the fracture occurred at the center of the weld, and the shape of pipe cross section did not change (Figure 4.6 – d & e). In this joining, filler does not penetrate inside the pipes to mix with pipes edges like V-welding pipes (Figure 4.5) & (Figure 4.7 – e & f). Hence, the heat does not affect the metal significantly. Although the V-welding technique known to be stronger than normal faced welding technique according to internationally recognized codes, the HAZ in V-

welding caused a considerable lack of properties and hence the results for both techniques did not differ a lot regarding ultimate flexural load. In addition, V-welded technique showed higher ductility than normal faced butt-welding which is another significant advantage.

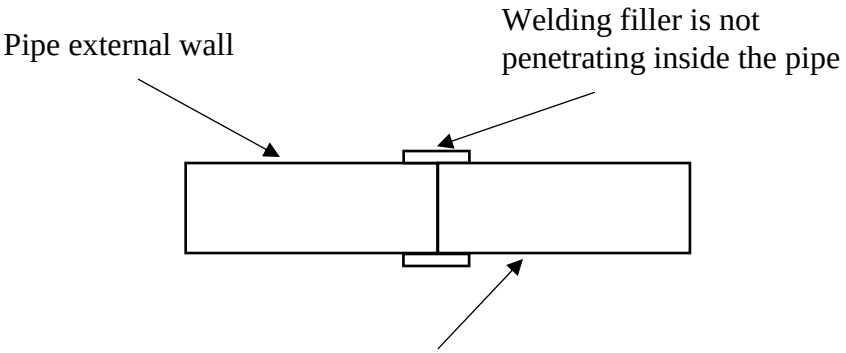

(a)

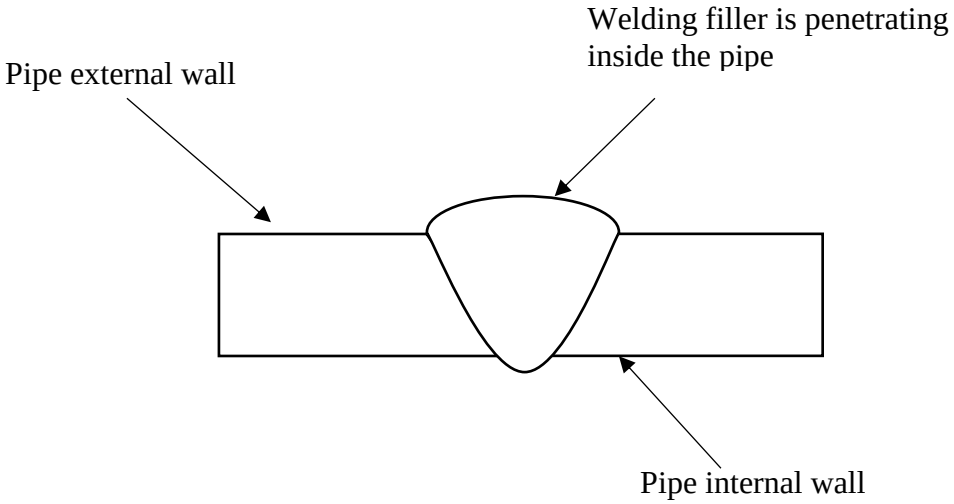

(b)

Figure 4.5: Sketch of welding filler and the pipe wall.

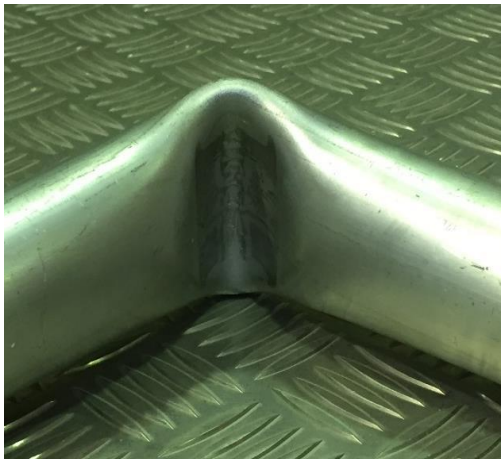

(a): Non-joined pipe in lower side

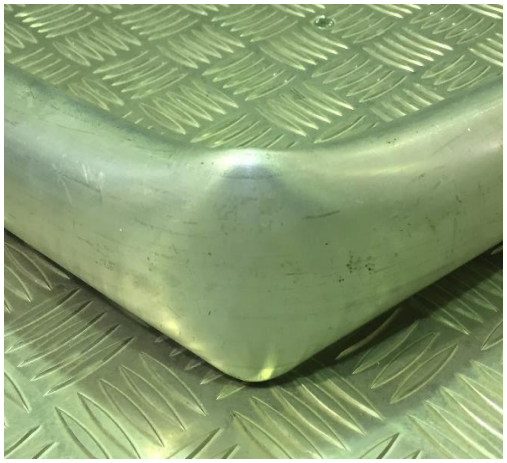

(b): Non-joined pipe in upper side

(b): V-welded pipe fracture in lower side

(c): V-welded pipe crushed in upper side

(d): Normal faced welded pipe fracture in lower side

(e): Normal faced welded pipe fracture in upper side

Figure 4.6: Welded and non-joined pipes after bending test.

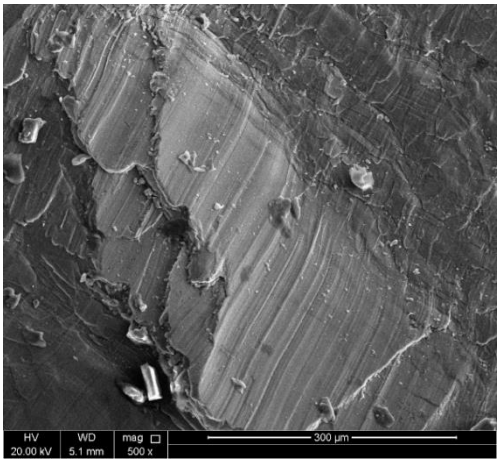

(a): Non – joined pipe Crushing on the upper side (compression).

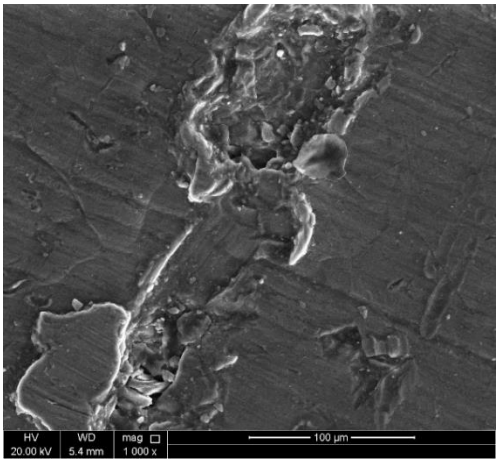

(b): Non – joined pipe micro crack in lower side (tension).

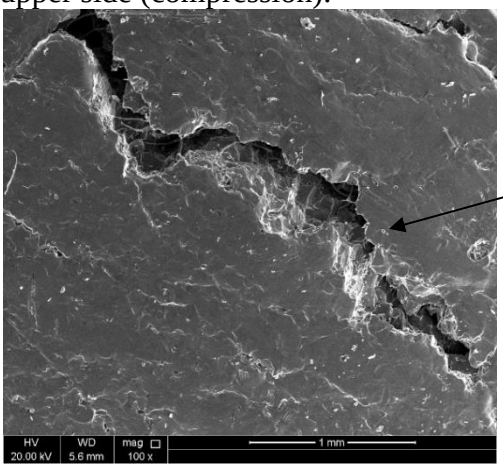

(c): Micro crack in Non – joined pipe.

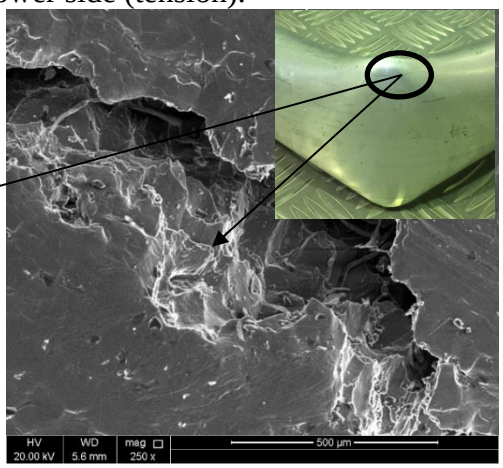

(d): Micro crack in Non – joined pipe.

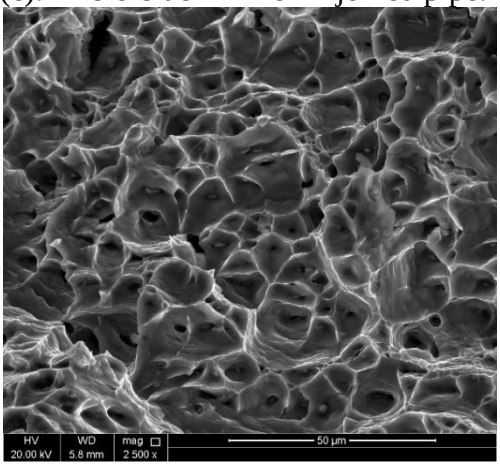

(e): V – welded pipe fracture at HAZ.

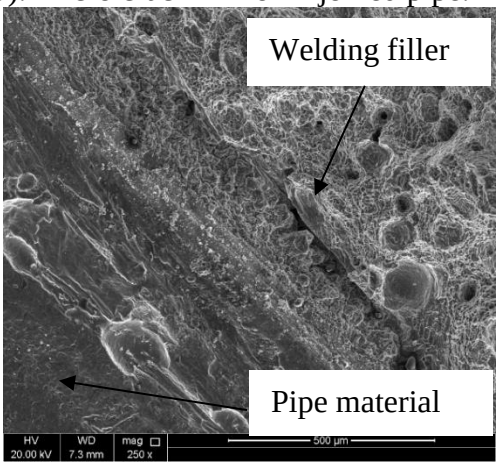

(f): Normal faced butt-welding fracture

Figure 4.7: SEM pictures of different sides of pipe subjected to bending test.

4.1.3 CFRP joining aluminum pipes

The bending behavior for CFRP joining system has been investigated for specimens with two different fiber orientations. The fiber orientations were chosen based on manufacturability and namely ±45º and 0º/90º angles. As stated before, specimens with best bending behavior have been candidates for more evaluation criteria related to the pressure carrying capacity.

- **CFRP with fiber orientation of ±45º**

The bending behavior of CFRP joining aluminum pipes with a fiber orientation of ±45º and four layers are shown in Figure 4.8. The response of joined aluminum pipes using CFRP with a fiber orientation of ±45º can be classified into four stages. In the first stage, elastic deflection was found to be 0.73 mm. As the pipe deflected beyond this point, the flexural load no longer proportional to deflection and plastic deformation was observed to occur. The change in pipe behavior from elastic to plastic has been noticed to be a gradual process, which results in the onset of plastic deformation. After attaining plastic deformation, the yielding stage has been found to continue without a significant increase in the pipe load carrying capacity. The deflection measured to be about 14 mm. Then after, in next stage, the load necessary to continue plastic deformation in pipe increases and the pipe demonstrated its ultimate load carrying capacity to 9.2 kN while the deflection was 24.5 mm. After that, the failure stage occurred, and the load decreased.

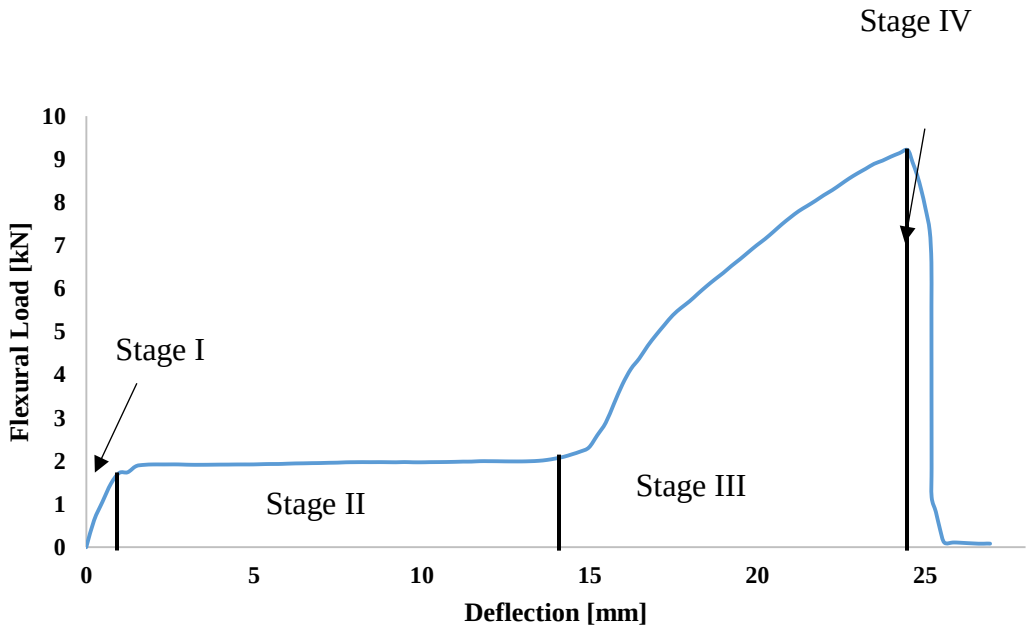

Figure 4.8: Flexural load vs. deflection curve for CFRP joining aluminum pipe with a fiber orientation of ±45º and 4-layers.

- **CFRP with fiber orientation of 0º/90º**

The bending behavior of CFRP joining aluminum pipes with a fiber orientation of 0º/90º and four layers are shown in Figure 4.9. The response of joined aluminum pipe using CFRP with a fiber orientation of 0º/90º can be classified into four stages. In the first stage, elastic deflection was found to be 0.5 mm. As the pipe deflected beyond this point, the flexural load no longer proportional to deflection and plastic deformation was observed to occur. The change in pipe behavior from elastic to plastic has been noticed to be a gradual process, which results in the onset of plastic deformation. After attaining plastic deformation, the yielding stage has been found to continue without a significant increase in the pipe load carrying capacity. The deflection measured to be about 13.5

mm. Then after, in next stage, the load necessary to continue plastic deformation in pipe increases and the pipe demonstrated its ultimate load carrying capacity to 10.7 kN while the deflection was 24.2 mm. After that, the failure stage occurred, and the load decreased.

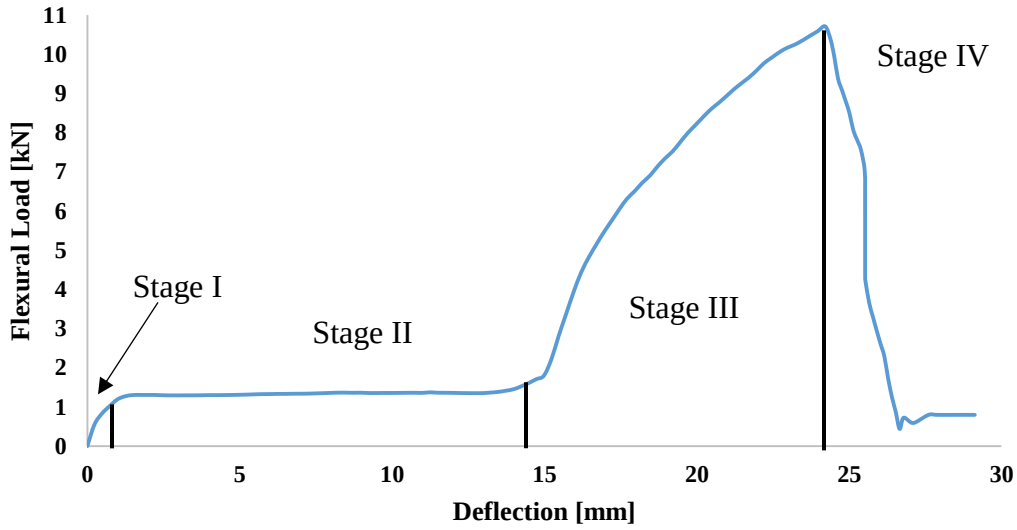

Figure 4.9: Flexural load vs. deflection curves for CFRP joining aluminum pipe with a fiber orientation of 0º/90º and 4-layers.

- **Effect of orientation on the bending behavior of CFRP joining aluminum pipes**

The orientations: ±45º and 0º/90º have been used to optimize the orientations for joining aluminum pipes. Figure 4.10 shows the difference between different orientations. In the first stage, the CFRP joining aluminum pipes with ±45º showed that the yielding (initial

failure) is 1.47 kN, which is higher than the 0º/90º orientation, which was 0.8 kN. The elastic deflection of ±45º was 0.73 mm, and it was 0.5 mm for 0º/90º. The deflection in yielding stage reached 14 mm for ±45º and 13.5 mm for 0º/90º. The ultimate flexural strength found to be 9.2 kN for ±45º, which is lower than 0º/90º, which was 10.7 kN. The deflection at the failure of both orientations showed similar behavior. It was 24.5 mm for ±45º and 24.2 mm for 0º/90º. These results showed that ±45º orientation is stiffer than 0º/90º orientation, while the significant effect of orientation appears at the maximum flexural load. The 0º/90º orientation showed the highest flexural load under bending load.

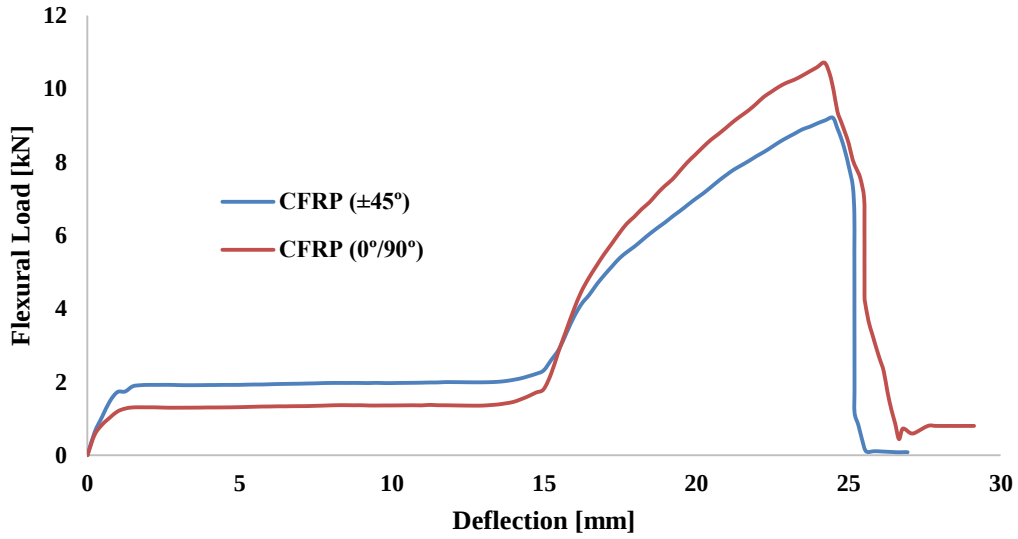

(a)

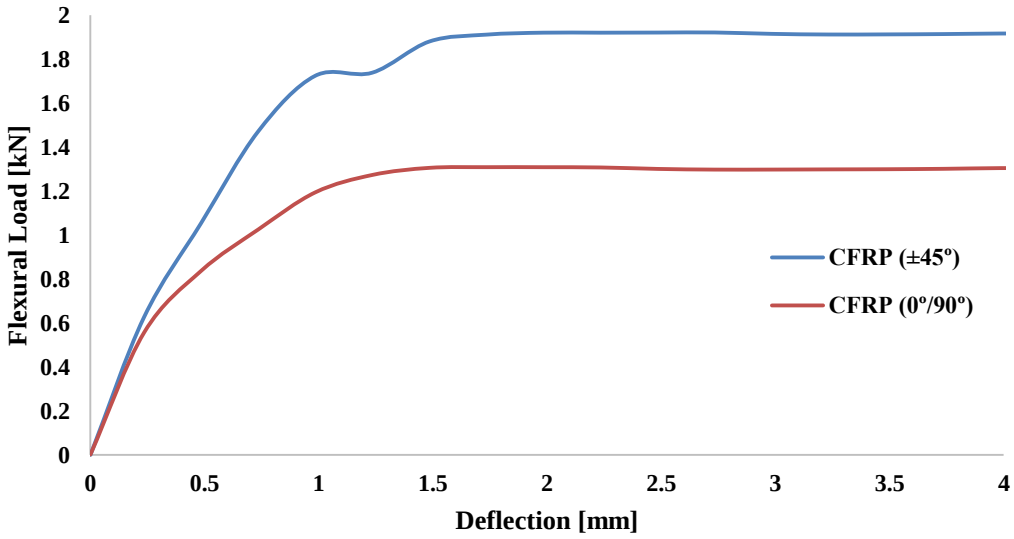

(b)

Figure 4.10: Flexural load vs. deflection curves for CFRP joining aluminum pipes with a fiber orientation of ±45º & 0º/90º with 4-layers, (a): full curve, (b): zoomed curve for initial failure.

Table 4.2: Observations summary for bending behavior of joined aluminum pipes with CFRP composites of ±45º & 0º/90º orientation

Type of joining	**Yielding**		**Ultimate failure**	
	Load [kN]	**Deflection [mm]**	**Load [kN]**	**Deflection [mm]**
CFRP ±45º	1.47	0.73	9.2	24.5
CFRP 0º/90º	0.80	0.50	10.7	24.2

The failure of both fiber orientations occurred very sharply, and a complete fracture occurred as shown in Figure 4.11. This type of failure is clearly, because of the fact that carbon fiber is a brittle material. The crack was not a straight crack as it was in welding. This is because cracks in carbon fiber follow the fiber paths of fast propagation crack line, which lead to this shape of failure. The pipe cross section at failure edge has been changed to an oval shape (Figure 4.11 – b & d).

(a): ±45º CFRP joining failure in tension side

(b): ±45º CFRP joining failure in compression side

(c): 0º/90º CFRP joining failure in tension side

(d): 0º/90º CFRP joining failure in compression side

Figure 4.11: Failure of CFRP joining aluminum pipes with a fiber orientation of ±45º & 0º/90º.

SEM pictures showed debonding failure mechanism in both ±45º & 0º/90º as shown in Figure 4.12-a & Figure 4.13-d, where some fibers are separated from the matrix. A pulling indication also is observed in both orientations as shown in Figure 4.12-c & Figure 4.13-c. No delamination has been observed in both orientations for CFRP joining.

The fracture surface of the fibers shows flat fracture representing the fast and sharp crack propagation of the brittle material.

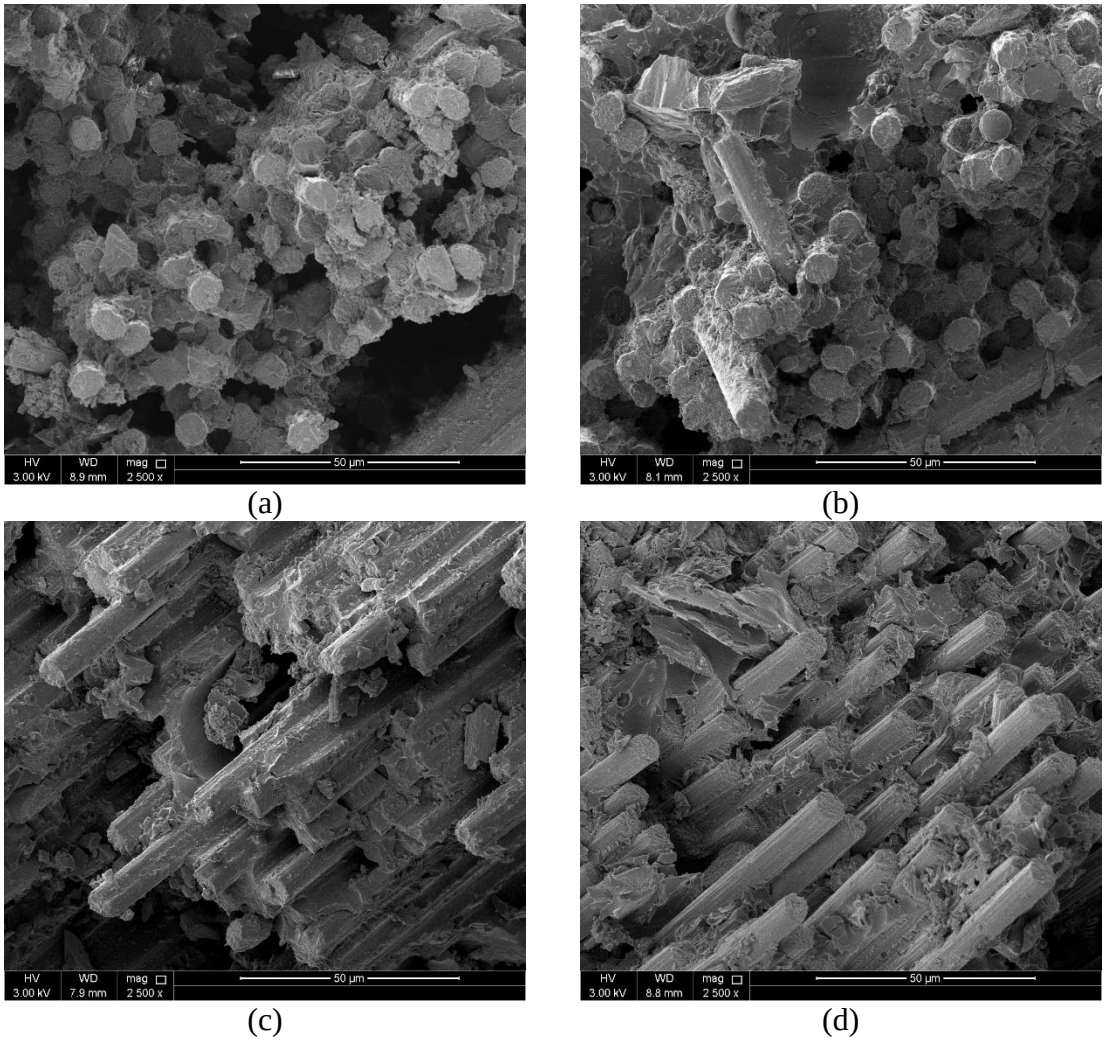

Figure 4.12: SEM pictures of CFRP fracture surface of ±45º orientation.

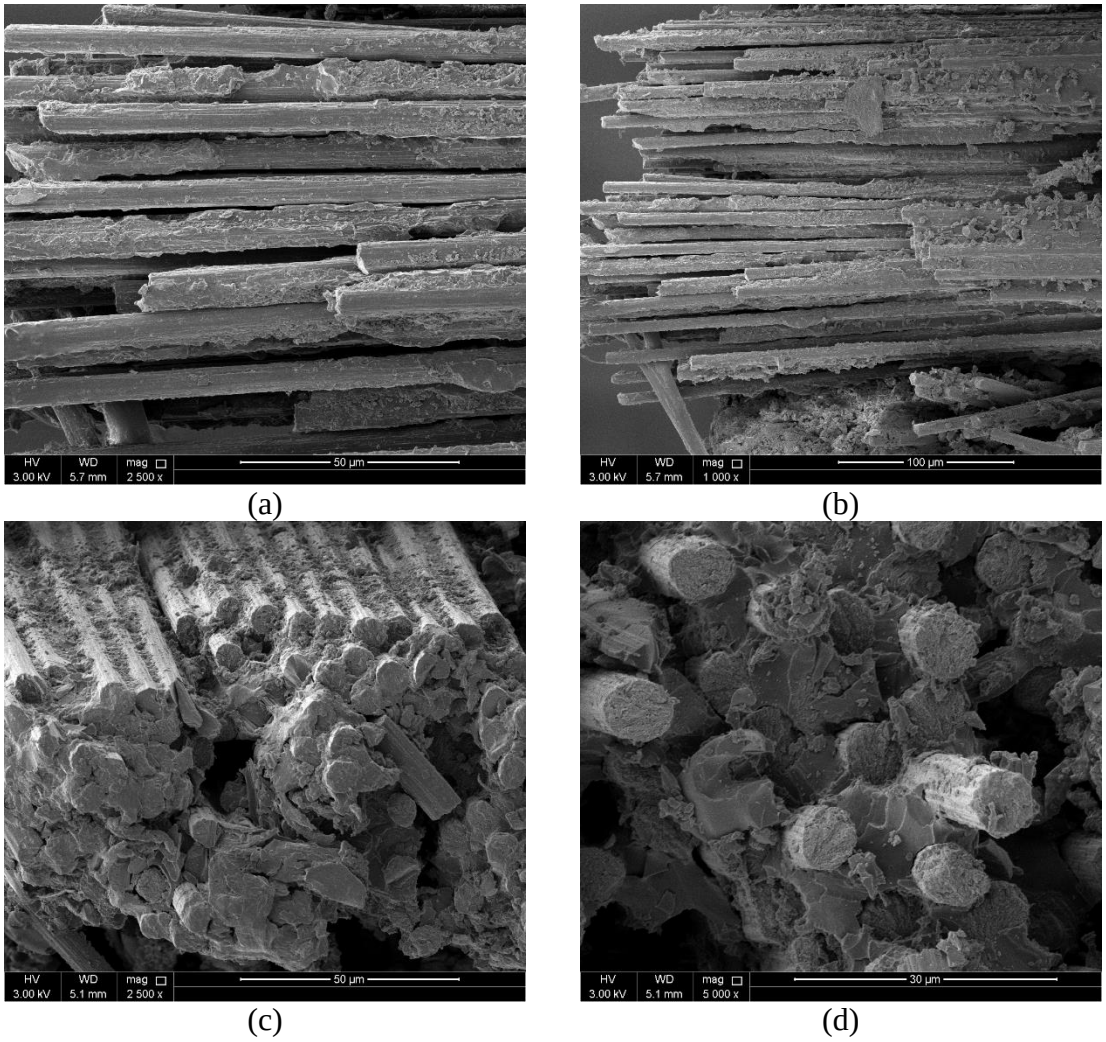

Figure 4.13: SEM pictures of carbon fiber fracture surface of CFRP of 0º/90º orientation.

Fiber Orientation angle optimization:

As expected, CFRP of 0º/90º orientation represented the higher flexural load values than CFRP of ±45º orientation. This because in 0º/90º orientation the maximum tension loads can be obtained as the uniaxial load in both tension directions in the pipe under bending. While, in ±45º orientation, the shear forces occur in both directions of tension, which

considered as a weakness in CFRP. In fact, this problem occurs in all other angles rather than 0º/90º, where it obtains the maximum load in both directions. Due to these results, only 0º/90º was considered for the rest of tests for other types of composites.

4.1.4 GFRP joining aluminum pipes

The response of joined aluminum pipes using GFRP with a fiber orientation of 0º/90º is shown in Figure 4.14. In the first stage, elastic deflection was found to be 1 mm. As the pipe deflected beyond this point, the flexural load no longer proportional to deflection and plastic deformation was observed to occur. The change in pipe behavior from elastic to plastic has been noticed to be a gradual process, which results in the onset of plastic deformation. After attaining plastic deformation, the yielding stage has been found to continue without a significant increase in the pipe load carrying capacity. The deflection measured to be about 14 mm. Then after, in next stage, the load necessary to continue plastic deformation in pipe increases and the pipe demonstrated its ultimate load carrying capacity to 6.8 kN while the deflection was 23.2 mm. After that, the failure stage occurred, and the load decreased.

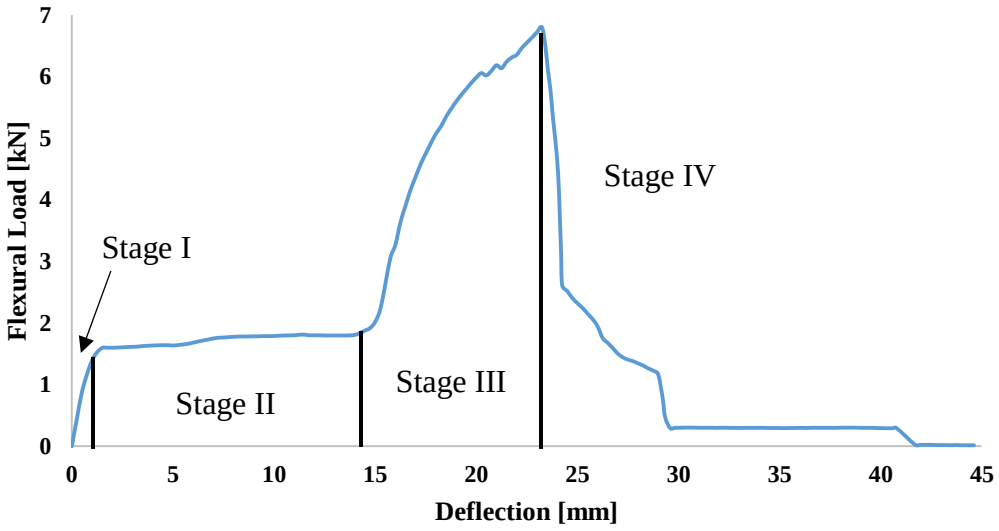

Figure 4.14: Flexural load vs. deflection curves for GFRP joining aluminum pipes with a fiber orientation of 0º/90º with 4-layers.

4.1.5 KFRP joining aluminum pipes

The response of joined aluminum pipes using KFRP with a fiber orientation of 0º/90º is shown in Figure 4.15. In the first stage, elastic deflection was found to be 1 mm. As the pipe deflected beyond this point, the flexural load no longer proportional to deflection and plastic deformation was observed to occur. The change in pipe behavior from elastic to plastic has been noticed to be a gradual process, which results in the onset of plastic deformation. After attaining plastic deformation, the yielding stage has been found to continue without a significant increase in the pipe load carrying capacity. The deflection measured to be about 14.5 mm. Then after, in next stage, the load necessary to continue plastic deformation in pipe increases and the pipe demonstrated its ultimate load carrying

capacity to 14.7 kN while the deflection was 52.4 mm. After that, the failure stage occurred, and the load decreased.

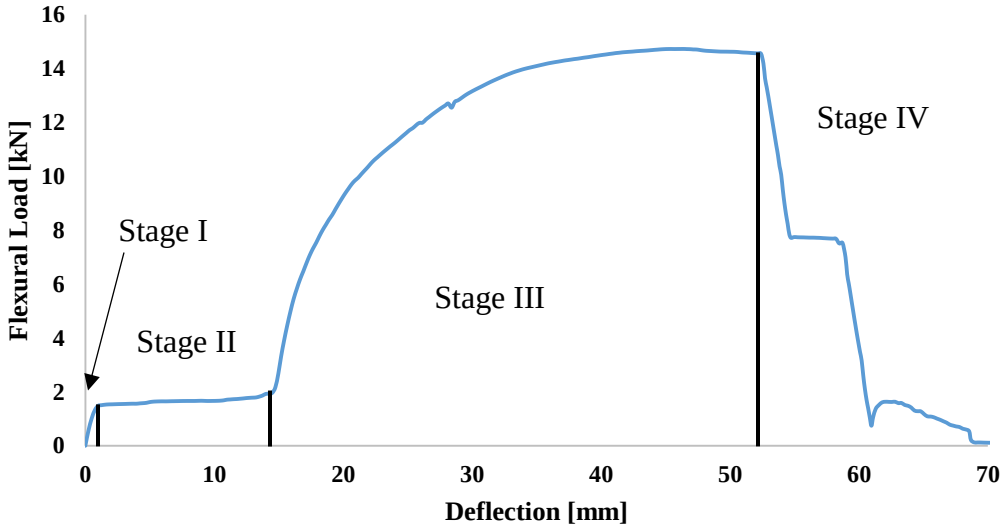

Figure 4.15: Flexural load vs. deflection curves for KFRP joining aluminum pipes with a fiber orientation of 0º/90º with 4-layers.

4.1.6 Effect of FRP type on bending behavior of joined aluminum pipes

Three types of FRP, including (KFRP, CFRP, and GFRP) have been used to join the aluminum pipes. The initial failure (yielding) is found to be similar in GFRP and KFRP, while it is much lower in CFRP as shown in Figure 4.16 & Table 4.3. In the second stage (yielding stage), the deflection also was almost similar in all types of composites. The ultimate flexural load found to be 6.8 kN for GFRP, which is lower than CFRP, which was 10.7 kN. The KFRP showed the highest value of an ultimate flexural load of 14.7

kN. The deflection at failure was 23.2 mm for GFRP and slightly higher in CFRP with 24.2 mm. Again, the KFRP showed the highest deflection at failure compared to GFRP and CFRP, which was 52.4mm.

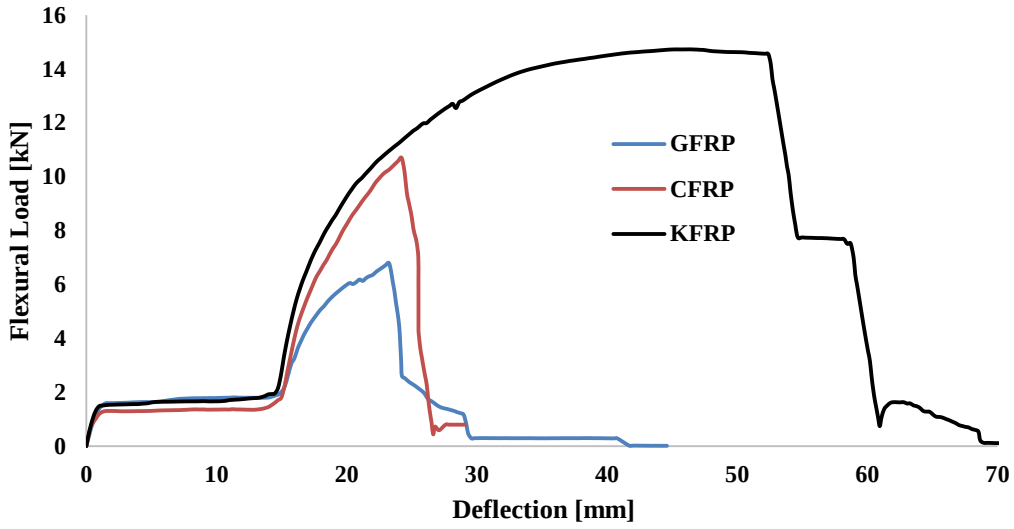

(a)

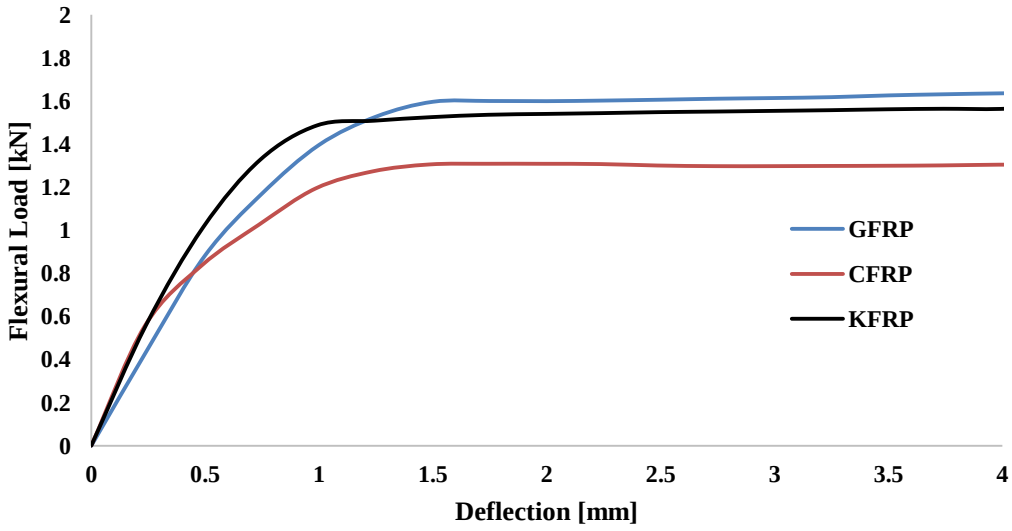

(b)

Figure 4.16: Flexural load vs. deflection curves for KFRP, CFRP, and GFRP with 4-layers, (a): full curve, (b): zoomed curve for initial failure.

Table 4.3: Observations summary for bending behavior of joined aluminum pipes with FRP composites of 0º/90º orientation

Type of joining	Yielding		Ultimate failure	
	Load [kN]	Deflection [mm]	Load [kN]	Deflection [mm]
GFRP	1.4	1	6.8	23.2
CFRP	0.8	0.5	10.7	24.2
KFRP	1.5	1	14.7	52.4

For failure investigation at the macro level, it has been noticed that GFRP, similar to CFRP where failure fracture edge was not straight because of same reasons that crack propagation follows a specific path. The failure also, showed that GFRP dissimilar to CFRP, where the curve fluctuated slightly before sharply decreasing occurred (Figure 4.16 – a & b).

For KFRP, the failure shows that fracture edges are not sharp as CFRP or GFRP. This is due to the high toughness of Kevlar. The failure occurred at the lower part of the pipe, which was under tension during bending test (Figure 4.17 – e & f).

(a): GFRP failure in tension side

(b): GFRP failure in compression side

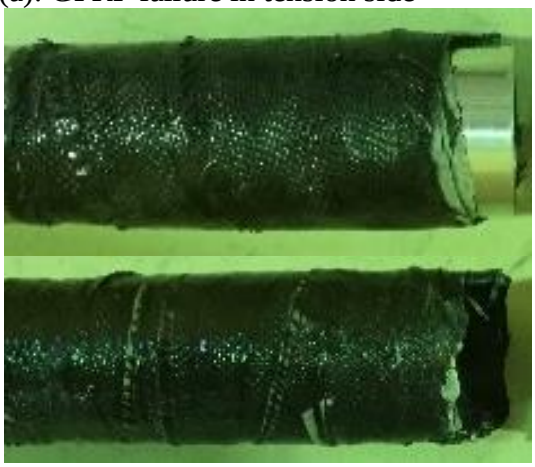

(c): CFRP failure in tension side

(d): CFRP failure in compression side

(e): KFRP failure in tension side

(f): KFRP failure in compression side

Figure 4.17: Failure of KFRP, CFRP & GFRP joined aluminum pipes of 0º/90º orientation.

SEM pictures showed debonding failure mechanism in GFRP as shown in Figure 4.19 - c, where some fibers are separated from the matrix similar to what has been observed in Figure 4.12 - a & Figure 4.13 - d for CFRP. The fracture for GFRP was not flat as it was in CFRP SEM pictures (Figure 4.19 - d). No delamination has been observed in GFRP as well as in CFRP. For KFRP it was difficult to observe the fracture surface of fibers or debonding occurrences due to the significant interaction between fibers (Figure 4.18). This can be explained as the high toughness of Kevlar, which prevents sharp and fast cracking. Instead, KFRP experienced tearing of fibers rather than fracture.

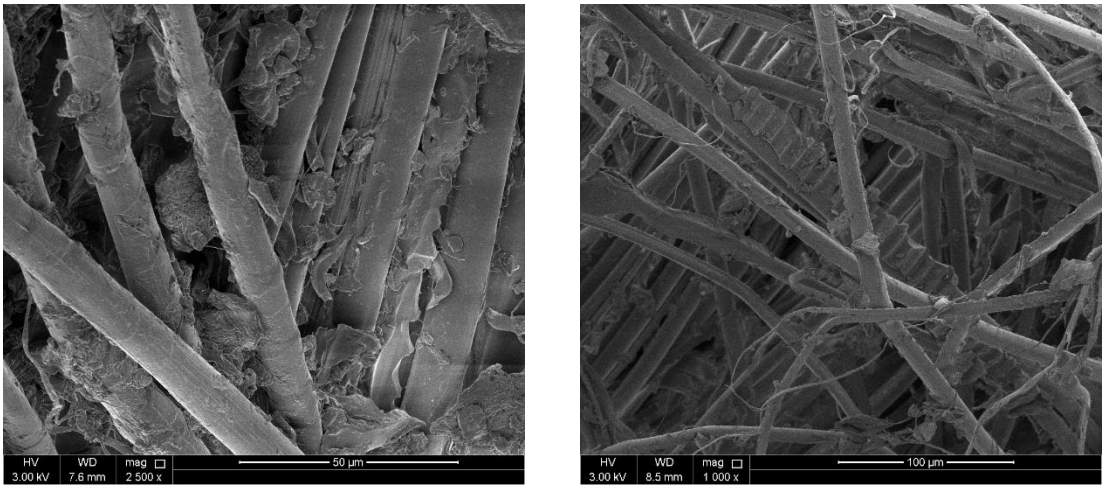

(a) (b)

Figure 4.18: SEM pictures of KFRP fracture surface of 0º/90º orientation.

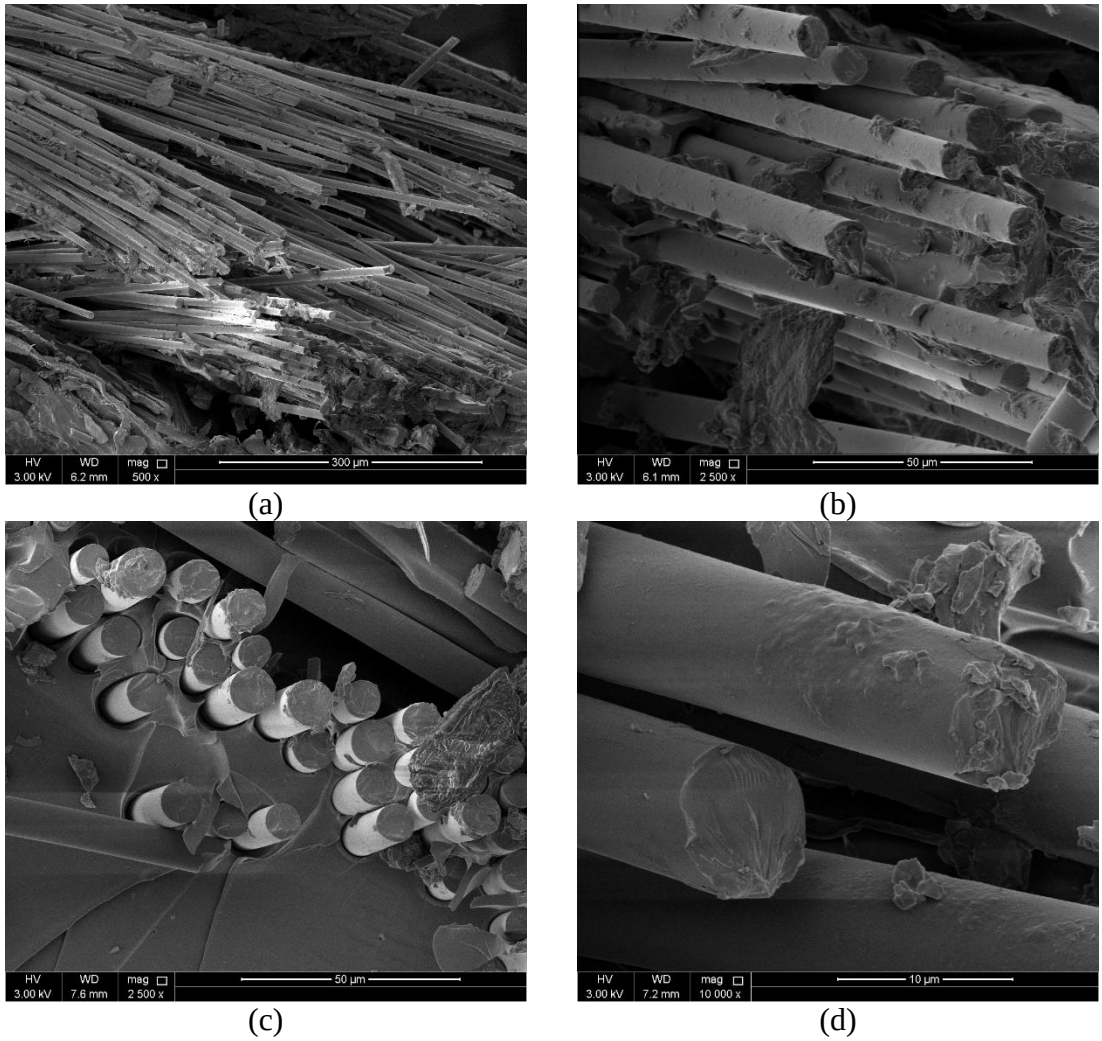

(a) (b)

(c) (d)

Figure 4.19: SEM pictures of GFRP fracture surface of 0º/90º orientation.

4.1.7 FRP joining versus welding

The results of different composites versus classical welding showed better behavior regarding flexural load, especially for KFRP and CFRP (Figure 4.20). To this extent, KFRP showed very high flexural load and high toughness compared to other types of composites and other welding techniques.

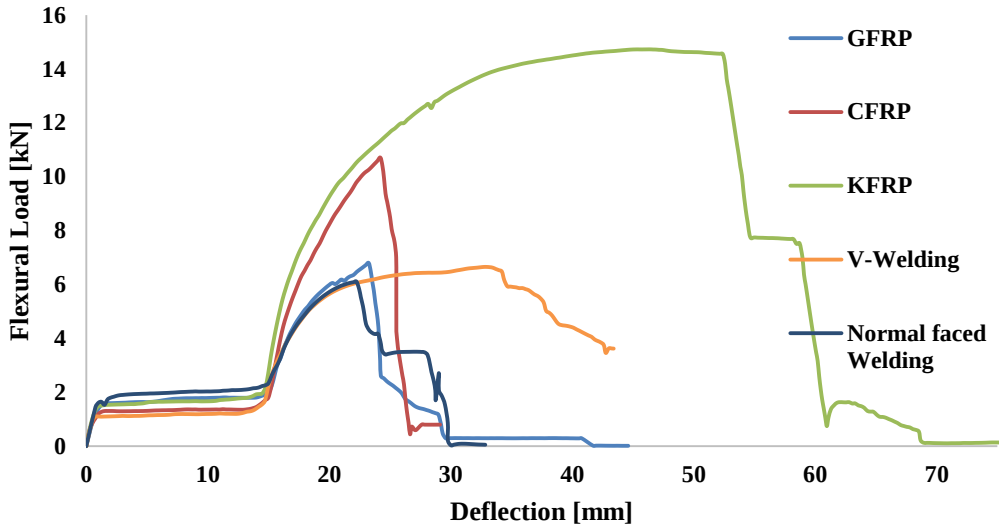

(a)

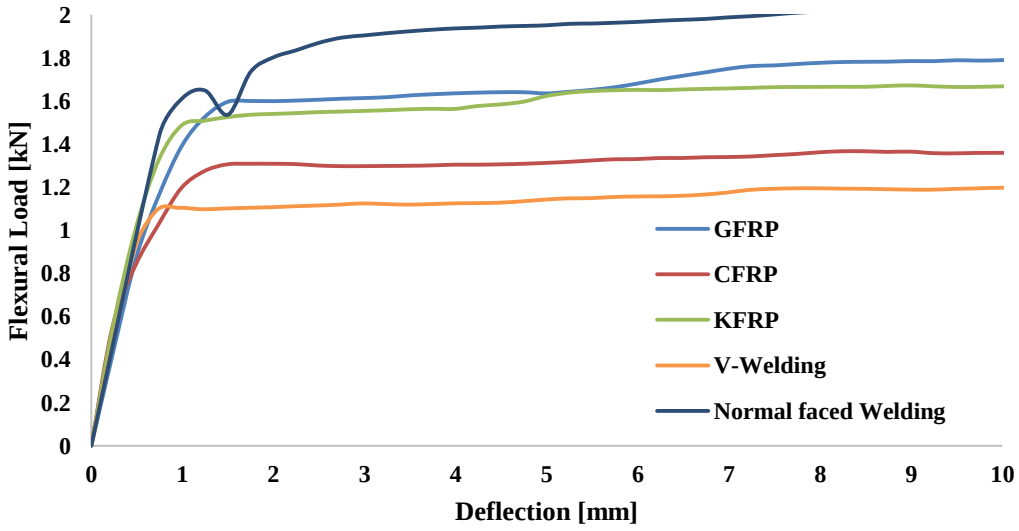

(b)

Figure 4.20: Flexural load vs. deflection curves for GFRP, CFRP, KFRP joined pipes and normal faced butt-welded & V-welded pipes, (a): full curve, (b): zoomed curve for initial failure.

Table 4.4: Observations summary for bending behavior of joined aluminum pipes with FRP composites of 0º/90º orientation compared to normal faced butt-welded & V-welded pipes

Type of joining	Yielding		Ultimate failure	
	Load [kN]	Deflection [mm]	Load [kN]	Deflection [mm]
V- welding	1.1	0.5	6.6	33.5
Normal faced welding	1.4	0.75	6.1	22.2
GFRP	1.4	1	6.8	23.2
CFRP	0.8	0.5	10.7	24.2
KFRP	1.5	1	14.7	52.4

4.1.8 The effect of hybridization on bending behavior of joined aluminum

The hybridization has been made for KFRP/CFRP & GFRP/CFRP, where both KFRP & GFRP has been chosen as starting material in contact with aluminum pipes due to their corrosion resistance comparing to CFRP, which cause galvanic corrosion due to its electrical conductivity. (Mandel & Krüger, 2015) & (Discussion with Dr.Elsadig AlTai for unpublished work at QU).

- **GFRP/CFRP with four layers**

Figure 4.21 shows the results for four layers hybridization of GFRP/CFRP. It showed that ultimate flexural load was 6.5 kN. Which was almost same as the behavior of joined aluminum pipe with GFRP of four layers, which was 6.8 kN. This can be explained as in GFRP the matrix is continues which give more capability to handle more load. While in

hybrid GFRP/CFRP, where there are two layers only of each. The behavior tends to show no advantage of using CFRP in addition to GFRP over continuous GFRP composite for the same total number of layers.

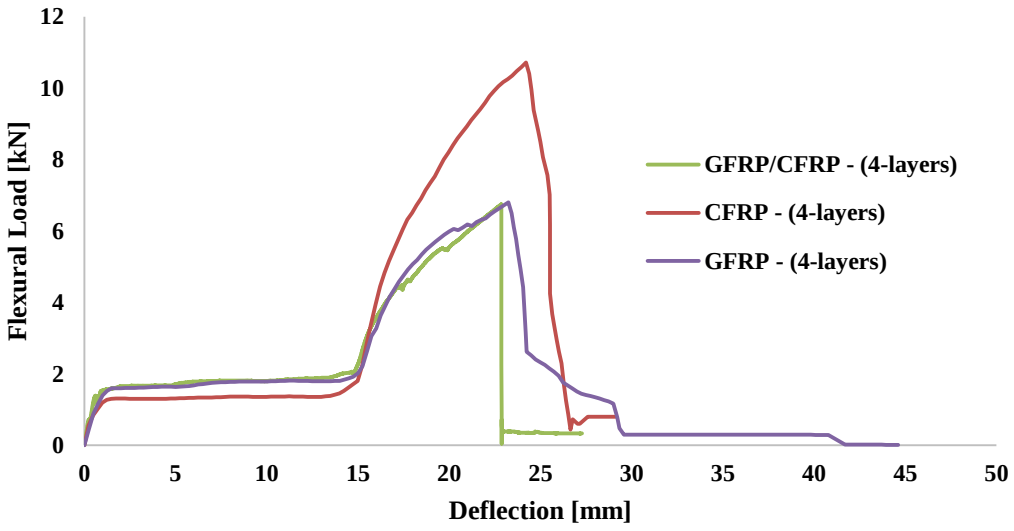

Figure 4.21: Flexural load vs. deflection curves for 4-layers hybridization of GFRP/CFRP compared to GFRP & CFRP.

Table 4.5: Observations summary for bending behavior of joined aluminum pipes with four layers of hybridization of GFRP/CFRP compared to four layers GFRP & CFRP

Type of joining	Yielding		Ultimate failure	
	Load [kN]	Deflection [mm]	Load [kN]	Deflection [mm]
(GFRP/CFRP)	1.1	0.7	6.5	23.4
GFRP	1.4	1	6.8	23.2
CFRP	0.8	0.5	10.7	24.2

- **KFRP/CFRP with four layers**

Figure 4.22 shows the results for four layers hybridization of KFRP/CFRP. It showed that ultimate flexural load was 10.8 kN, which was almost same as joined aluminum pipe with CFRP of four layers, which was 10.7 kN. Again, as discussed for GFRP/CFRP, the KFRP/CFRP results showed there is no advantage of using KFRP in addition to CFRP over continuous CFRP composite for the same total number of layers.

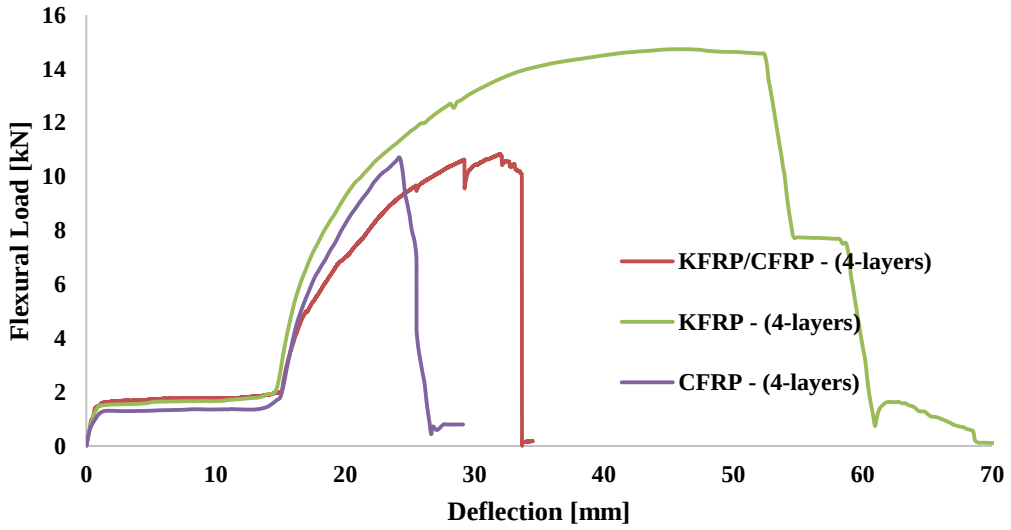

Figure 4.22: Flexural load vs. deflection curves for 4-layers hybridization of KFRP/CFRP compared to KFRP & CFRP.

Table 4.6: Observations summary for bending behavior of joined aluminum pipes with four layers of hybridization of KFRP/CFRP compared to four layers KFRP & CFRP

Type of joining	Yielding		Ultimate failure	
	Load [kN]	Deflection [mm]	Load [kN]	Deflection [mm]
(KFRP/CFRP)	1.4	0.7	10.8	32.5
CFRP	0.8	0.5	10.7	24.2
KFRP	1.5	1	14.7	52.4

According to these results, the tests for hybridization has been carried out again with eight layers to investigate their behavior.

- **GFRP/CFRP with eight layers**

Figure 4.23 shows the results for eight layers hybridization of GFRP/CFRP. It showed that ultimate flexural load had been increased to 11.9 kN. Which higher than values obtained for joined aluminum pipe with CFRP of four layers, which was 10.7 kN. In this case, it required more layers and two material to overcome slightly the value obtained for CFRP four layers. Again, as discussed previously, results showed that using GFRP in addition to CFRP overcome the continuous CFRP with four layers when only the number of layers is increased.

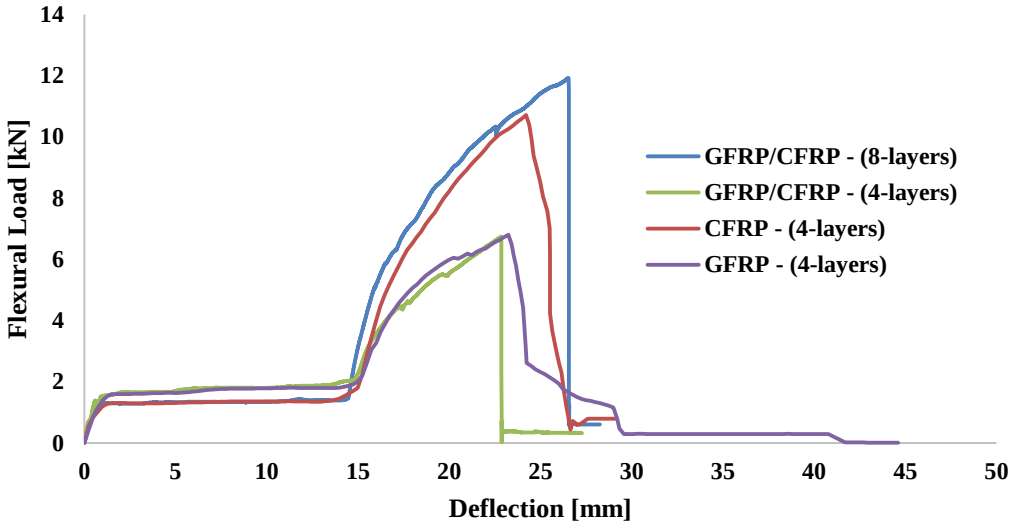

Figure 4.23: Flexural load vs. deflection curves for 8-layers hybridization of GFRP/CFRP compared to four layers GFRP/CFRP, CFRP, and GFRP.

Table 4.7: Observations summary for bending behavior of joined aluminum pipes with eight layers of hybridization of GFRP/CFRP compared to four layers GFRP, CFRP, and hybridization of GFRP/CFRP

Type of joining	**Yielding**		**Ultimate failure**	
	Load [kN]	**Deflection [mm]**	**Load [kN]**	**Deflection [mm]**
(GFRP-CFRP) (8-layers)	1.3	0.8	11.9	26.6
(GFRP-CFRP) (4-layers)	1.1	0.7	6.5	23.4
CFRP (4-layers)	0.8	0.5	10.7	24.2
GFRP (4-layers)	1.4	1	6.8	23.2

(a): KFRP/GFRP joined pipe failure in tension side

(b): KFRP/GFRP joined pipe failure in compression side

Figure 4.24: Fracture of hybrid GFRP/CFRP joined aluminum pipes.

- **KFRP/CFRP with eight layers**

Figure 4.25 shows the results for eight layers hybridization of KFRP/CFRP. It showed that ultimate flexural load had been increased significantly to 16 kN. Which gives higher flexural load than continuous CFRP of four layers, which was 10.7 kN, as well as continuous KFRP with four layers, which was 14.7 kN. For total deflection, the effect of KFRP/CFRP with eight layers showed decreasing compared to continuous KFRP with four layers, while it was higher compared to continuous CFRP with four layers.

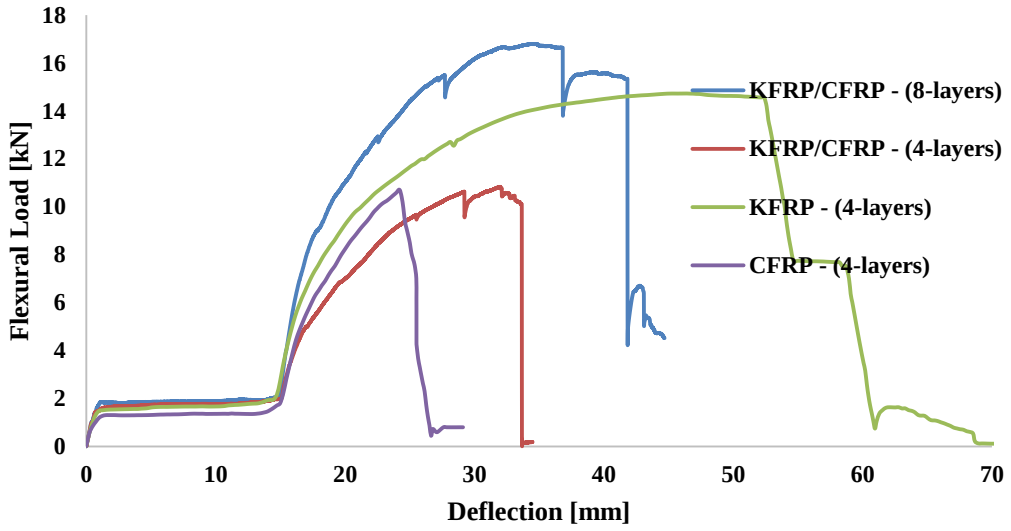

Figure 4.25: Flexural load vs. deflection curves for 8-layers hybridization of KFRP/CFRP compared to four layers KFRP/CFRP, CFRP, and KFRP.

Table 4.8: Observations summary for bending behavior of joined aluminum pipes with eight layers of hybridization of KFRP/CFRP compared to four layers KFRP, CFRP, and hybridization of GFRP/CFRP

Type of joining	**Yielding**		**Ultimate failure**	
	Load [kN]	**Deflection [mm]**	**Load [kN]**	**Deflection [mm]**
(KFRP/CFRP) (8-layers)	1.8	1.2	16	41
(KFRP/CFRP) (4-layers)	1.4	0.7	10.8	32.5
CFRP (4-layers)	0.8	0.5	10.7	24.2
KFRP (4-layers)	1.5	1	14.7	52.4

(a): KFRP/CFRP joined pipe failure in tension side

(b): KFRP/CFRP joined pipe failure in compression side

Figure 4.26: Fracture of hybrid KFRP/CFRP joined aluminum pipe.

FRP joining type optimization:

For finding the optimum type of joining, an optimization process has been carried using a matrix to calculate the weight of each type of joining depending on the following factors and their weight values:

1. Flexural Load: (1-7), where the higher number for the higher value.
2. Total Deflection: (1-7), where the higher number for the higher value.
3. Yielding Load: (1-7), where the higher number for the higher value.
4. Cost: (1-2), where (2) for four layers (less cost) and (1) for eight layers (more cost).

Different types of joining have been sorted from the maximum value to the lowest for each factor. The highest value of each type of joining has been given the highest weight

number. The total summation of weight numbers for each type of joining represent their level in the optimization process. The highest number is the optimized type.

Table 4.9: Type of joining optimization matrix

Joining material	Cost		Yielding Load		Total Deflection		Flexural Load		Sum of Ranking
	Ranking (1-2)	Number of layers (1-2)	Ranking (1-7)	Load [kN]	Ranking (1-7)	Deflection [mm]	Ranking (1-7)	Load [kN]	
KFRP-4	2	4	6	1.5	7	52.4	6	14.7	**21**
CFRP-4	2	4	2	0.8	3	24.2	3	10.7	10
GFRP-4	2	4	5	1.4	1	23.2	2	6.8	10
(KFRP/CFRP)-4	2	4	5	1.4	5	32.5	4	10.8	16
(GFRP/ CFRP)-4	2	4	3	1.1	2	23.4	1	6.5	8
(KFRP/CFRP)-8	1	8	7	1.8	6	41	7	16	**21**
(GFRP/CFRP)-8	1	8	4	1.3	4	26.6	5	11.9	14

The optimization process showed that both four layers of KFRP and eight layers of hybrid KFRP/CFRP are the optimized types of joining the aluminum pipes to be considered for an internal pressure test.

Summary of bending test outcomes:

1. Using FRP in joining resulted in a significant improvement of ultimate flexural load compared to welding techniques.
2. FRP joining system with a fiber orientation of $0^{o}/90^{o}$ demonstrated highest flexural load carrying capacity.
3. KFRP joining system showed the highest ultimate flexural load and toughness compared to GFRP and CFRP.
4. CFRP joining system showed a high value of flexural load compared to welding, while it showed lower deflection than V- welded pipes due to the brittleness of CFRP.
5. The effect of hybridization system of four layers of GFRP/CFRP on load carrying capacity found to be insignificant compared to continuous GFRP of the same total number of layers.
6. The effect of hybridization system of four layers of KFRP/CFRP on load carrying capacity found to be insignificant compared to continuous CFRP of the same total number of layers.

7. Hybridization of eight layers of GFRP/CFRP resulted in an improvement in ultimate flexural load, compared to four layers of GFRP/CFRP, GFRP, and CFRP.
8. Hybridization of eight layers of KFRP/CFRP resulted in a significant improvement in ultimate flexural load compared to four layers of KFRP/CFRP, CFRP, and KFRP.

4.2 Internal pressure capacity of joined pipes

In this section, the internal pressure test results for KFRP with four layers and CFRP/KFRP with eight layers, which have been selected through optimization for the results obtained from bending test are presented and discussed.

4.2.1 KFRP with four layers

In this section, results of combined axial and radial internal pressure test as well as radial internal pressure test are presented and discussed.

- **Combined axial and radial internal pressure**

The test for KFRP under combined axial and radial internal pressure has been conducted by connecting both sides of the pipes with the inlet and outlet hoses using cylindrical

fixtures (Figure 4.27).

Figure 4.27: Aluminum pipe joined with KFRP joining under combined axial and radial internal pressure test.

The results obtained showed that the pipe has been in filling the stage for 16 s before it pressurized through the cyclic internal pressure until failure after for 4 s with 100 bar of internal pressure (Figure 4.28).

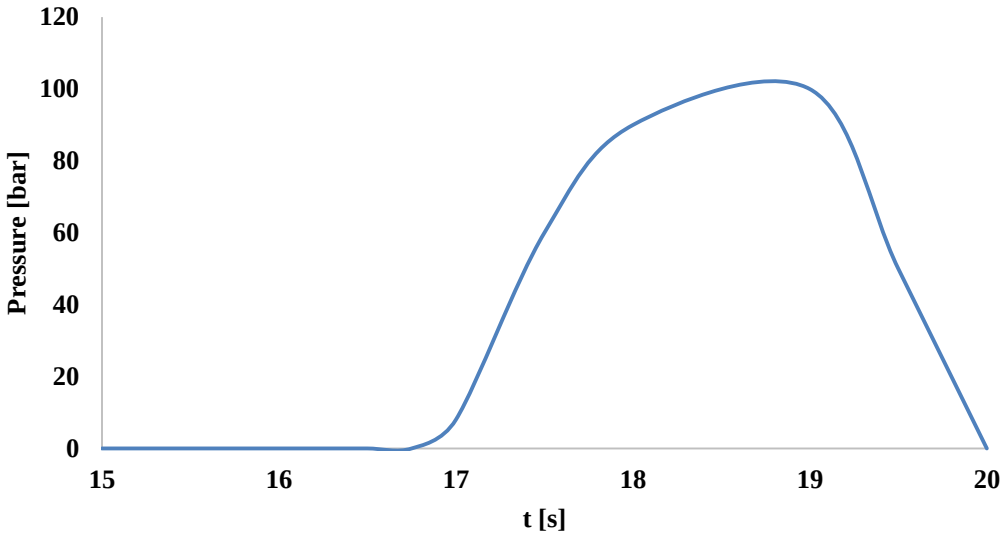

Figure 4.28: Kevlar joining under combined axial & radial internal pressure.

The failure occurred when the leakage started, and at the same time, the joint has been split from one side of the pipe without breakage in the main pipe body or the joint itself (Figure 4.29). This indicates that the failure is related to resin crack in the layer in contact with the pipe's surface.

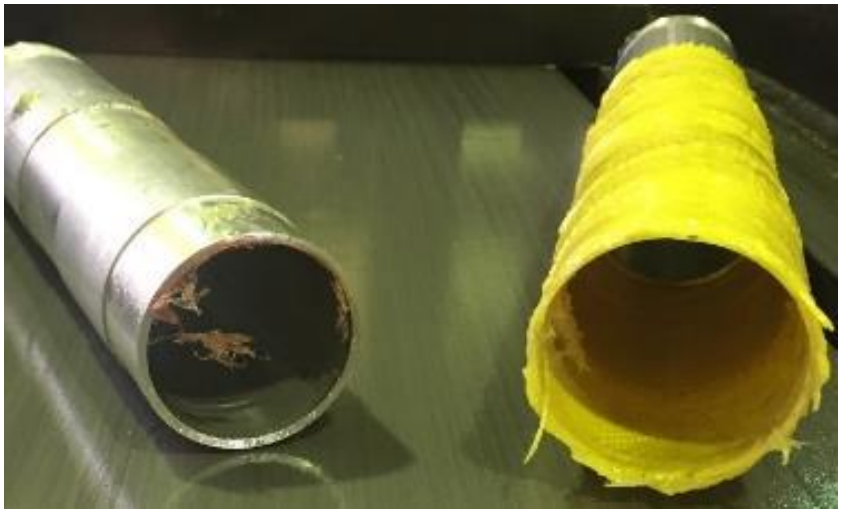

Figure 4.29: Splitting of the joint from the pipe.

According to these results, it has been decided to design another fixture to fix the pipe from each side, to allow only radial pressure, which gives more realistic results, and to represent the reality where joined pipes always fixed.

- **Radial internal pressure**

For radial internal pressure test, a new fixation has been used as a case to hold both sides of the pipe (Figure 4.30). This fixation has been designed as two plates connected to each other using four long threaded rods with nuts for tiding. These two plates have a cup groove where the original two fixtures of the pipe can be placed.

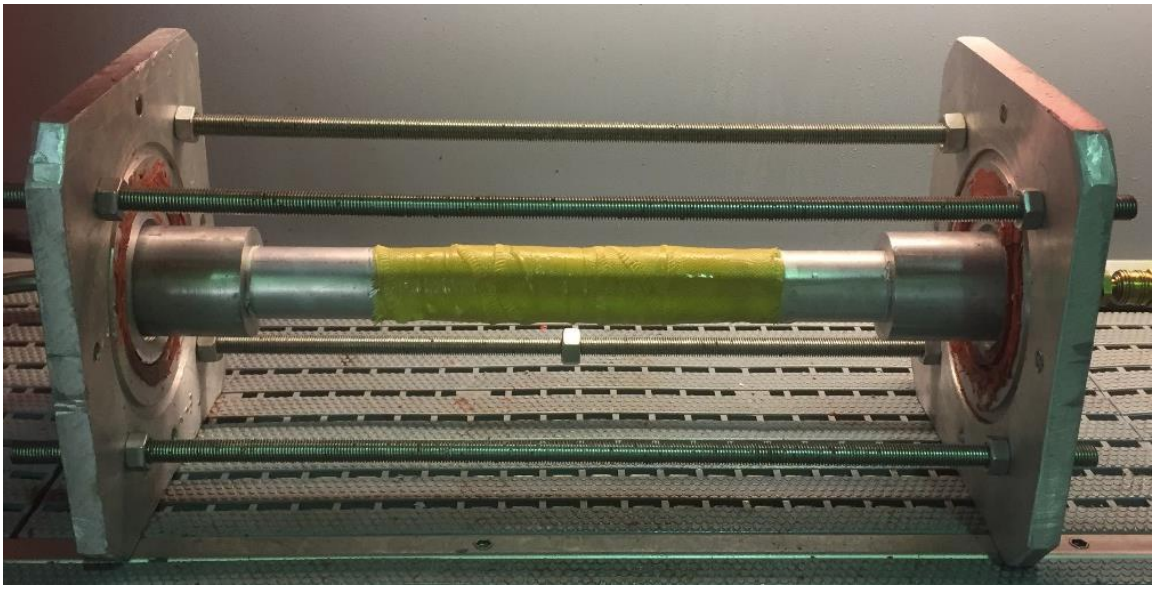

Figure 4.30: Fixation for radial internal pressure test.

The result of KFRP under radial internal pressure test showed a significant increase in the internal pressure capacity of the pipe. The pressure reached 200 Bar after 5 s from filling completion, where slightly decreasing occurred until failure occurred when the pressure reached 171 Bar after 30 s from filling completion. (Figure 4.31). The failure occurred as leakage from the KFRP joint edges, without any breakage or visual deformation in the pipe or the joint. Again, this failure is related to resin cracks in the layer, which is in contact with pipe's surface. After removal of the pipe from the test fixtures, it has been noticed that the joint is still connected to the pipe and cannot be removed by hand.

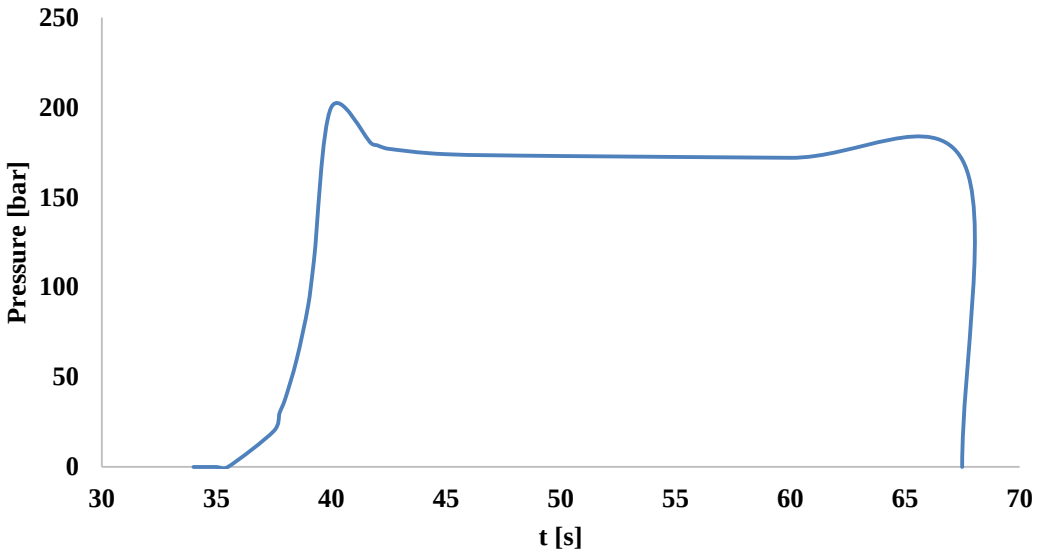

Figure 4.31: KFRP with 4-layers joining under radial internal pressure.

4.2.2 CFRP/KFRP with eight layers

The result of CFRP/KFRP with eight layers joining aluminum pipes under radial internal pressure test failed at 165 Bar after 20 s from filling completion, where slightly decreasing occurred until the pressure reached 150 Bar after 45 s from filling completion when the failure occurred (Figure 4.32). The failure occurred as leakage from the composite joint edges, without any breakage or visual deformation in the pipe or the joint, as it has been observed in KFRP with four layers. Again, this failure is related to resin cracks in the layer, which is in contact with pipe's surface. After removal of the pipe from the test fixtures, it has been noticed that the joint is still connected to the pipe and cannot be removed by hand.

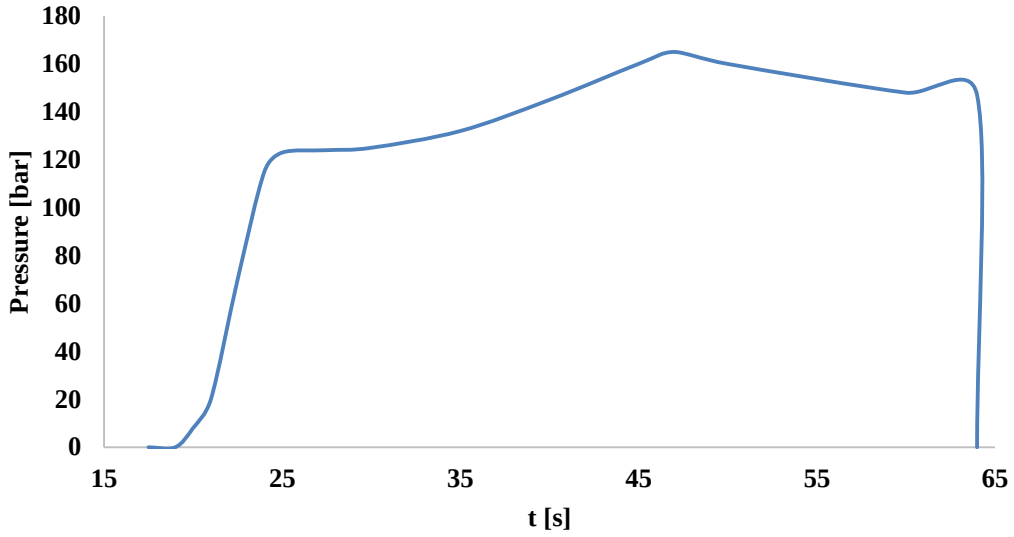

Figure 4.32: KFRP/CFRP with 8-layers joining under radial internal pressure.

This result was lower than the results obtained from KFRP with four layers test, although it took a long time to occur. This can be referred to hand layup problems during the fabrication process, which includes the amount of resin used for it. It indicates that the fabrication process quality could affect the results significantly.

4.2.3 FRP composite versus welding

The results for welded aluminum pipe under radial internal pressure test showed failure at 165 bar. The KFRP with four layers showed higher internal pressure capacity of 200 bar (Figure 4.33). Although CFRP/KFRP with eight layers showed similar internal pressure capacity to the welded aluminum pipe, it is believed that higher quality of the fabrication

process could improve this result. In general, using composites for joining pipes is showing a promising method for higher performance regarding internal pressure compared to welding methods.

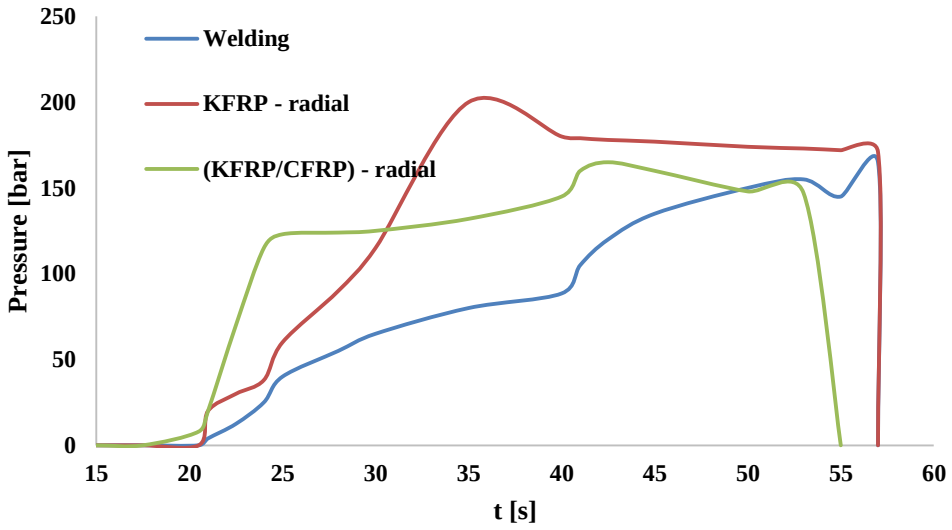

Figure 4.33: Internal pressure capacity of composite joining vs. welding.

Summary of internal pressure test outcomes:

1. Using composites of fiber in joining resulted in a significant improvement of internal pressure capacity of joined pipes compared to welding.
2. The failure in FRP composite joined pipes occurred at the edge of joint as leakage due to resin cracking in the attached layer to the pipe's surface and before any visual deformation in the pipe or the joint.

3. The quality of fabrication process can significantly affect the internal pressure capacity of FRP joined pipes.

4.3 Corrosion in joined pipes

Corrosion experiment has been designed to investigate the corrosion resistance of different FRP composites types comparing to weld and base metal. The figures for different specimens before and after immersing them in 1.5 M HCl solution are presented. The experiment showed that corrosion was formed in both welded pipe and non-joined pipe. The three types of FRP composites including KFRP, CFRP, and GFRP showed corrosion resistance after one week from experimenting (Figure 4.37).

The pitting corrosion started in both welded and non-welded aluminum pipes after one week of conducting corrosion experiment (Figure 4.36), due to acid attacking of the oxide film on aluminum pipes.

(a) (b)

Figure 4.34: Aluminum pipe specimens before corrosion experiment, (a): Welded aluminum pipe, (b): Non welded aluminum pipe.

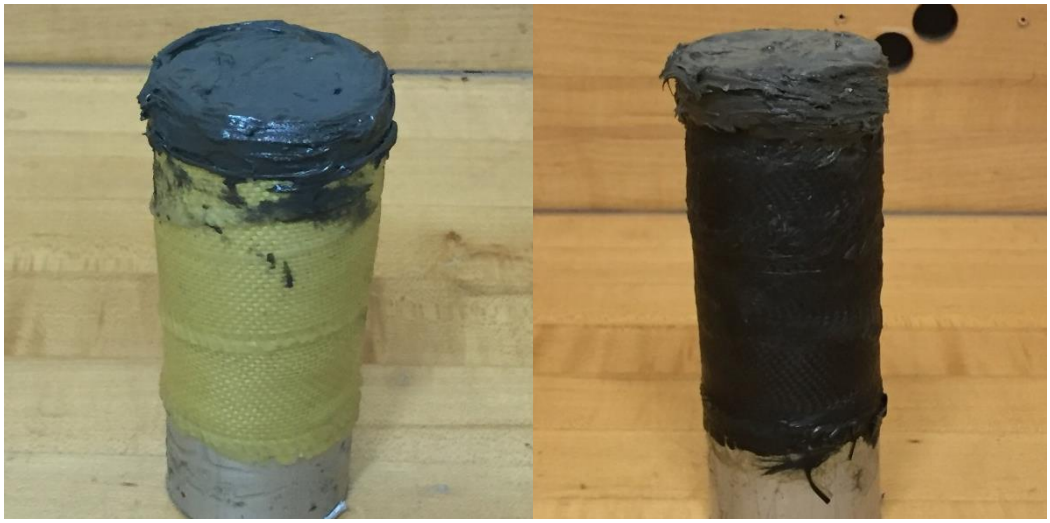

(a): Aluminum pipe joined with KFRP (b): Aluminum pipe joined with CFRP

(c): Aluminum pipe joined with GFRP

Figure 4.35: Aluminum pipe specimens joined with FRP before corrosion experiment, (a): KFRP, (b): CFRP, (c): GFRP.

(a): Corrosion in welded aluminum pipe

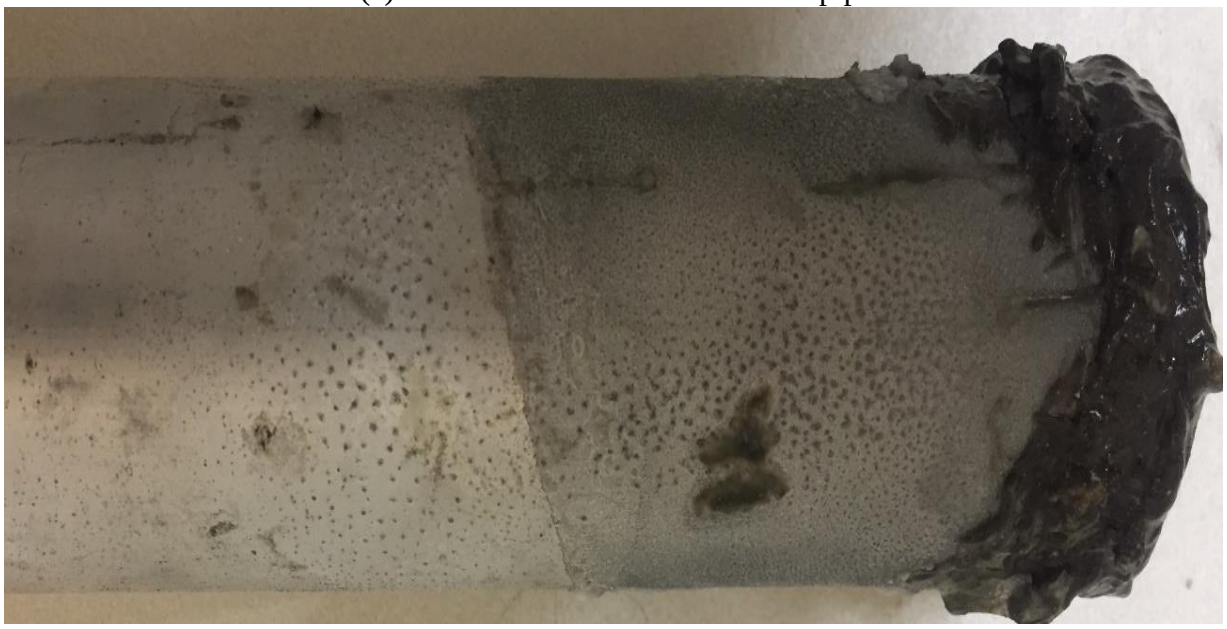

(b): Corrosion in non – joined aluminum pipe

Figure 4.36: Corrosion of welded and non-welded aluminum pipe.

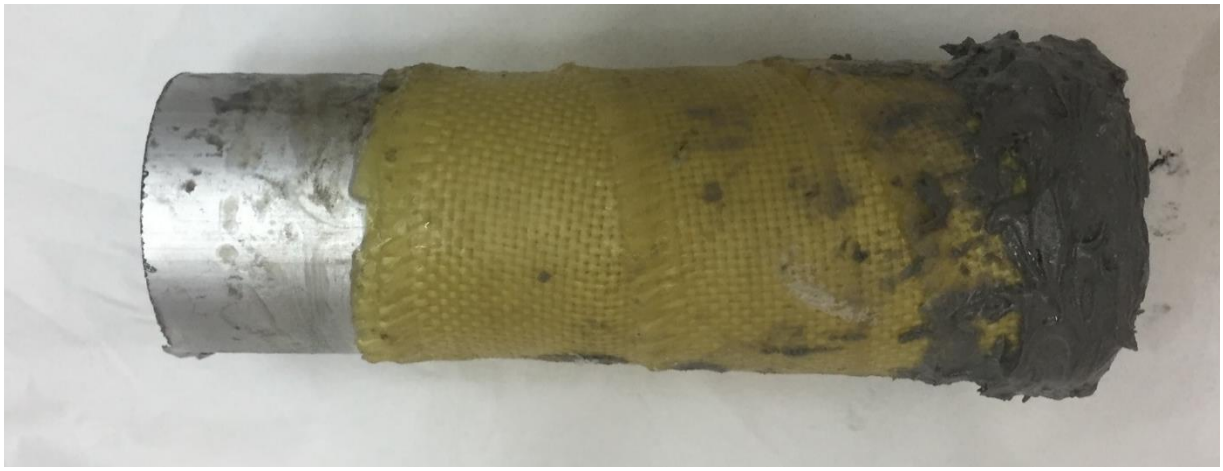

(a): Aluminum pipe joined with KFRP

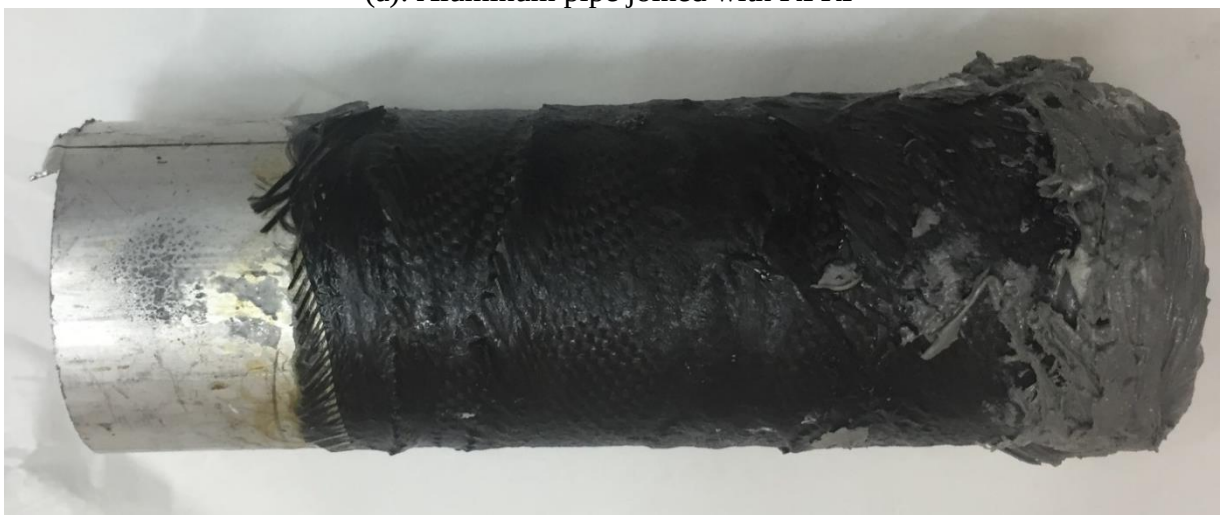

(b): Aluminum pipe joined with CFRP

(c): Aluminum pipe joined with GFRP

Figure 4.37: Aluminum pipe joined with FRP composites after one week of corrosion experiment.

CHAPTER 5

CONCLUSION AND RECOMMENDATIONS

5.1 Conclusion

In this study, using of fiber reinforced plastics (FRP) composites in pipe joining has been investigated regarding bending behavior and internal pressure capacity and compared to welding through six phases. In Phase1, a fabrication process has been carried out. The aluminum pipes samples have been prepared for winding by making grooves in the pipes, and different FRP materials which are Kevlar fiber (KFRP), carbon fiber (CFRP), and glass fibers (GFRP) have been cut as long strips and utilized in the joining systems using fabric winding method. On the other hand, the welded pipes involved V-welding technique and normal faced butt-welding technique, with (4043) aluminum alloy wire as filler material. Moreover, Phase2 involved optimization of fiber orientation of joining system under bending test, where CFRP has been used with $0^0/90^0$ and $\pm45^0$ orientations. The results showed that $0^0/90^0$ orientation has the highest flexural load values. In Phase3, evaluation of fiber type effect on bending behavior of joined pipes has been carried out for different FRP composites types with four layers and compared to welding. For comparison purpose, the non-joined aluminum pipe has been investigated under three-point bending test as a control for the study. Also, the V-welded pipes, as well as normal faced butt-welded pipes, have been investigated under three-point-bending test. The results for V-welded pipes showed higher flexural load than normal faced butt-welded

pipes. Both types of welding resulted in a significant reduction of flexural load compared to non – joined aluminum pipe, while the V – welded pipe showed failure at a higher deflection than non – joined aluminum pipe. To this extent, using of FRP composites in pipes joining resulted in a significant improvement of ultimate flexural load compared to welding techniques. The pipes joined with KFRP showed the highest flexural load. The pipes joined by CFRP showed a high value of flexural load under bending compared to welding techniques, while it showed lower deflection than welded pipes due to the brittleness of carbon fiber. On the other hand, the pipes joined with GFRP showed similar ultimate flexural load to welding. In addition, Phase4 involved assessment of FRP hybridization on bending behavior of joined pipes, where GFRP/CFRP and KFRP/CFRP of four layers and eight layers have been assessed. The results showed that four layers of FRP hybridization are insignificant compared to four layers of single FRP type. The results indicated the need to increase the number of layers to get better results of bending flexural load than using only one type of lower number of layers. Accordingly, eight layers of GFRP/CFRP and KFRP/CFRP resulted in an improvement in flexural loads compared to four layers of single FRP type. Based on the bending results, the Phase5 has been established, where the internal pressure capacity of the pipe has been investigated for the optimized type of joining, which found to be KFRP of four layers and KFRP/CFRP of eight layers. The results showed improvement in the pipes internal pressure capacity compared to welding. The failure in case of FRP composites joining under internal pressure test has been observed as leakage from the joint edges without any visual deformation in the joint structure or pipe. Finally, corrosion test has been carried out in Phase6. The results showed that FRP joining systems have higher corrosion

resistance compared to welded and non – joined pipes. These results revealed that using FRP composites in pipes joining showing a promising future for pipes joining to achieve the free corrosion pipelines.

5.2 Recommendations for future work

1. Studying the effect of resin type on improving the adhesive between matrix and surface of the joined pipes.
2. Studying the fatigue behavior of FRP composite joining of pipes compared to welding joining.
3. Studying corrosion with and without fatigue for FRP composites joining pipes compared to welding joining.
4. Studies to optimize the performance of FRP composite joining alongside with cost to establish a fiber composite cost-effective solution for pipe joining.
5. Establishment of numerical study using simulation software to compare to the results from this study and to provide a sufficient tool for predicting the behavior of FRP composite joining pipes.

REFERENCES

ASTM, I. (2006). *Terminology Relating to Corrosion and Corrosion Testing ASTM Book of Standards* (Standard G15 ed.). West Conshohocken: PA.

ASTM-G46. (2013). *Standard Guide for Examination and Evaluation of Pitting Corrosion.*

Bae, W.-G., Chang, K.-H., & Lee, C.-H. (2016). Progressive inelastic deformation of a girth-welded stainless steel pipe under internal pressure and cyclic bending. *Ocean Engineering, 128*, 81-93.

Barsoum, I., & Khalaf, A. (2015). Evaluation of a pipe - flange connection replacing fusion welding. *Procedia Engineering*, 446-452.

Budiansky, B., & Fleck, N. (1993). Compressive failure of fiber composites. *J. Mech. Phys. Solids*, 41-183.

Budyans, R. G., & Nisbett, K. (2011). *Shigley's mechanical engineering design.* McGraw-Hill series in mechanical engineering.

Chaves, I. A., & Melchers, R. E. (2011). Pitting corrosion in pipeline steel weld zones. *Corrosion Science, 53*, 4026-4032.

Chen, X., Lu, H., Chen, G., & Wang, X. (2015). A comparison between fracture toughness at different locations of longitudinal submerged arc welded and spiral submerged arc welded joints of API X80 pipeline steels. *Engineering Fracture Mechanics, 148*, 110-121.

Cooper, G. (1974). Micromechanics aspects of fracture and toughness, Composite

Materials. *Fracture and Fatigue*, 415.

Eliyan, F. F., Mahdi, E.-S., & Alfantazi, A. (2012). Electrochemical evaluation of the corrosion behaviour of API-X100 pipeline steel in aerated bicarbonate solutions. *Corrosion Science, 58*, 181-191.

Francis, R. (2001). *Galvanic Corrosion: A Practical Guide for Engineers.* Houston: NACE.

Fukunaga, H., & Chou, T. (1988). Simplified Design Techniques for Laminated Cylindrical Pressure Vessels under Stiffness and Strength Constraints. *Journal Composite Material, 22*, 1156-1169.

Gohari, S., Golshan, A., Mostakhdemin, M., Mozafari, F., & Momenzadeh, A. (2012). Failure Strength of Thin-walled Cylindrical GFRP Composite Shell against Static Internal and External Pressure for various Volumetric Fiber Fraction. *International Journal of Applied Physics and Mathematics*, 111-116.

Hack, H. P. (2010). Galvanic Corrosion. *Reference Module in Materials Science and Materials Engineering, 2*, 829-855.

Huang, Z. m. (2000). The mechanical properties of composites reinforced with woven and braided fabrics. *Composites Science and Technology*, 479-498.

Kennedy, J. L. (1993). Pipeline industry overview. In J. L. Kennedy, *Oil and Gas Pipeline Fundamentals* (pp. 3-6). PennWell Books.

Krikanov, A. A., & Soni, S. (1995). Minimum Weight Design of Pressure Vessel with Constraint on Stiffness and Strength. (pp. 107-113). Santa Monica, CA: 10th ASC Technical Conference on Composite Materials.

Kumar, P., Singh, R. K., & Kumar, R. (2007). Joining similar and dissimilar materials

with GFRP. *International Journal of Adhesion & Adhesives 27 (2007) 68–76, 27,* 68-76.

Lee, C.-H., & Chang, K.-H. (2013). Study on the residual stresses in girth-welded steel pipes and their evolution under internal pressure. *Marine Structures, 34*, 117-134.

Lotsberg, I. (2008). Stress concentration factors at welds in pipelines and tanks subjected to internal pressure and axial force. *Marine Structures, 21*, 138-159.

Lyu Jin. A. (2014, April). *Metal-plastic composite pipe*. Retrieved from Google Patent: CN103727324

Mahdi, E. (2015). *UREP 10 - 053 - 2 - 015.*

Mahdi, E., Hamouda, A., Sahari, B., & Khalid, Y. (2003). Effect of hybridisation on crushing behaviour of carbon/glassfibre/epoxy circular–cylindrical shells. *Journal of Materials Processing Technology*, 49-57.

Mahdi, E., Hamouda, A., Sahari, B., & Khalid, Y. (2003). Experimental quasi-static axial crushing of cone–tube–cone composite system. *Composites: Part B 34;* , 285-302.

Mahdi, E., Mokhtar, A., Asari, N., Elfaki, F., & Abdullah, E. (2006). Nonlinear finite element analysis of axially crushed cotton fiber composite corrugated tubes. *Composite Structures*, 39-48.

Mahdi, E., Rauf, A., Ghani, S., El-Noamany, A., & Pakari, A. (2013). Erosion-Corrosion Behavior and Failure Analysis of Offshore Steel Tubular Joint. *Int. J. Electrochem. Sci., 8*, 7187-7210.

Mahmoodian, M., & Li, C. Q. (2016). Chapter 11 - Stochastic failure analysis of defected oil and gas pipelines. In M. Mahmoodian, & C. Q. Li, *Handbook of Materials Failure Analysis with Case Studies from the Oil and Gas Industry* (pp. 235-255).

Butterworth-Heinemann.

Mallick, P. K. (2007). *Fiber-Reinforced Composites: Materials, Manufacturing, and Design* (Third edition ed.). Florida: CRC Press.

Mandel, M., & Krüger, L. (2015). Long-term corrosion studies of a CFRP / EN AW-6060-T6 self - piercing rivet joint and a steel / EN AW-6060-T6 blind rivet joint. *Materials Today*, 131 – 140.

Mathias, L. L., Sarzosa, D. F., & Ruggieri, C. (2013). Effects of specimen geometry and loading mode on crack growth resistance curves of a high-strength pipeline girth weld. *International Journal of Pressure Vessels and Piping, 111-112*, 106–119.

Pluvinage, G., & Elwany, M. H. (2008). *Safety, Reliability and Risks Associated with Water, Oil and Gas Pipelines.* Springer in cooperation with NATO Public Diplomacy Division.

Popoola, L. T., Grema, A. S., Latinwo, G. K., & Gutti, B. (2013). Corrosion problems during oil and gas production and its mitigation. *International Journal of Industrial Chemistry*.

Popoola, L. T., Grema, A. S., Latinwo, G. K., Gutti, B., & Balogun, A. S. (2013). Corrosion problems during oil and gas production and its mitigation. *International Journal of Industrial Chemistry, 35*(4), 2228-5547.

Popoola, L. T., Grema, A. S., Latinwo, G. K., Gutti, B., & Balogun, A. S. (2013). Corrosion problems during oil and gas production and its mitigation. *International Journal of Industrial Chemistry, 35*(4), 2228-5547.

Sebaey, T., & Mahdi, E. (2014). Lateral Compression after Impact of GFRP Composite Pipes . *Int'l Conference on Advances in Materials (AMMIE-2014), Mechanical*

and Industrial Engg. Phuket - Thailand.

Sebaey, T., & Mahdi, E. (2014). Crushing after impact of GFRP composite tubes. *Journal of Impact Engineering*.

Sebaey, T., Mahdi, E., Shamseldin, A., & Eltai, E. (2014). Crushing behavior of hybrid hexagonal/octagonal cellular composite system: All made of CFRP composite. *Materials & Design*, 556-562.

Senkine, H., & Shin, E. (1999). Optimum Design of Thick-Walled Multi-Layered CFRP Pipes to Reduce Process-Induced Residual Stresses. *Applied Composite Materials*, 289-307.

Sharma, S. K., & Maheshwari, S. (2017). A review on welding of high strength oil and gas pipeline steels. *Journal of Natural Gas Science and Engineering, 38*, 203-217.

Toutanji, H., & Dempsey, S. (2001). Analytical Study of the Use of Advanced Composites for Repair and Rehabilitation of Pipelines. *Journal of Thin-Walled Structures, 39*(2).

Vanaei, H., Eslami, A., & Egbewande, A. (2017). A review on pipeline corrosion, in-line inspection (ILI), and corrosion growth rate models. *International Journal of Pressure Vessels and Piping, 149*, 43-54.

Vasiliev, V., Krikanov, A., & Razin, A. (2003). New generation of filament-wound composite pressure vessels for commercial applications. *Composite Structures, 62*(3-4), 449-459.

Welding and Pipe Fabrication: Different Processes for Different Grades of Piping. (2015, Jul 29). Retrieved from STI group: http://setxind.com/fabrication/welding-pipe-fabrication-different-processes-different-grades-piping/

Xu, S., Wang, H., Li, A., Wang, Y., & Su, L. (2016). Effects of corrosion on surface characterization and mechanical properties of butt-welded joints. *Journal of Constructional Steel Research, 126*, 50-62.

Yang, Y., Shi, L., Xu, Z., Lu, H., Chen, X., & Wanga, X. (2015). Fracture toughness of the materials in welded joint of X80 pipeline steel. *Engineering Fracture Mechanics, 148*, 337-349.

Zhu, J., Xu, L., Chang, W., Hub, L., & Lu, M. (2014). Microstructures and mechanical properties of welded joints of novel 3Cr pipeline steel using an inhouse and two commercial welding wires. *Materials and Design, 53*, 405-411.